AD/A-001 832

ANALYSIS OF THE MOBILIZATION OF DEBRIS FLOWS

James D. Rodine, et al

Stanford University

Prepared for:

Army Research Office-Durham

October 1974

SECURITY CLASSIFICATION OF THIS PAGE (When Data Entered)

REPORT DOCUMENTATION PAGE

READ INSTRUCTIONS BEFORE COMPLETING FORM

1. REPORT NUMBER: ARO-9973.1-EN
2. GOVT ACCESSION NO.
3. RECIPIENT'S CATALOG NUMBER: AD/A001 832

4. TITLE (and Subtitle): ANALYSIS OF THE MOBILIZATION OF DEBRIS FLOWS
5. TYPE OF REPORT & PERIOD COVERED: Final Report
6. PERFORMING ORG. REPORT NUMBER

7. AUTHOR(s): James D. Rodine, Arvid M. Johnson and E.I. Rich
8. CONTRACT OR GRANT NUMBER(s): DA-ARO-D-31-124-71-G158

9. PERFORMING ORGANIZATION NAME AND ADDRESS: School of Earth Sciences, Stanford University, Stanford, Calif. 94305
10. PROGRAM ELEMENT, PROJECT, TASK AREA & WORK UNIT NUMBERS

11. CONTROLLING OFFICE NAME AND ADDRESS: U. S. Army Research Office, Box CM, Duke Station, Durham, North Carolina 27706
12. REPORT DATE: October 1974
13. NUMBER OF PAGES: ~~235~~ 237
14. MONITORING AGENCY NAME & ADDRESS (if different from Controlling Office)
15. SECURITY CLASS. (of this report): Unclassified
15a. DECLASSIFICATION/DOWNGRADING SCHEDULE: NA

16. DISTRIBUTION STATEMENT (of this Report)

Approved for public release; distribution unlimited.

17. DISTRIBUTION STATEMENT (of the abstract entered in Block 20, if different from Report)

NA

18. SUPPLEMENTARY NOTES

The findings in this report are not to be construed as an official Department of the Army position, unless so designated by other authorized documents.

19. KEY WORDS (Continue on reverse side if necessary and identify by block number)

Debris flow, conical penetrometer, packing of sedimentary particles, initiation of debris flow, mudflow, debris avalanche, debris slide, mudslide, mobility index, Coulomb properties of debris, size distribution of debris, slurries, strength of debris, mobility of debris.

20. ABSTRACT (Continue on reverse side if necessary and identify by block number)

(abstract enclosed)

DD FORM 1 JAN 73 1473 EDITION OF 1 NOV 65 IS OBSOLETE

Unclassified
SECURITY CLASSIFICATION OF THIS PAGE (When Data Entered)

ANALYSIS OF THE MOBILIZATION OF DEBRIS FLOWS

Final report to U. S. Army Research Office

Durham, North Carolina

Grant No. DA-ARO-D-31-124-71-G158

By

James Dwain Rodine
Department of Geology
Stanford University
Stanford, California 94305

Principal Investigators
Arvid M. Johnson
Ernest I. Rich

October 1974

ia

ANALYSIS OF THE MOBILIZATION OF DEBRIS FLOWS

James Dwain Rodine, Ph.D.
Stanford University, 1975

The purpose of this study was to learn how to predict the potential for debris flow. Many people living in the southwestern United States face the eventual prospect of a visit by a devastating debris flow. Geologists familiar with the process of debris flow have recognized debris-flow deposits in alluvial fans and, based on this historical record, have accurately predicted future debris-flow activity. Unfortunately, the historical approach to the prediction of debris flows is not always reliable because areas can change, as by destruction of the native vegetation or by man's alteration of the landscape by construction. Therefore, this study was designed to analyse the processes of mobilization of debris flows in order to develop a method of quantitatively evaluating the susceptability of an area to erosion by debris-flow activity.

Prediction of the debris-flow potential for an area is possible if one considers six, critical, quantifiable factors: Slope angle and shape of the channel in the source area, water content of saturated, in-situ soil, debris unit weight, and apparent cohesion and apparent friction angle of the debris. Five of the factors, slope angle, channel shape, and unit weight, apparent cohesion and apparent friction angle of the debris, theoretically can be related. The water content of saturated soil, or field capacity, is a measure of the in-situ properties of the soil. The debris properties, unit weight, apparent cohesion and apparent friction angle, can be determined experimentally, with paired conical penetrometers as a

function of the water content. The water content at which debris flow begins in a channel in the source area divided by the field capacity is defined as the mobility index. Mobility index values greater than one indicate low susceptability and values less than one high susceptability to the formation of debris flows.

Computation of mobility index for selected source areas yields values of 1.15 to 1.77 for non debris-flow materials and values of .98 to 1.02 for debris-flow materials.

Study of source areas ranging from large landslide masses at Wrightwood, California, and Thompson Creek, Utah, to small rill-like gullies at Big Sur and at Arroyo Hondo, California, suggests that most debris flows initiate from landslides. Mobilization of the debris is accomplished as the landslide mass moves downhill. The sliding jostles, rotates and dilates blocks of landslide material until enough water is incorporated for flow to begin.

Debris flows can move on gentle slopes yet transport large amounts of clastic materials, including large blocks. Experimental and theoretical studies of artificial mixtures of spherical particles and clay-water slurries suggest that flow on gentle slopes is due to low internal friction brought about by poor sorting. Poor sorting reduces sliding friction and particle interlocking within the debris. The ability of debris flows to transport large blocks is apparently due to buoyancy and the cohesive strength of the clay-water slurry.

Approved for publication:

By _____
For Department of Geology

By _____
Dean of Graduate Studies

PREFACE

This study has been largely supported by the U. S. Army, Grant Number ARO-D-31-124-71-G158, under the supervision of Finn Bronner. I wish to thank Dr. Bronner for his helpful criticism and encouragement during this study. Support for early phases of this study was provided by the U. S. Geological Survey, Contract Number 14-09-0001-10884, and by the Geological Society of America, Grant Number 1537-71.

Review of various portions of this thesis have been made by Dr. Monty A. Hampton, University of Rhode Island, and by Dr. Robert W. Fleming, University of Cincinnati. Their helpful comments have resulted in many improvements to the text.

Arvid M. Johnson, principal thesis advisor, has given so freely of his time that the scope and depth of this study are primarily the results of his insights and ability to illuminate the path toward knowledge.

John Baltierra and Kent McMillan, fellow graduate students at Stanford University, provided laboratory assistance for which I am grateful.

To my wife, Marcia, and daughters, Cybele, Wendy, and Heidi, I offer my thanks for patience and emotional support.

TABLE OF CONTENTS

LIST OF TABLES

PART I: PROCESSES OF INITIATION OF DEBRIS FLOWS

PART II: A METHOD OF DETERMINING COULOMB STRENGTH PROPERTIES OF SOFT, REMOLDED DEBRIS USING PAIRED CONICAL PENETROMETERS

PART III: THE ABILITY OF DEBRIS, HEAVILY FREIGHTED WITH COARSE CLASTIC MATERIALS, TO FLOW ON GENTLE SLOPES

LIST OF FIGURES

PART I: PROCESSES OF INITIATION OF DEBRIS FLOWS

PART II: A METHOD OF DETERMINING COULOMB STRENGTH PROPERTIES OF SOFT, REMOLDED DEBRIS USING PAIRED CONICAL PENETROMETERS

PART III: THE ABILITY OF DEBRIS, HEAVILY FREIGHTED WITH COARSE CLASTIC MATERIALS, TO FLOW ON GENTLE SLOPES

PART IV: MOBILITY INDEX-- A MEASURE OF THE POTENTIAL FOR DEBRIS FLOW

ANALYSIS OF MOBILIZATION OF DEBRIS FLOWS

PART I: PROCESSES OF INITIATION OF DEBRIS FLOWS

ABSTRACT

Observations of debris flows developing on hillslopes throughout the world indicate that debris is mobilized by mass movement of in-situ soil, typically by landsliding. Some debris flows initiate in tiny rills, a few centimeters in depth and width but close inspection indicates that even these form by small-scale landsliding at the heads of the rills.

The mobilization process begins by progressive failure of blocks of soil by landsliding or, in some places, by the energy of impacting water. The slide blocks jostle, rotate, slide downhill, dilate and incorporate water. Then debris flow begins.

The most important conditions to the initiation of debris flows appear to be: Available water and unconsolidated soil containing at least a small fraction of clay, a mechanism for mixing the soil and water and favorable geometry of the source area and of the channel through which the debris must flow.

INTRODUCTION

Suddenly a wall of boulders, rocks of all sizes and oozing mud appears at the mouth of a canyon preceeded by a thunderous roar. The debris-laden torrent flows across an alluvial fan, engulfing structures and cars in its path, covering roads, fields and pastures with a blanket of muck, and slowly coming to a stop as the debris spreads out in a lobate form with steep terminal snout and margins. The event described is a debris flow and its mode of flow and characteristic deposits have long excited the academic interests of students as well as aroused the practical interests of local people faced with the task of cleaning up the mess.

Debris flows have wreaked misery on the lives of many people. In 1919 a volcanic ejection of the water in a crater lake created massive debris flows that killed 5110 people, destroyed 104 villages, and buried 131.2 square kilometers of Java (Scrivenor, 1929, p. 434). Shortly after midnight on New Years Eve, 1934, a flood and debris wave crossed La Cañada Valley, Los Angeles County, California, causing property damage in excess of five million dollars, including loss of 400 houses, and taking more than 40 lives (Troxell and Peterson, 1937). Near record rainfall on March 2, 1938 triggered massive floods and debris flows in the Los Angeles, California, region that caused about $380,000 damage in the Arroyo Seco drainage basin alone (Krumbein, 1942). In the spring of 1941 debris flows coursed through the town of Wrightwood, California, damaging roads and burying three cabins (Sharp and Nobles, 1953). In the summer of 1969 rains generated by Hurricane Camille triggered debris flows which killed about 150 people

and inflicted tens of millions of dollars worth of damage in Nelson County, Virginia (Williams and Guy, 1973). A heavy rainfall in the Mgeta Area, Western Ulugura Mountains, Tanzania, initiated about 1000 debris flows and caused well over $90,000 damage (Temple and Rapp, 1972). Also, heavy rains in October and again in November of 1972 were followed by bouldery debris flows that inundated the village of Big Sur, California and smashed a dozen cars (Cleveland, 1973).

The ability to predict debris-flow activity is of special interest to agencies and officials responsible for the protection of life and property in developed areas, some of which are visited repeatedly by damaging flows. The purpose of our study is to learn how to predict debris flows and to explain why debris flows are common in some areas and uncommon in others. Our approach has been to study processes of initiation and mobilization in the field, in the laboratory, and in theory.

This paper is the first part of a series of four dealing with various aspects of the mobilization of debris flows. The purpose of this first part is to describe source areas of debris flows and to deduce mechanisms of debris-flow initiation and mobilization. Part II describes a method by which Coulomb strength properties of soft, remolded debris can be determined. Part III analyzes the ability of debris to flow on gentle slopes yet freight large amounts of clastic materials. Part IV synthesizes a measure of the potential of soil in various settings to become mobilized as debris flows.

The financial support of the U.S. Army, Grant No. ARO-D-31-124-71-G158, is gratefully acknowledged. Early stages of the research were supported by the U.S. Geological Survey, Contract No. 14-09-0001-10884, and by the Geological Society of America, Grant No. 1537-71.

OBSERVATIONS OF DEBRIS FLOWS INITIATING

Heath Canyon, San Bernardino County, California

Heath Canyon, about 65 km northeast of Los Angeles, California, has been the source of many debris flows which have flowed northeast about one mile down the canyon, moved through the town of Wrightwood, and on into the desert beyond (Fig. 1, Table 1). The head of Heath Canyon, Wright Mountain, which has an elevation of 2580 meters, about 700 meters above and 2100 meters south of the town of Wrightwood, is shown in Fig. 2 where the lack of vegetation denotes the general source area of the debris-flow material. Wrightwood is in Swarthout Valley, a north-northwest trending valley formed along the San Andreas Rift Zone. Heath Canyon is approximately perpendicular to Swarthout Valley and is cut into the north flank of Blue Ridge, on the north side of the San Gabriel Mountains.

Climatic conditions in the Wrightwood area range widely, from cold, snowy, alpine-type winters to hot, dry, desert-type summers. Annual precipitation at Wrightwood is estimated to average 64 cm (Sharp and Nobles, 1953, p. 550). The marked increase in density of vegetation and sizes of trees from Wrightwood to Wright Mountain suggest that the debris-flow source area receives more than 64 cm of precipitation annually. Most of the precipitation is in the form of snow during the winter months, which melts in the spring providing the water for a stream which intermittently flows in Heath Canyon. Much of the year Heath Canyon is dry except for a few springs near the base of the source area.

Figure 1. Locations of debris-flow source areas.

TABLE 1

NAME	SECTION	TOWNSHIP	RANGE	U.S.G.S. TOPOGRAPHIC MAP
Heath Canyon, San Bernardino Co., Calif.	N 1/2 of 20, S 1/2 of 17	3 N.	7 W.	Mount San Antonio, Calif. 7 1/2 min. quad.
Thompson Creek, Sevier Co., Utah	8, 17	25 S.	2 W.	Monroe, Utah 15 min. quad.
Roofing Granule Quarry, San Bernardino Co., Ca.	NW 1/4 of 4	3 N.	7 W.	Phelan, Calif. 7 1/2 min. quad.
Arroyo Hondo, Fresno Co., Calif.	N 1/2 of 14	17 S.	13 E.	New Idria NE, Calif. 7 1/2 min. quad.
Big Sur, Monterey Co., Calif.	13, 24; 18, 19, 20, 29, 30	19 S.	1 E.; 2 E.	Big Sur, Calif. 7 1/2 min. quad.
San Rafael, Marin Co., Calif.	25 (projected)	2 N.	6 W.	San Quentin, Calif. 7 1/2 min. quad.
Woodside, San Mateo Co., Calif.	NW 1/4 of NW 1/4 of 25 (projected)	6 S.	4 W.	Woodside, Calif. 7 1/2 min. quad.
Lead Canyon, Inyo Co., Calif.	NE 1/4 of NW 1/4, NW 1/4 of NE 1/4	12 S.	37 E.	Waucoba Wash, Calif. 15 min. quad.

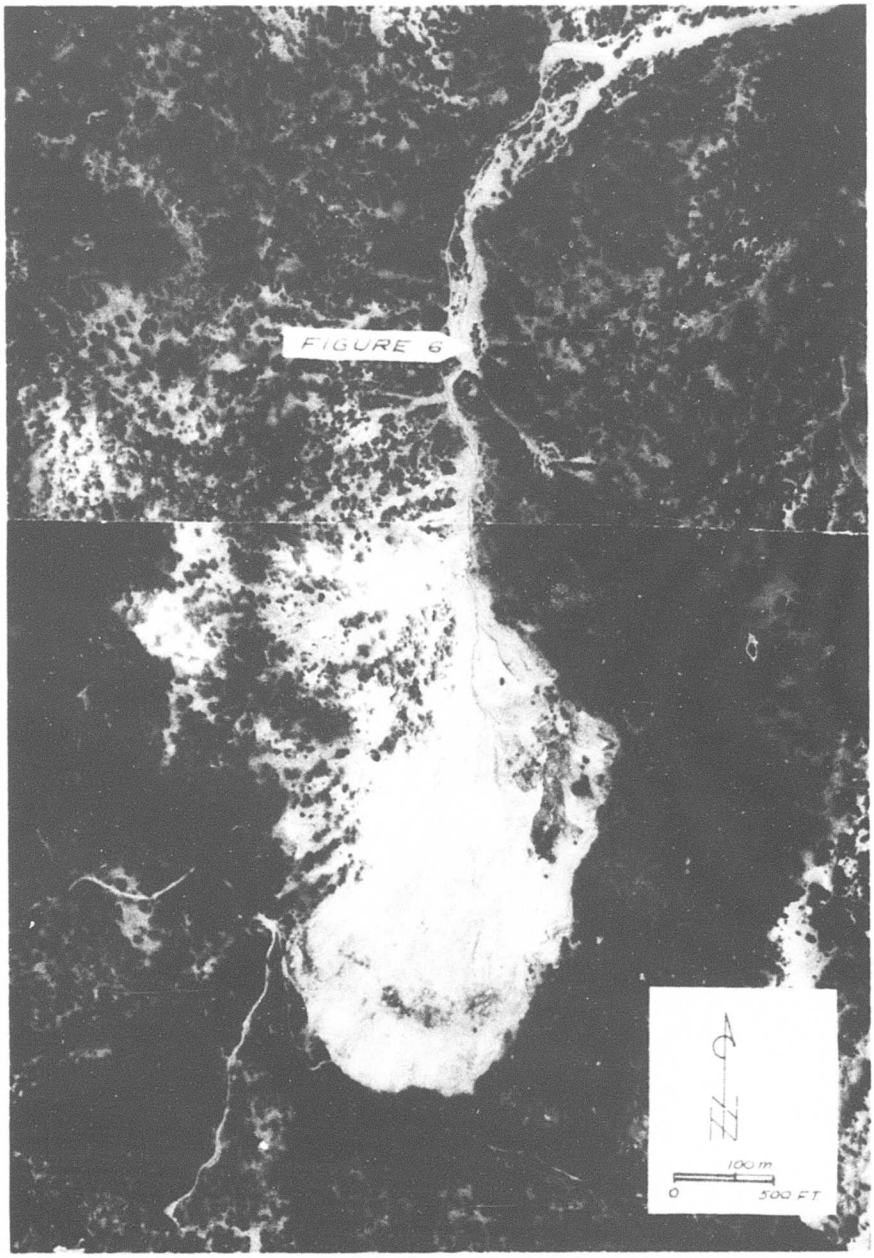

Figure 2. Heath Canyon, San Bernardino County, California is the central canyon in this photograph.

The bedrock at Heath Canyon is primarily mica-quartz schist, called the Pelona Schist (Noble, 1927, ref. in Sharp and Nobles, 1955, p. 549). Foliation of the bedrock strikes roughly parallel to Blue Ridge and dips. south, into the ridge, at an angle averaging 35 degrees (Sharp and Nobles, 1953). The bedrock between Wright Mountain and Wrightwood has been generally sheared and otherwise disturbed by movements within the San Andreas Rift Zone. Landslide activity in the source area has reoriented fragments and reduced particle sizes of schist. Samples of the debris-flow material, collected from the source area, have about 10 percent clay-sized particles, with a wide distribution through the coarser size ranges (Fig. 3).

The entire head of Heath Canyon has been formed by landslide activity. The large slide block shown in Fig. 4 is about 100 meters wide at the top and is more than 300 meters long. Several residents of Wrightwood remember when this block was in place near the top of Wright Mountain. The landslide began to move after 1952, according to examination of aerial photographs, so that the slide block has dropped about 70 meters during the past 20 years.

At the base of the source area is a narrow rock-walled gorge ranging in width up to four meters (Fig. 5). About 1000 meters north of the rock gorge, toward the town of Wrightwood, Heath Canyon widens to about 100 meters where a small bouldery debris flow filled an old channel (Fig. 6a, 6b).

Initiation of several debris flows were observed and photographed with a movie camera on the 20th of May 1969 by Arvid Johnson and several of his students (Hampton, 1972). The initiation sites were

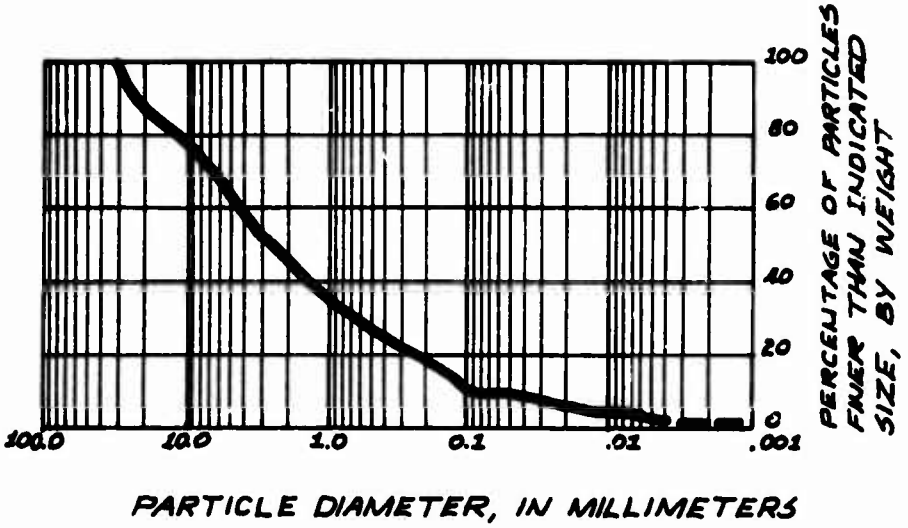

Figure 3. Size distribution of debris-flow material from Heath Canyon, San Bernardino County, California.

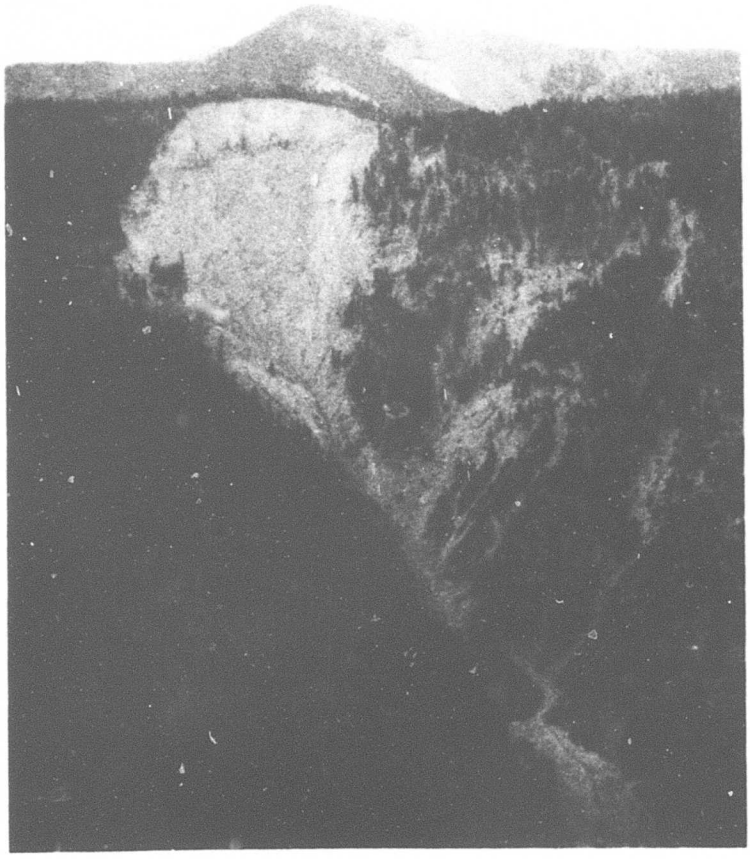

Figure 4. Looking south at Heath Canyon debris-flow source area with Mount San Antonio, Old Baldy, in the distance. The top of the landslide block is marked by the line of trees across the upper third of the raw scar.

Figure 5. Below base of the north-facing source area in Heath Canyon, San Bernardino County, California, with the dry stream bed in the foreground. The width of the narrow rock gorge in the middle ground, through which the debris flows move, is about 4 meters.

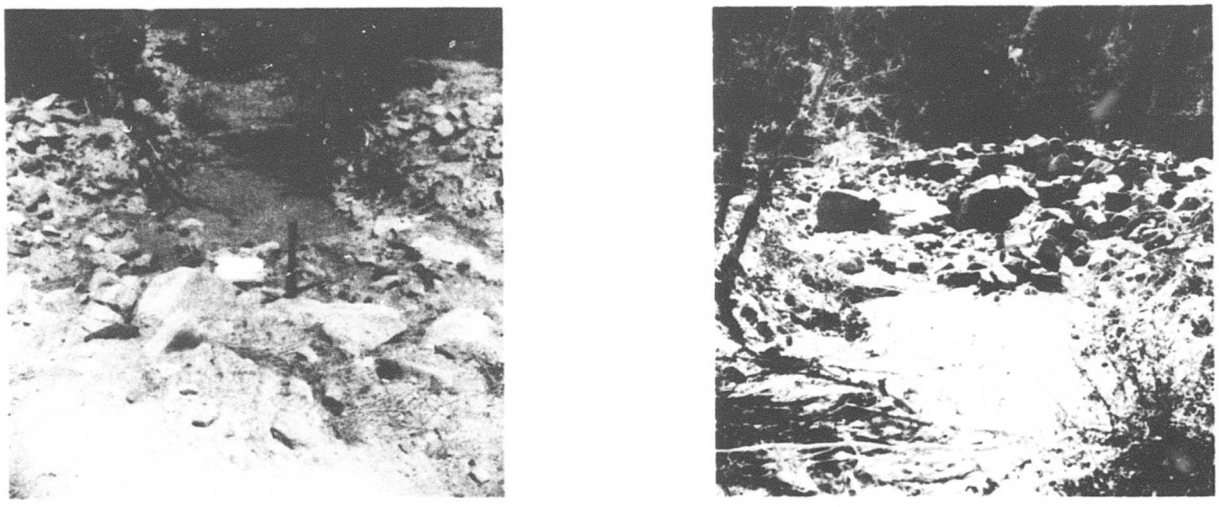

A

B

Figure 6. Debris-flow deposit in Heath Canyon, San Bernardino County, California. Location shown in Fig. 2.

A. Snout of debris-flow deposit as viewed downstream.

B. Snout of debris-flow deposit as viewed upstream.

at the head of Heath Canyon in a small swale cut into comminuted landslide material about 200 to 300 meters above the narrow gorge at the base of the source area. The swale has a semi-elliptical channel cross-section about four meters wide at the top with a depth of one meter (Fig. 7). The ground slopes at an angle averaging forty degrees over a length of about 200 meters. Johnson's movies of the initiation process show the debris changing rapidly from an in-situ solid to a flowing mass.

One debris mass that mobilized was about 4 to 6 meters long, 1 to 2 meters wide, and as much as 1/2 meter in depth, lying in the axis of the swale. The onset of movement was signalled by the loosening of a large rock from near the upper end of the debris mass. As the rock began to roll downhill, cracks trending horizontally across the debris mass appeared in the lower third of the debris mass and the lower blocks of debris began to slide downhill slightly, rotating into the slope. The cracks were first widest in debris near the base and narrowed uphill, but sliding and cracking quickly propagated until the entire mass exhibited large cracks. As a lower part of the mass began to break and slide away it was followed by the block immediately above and thus the movement propagated headward. The appearance was one of uphill progressive formation of cracks and sliding of blocks, and then of sliding and rotation of individual blocks of debris. As the blocks of debris moved down the swale they were jostled and deformed until they lost their individuality. The debris mass looked as if it were flowing much as wet concrete after it had travelled a distance of only a few meters. The entire sequence, from the time

Figure 7. Debris-flow source area in Heath Canyon, San Bernardino County, California, viewed downslope from side of swale.

the large rock started to roll to the time the debris was flowing, is estimated to have occurred within a few seconds time.

Other debris-flow initiations witnessed and photographed by Johnson appear to follow the same pattern. Some of the debris was transformed nearly instantaneously into flowing debris. At times various debris masses slid into the axis of the swale until enough debris had accumulated to begin the sliding-jostling-flow process. The swale contained some running water, attributed to snowmelt (Johnson, Pers. Comm.). Thus the jostling of the debris blocks in the swale may have encouraged incorporation of water, aiding in the transformation from sliding to debris flow.

The debris flows from Heath Canyon, which occurred during the spring of 1969, were witnessed by other observers. According to two members of the U. S. Geological Survey: "Flows formed when small masses of debris fell or slid from the surface of the landslide mass into the steep channel. Some of the masses were fluid enough to continue downstream without interruption; others stopped in the channel until remobilized by added meltwater or the passage of a mudflow from a higher altitude. Both processes resulted in discrete slugs which continued down the steep ravine, through an alluviated canyon, to a fan where most of the debris was deposited" (Morton and Campbell, 1973).

Woodside, San Mateo County, California

The process of debris-flow initiation was repeatly observed and recorded at Woodside in February of 1969 by Johnson and Hampton (Johnson and Rahn, 1970; Hampton, 1970). The source area is described

as a broken landslide mass composed principally of clay with some silt and sand with scant pebbles and cobbles. The initiation of debris-flows is described as:

> "The first indication of activity was usually the falling of small clods of soil from the vertical bank above a spring. Then larger masses of soil slightly shifted as units and cracks opened behind them. This action caused the spring to slow momentarily, presumably as the water flowed into the cracks and seeped into the soil along the freshly created surfaces of the cracks. This type of movement continued for a few minutes, punctuated now and then by tumbling of one of the loosened masses into the rivulet below. A trickle of spring water flowed over the loosened masses in the rivulet and became quite turbid as the water slightly eroded them. They remained stationary in the rivulet, however, until two or three masses, aggregating perhaps a third of a cubic foot, had fallen into the rivulet. Then the combined material began to shift slowly down the rivulet. It moved by segments so that now the front moved faster, and then the back moved up and overrode the front. During these movements, part of the trickling water was incorporated into the mass. In this manner, the water content of the mass increased and the mass became much like wet concrete in appearance. Meanwhile, the rate of the flow of the mass drastically increased from about one-half inch per second, when it first started moving as a rigid unit, to perhaps a foot per second, when it had the consistency of wet concrete. The transition from a slide or slump mass slowly moving in a channel to a debris-flow mass rapidly flowing in a channel took place over a horizontal distance of about three or four feet."

I visited the Woodside source area in the spring of 1971. No debris-flows were actively mobilizing at the time although they were easily started if the disarticulated landslide material was disturbed slightly with a stick. After jostling slightly a small mass of stiff clay-rich material, a volume totaling about ten liters would begin to slide about 2 to 3 cm a minute down a channel about 12 to 16 cm wide with a 35 degree slope. Water, oozing out of the landslide mass into

the debris channel, tended to pond behind the sliding debris and to seep into the outer edges of the mass. Rotation and flexure of the block as it overrode small irregularities in the channel opened small cracks allowing the further incorporation of water. After a few minutes the slide mass became thoroughly soaked and began to segregate into a soup-like matrix carrying small chunks of stiffer debris. At this time the debris began to flow about five to ten cm per second. The debris chunks sometimes broke up during the flow and were incorporated, or they simply rode in the flow about three meters to the base of the toe of the landslide where the flow stopped.

Thompson Creek, Sevier County, Utah

During the night of 20 July 1971 a desert rainstorm of high intensity inundated an area near Richfield, about 225 km south of Salt Lake City, Utah (Fig. 1, Table 1). Flood waters and debris flows poured out of several canyons, inflicting damage to farms and ranches located nearby. Aerial and field reconnaissance showed that Thompson Creek had produced a series of debris flows with little flood water, whereas other nearby canyons had yielded primarily flood waters. My investigation was concentrated on Thompson Creek because the conditions for debris-flow mobilization appear to be most favorable there.

Thompson Creek is about 16 km south of Richfield where it drains the northeastern flanks of the Sevier Plateau (Fig. 8). It heads at an elevation of about 3350 meters near Glenwood Mountain and terminates near the Sevier River at an elevation of about 1740 meters. The Thompson Creek debris flow overtopped the creek bed in some places

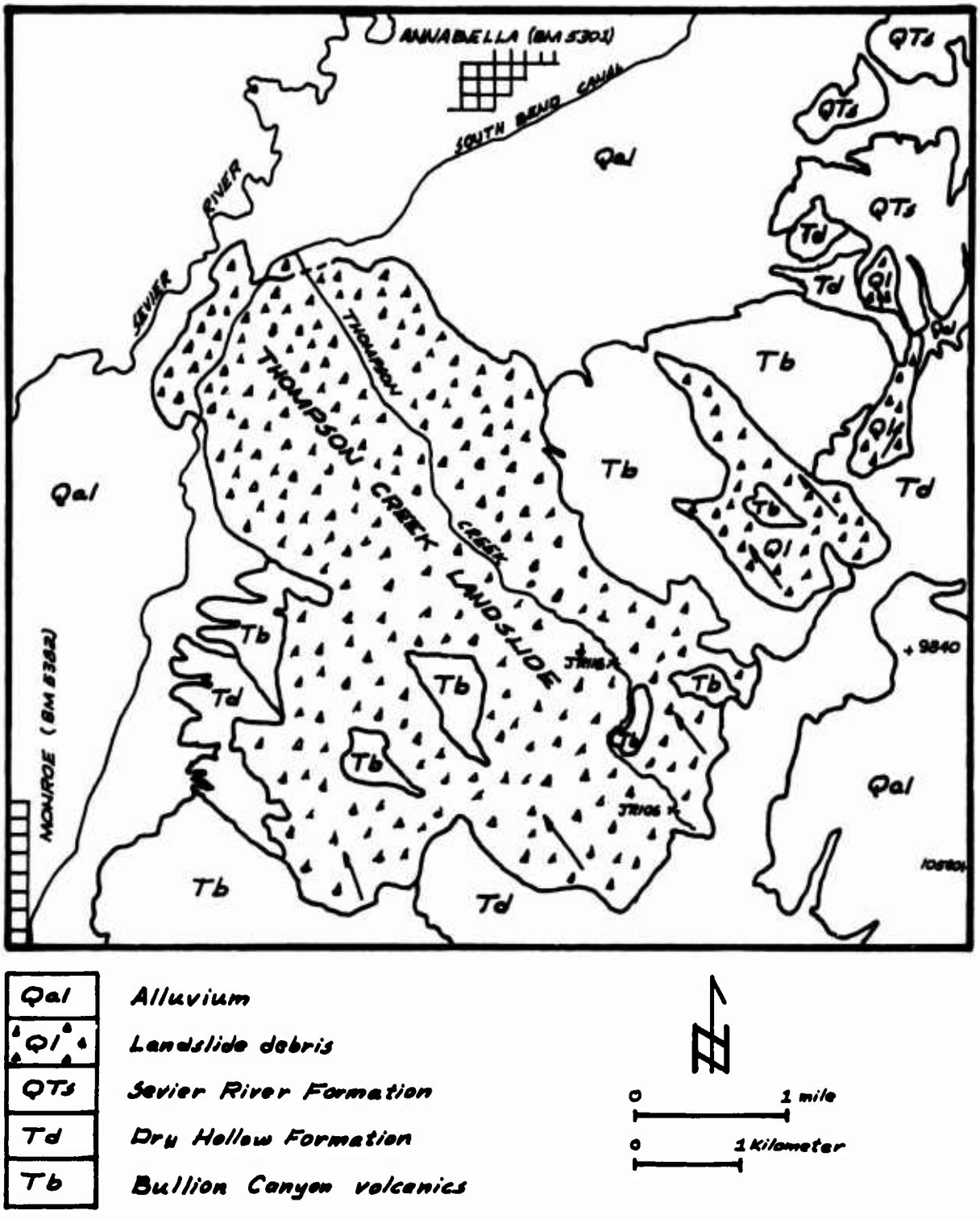

Figure 8. Thompson Creek, Sevier County, Utah, drainage system and Thompson Creek Landslide. Geology modified after Callaghan and Parker (1961). JR106 and JR116 mark the locations of debris-flow source areas shown on Figs. 12 and 13.

but it was largely channelized until it reached the South Bend Canal where it spread out, forming lobate deposits (Fig. 9a, 9b). One deposit contained boulders as large as two meters in diameter (Fig. 10). The debris flowed as far as 8 km, carrying about 3000 cubic meters of material. Thompson Creek drains an old landslide complex called the Thompson Creek Landslide, described as the largest and most spectacular in the Monroe Quadrangle (Callaghan and Parker, 1961). Steep cliffs, which are in places over 600 meters high, mark the head of the landslide complex (Fig. 11). The landslide debris is distributed over an area of about 30 square kilometers and is covered with vegetation except in steep areas near Thompson Creek.

The landslide material was derived from volcanic rocks exposed higher on Glenwood Mountain. The volcanic bedrock is also exposed under the landslide debris in places along the creek bed in the source area. The rocks are reddish to greenish-brown, extrusive latites and basaltic andesites of the Bullion Canyon and Dry Hollow Formations (Callaghan and Parker, 1961). The landslide debris is composed of soil, weathered volcanic debris, and clasts of sound volcanic rock. Landsliding has comminuted the rocks and destroyed most original structures (Fig. 11, Fig. 12).

The origin of the debris for the debris flows was determined by walking upstream from the deposits, following lateral ridges of debris and debris plastered along the creek walls, until fresh, bare earth scars were found. The scars were in areas of recent ground movement within the old landslide. At the bases of some of the scars are lobate snouts of debris that did not reach the channel. Some of the bare

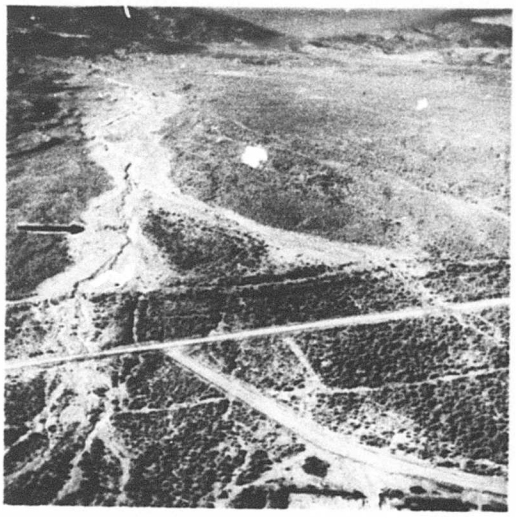

A

B

Figure 9. Debris-flow deposits along Thompson Creek, Sevier County, Utah.

A. Richfield, Utah, visible under the wingtip. Sevier River in the upper middle distance.

B. Distal end of bouldery debris-flow deposits. Arrow indicates bouldery snout shown in Fig. 13.

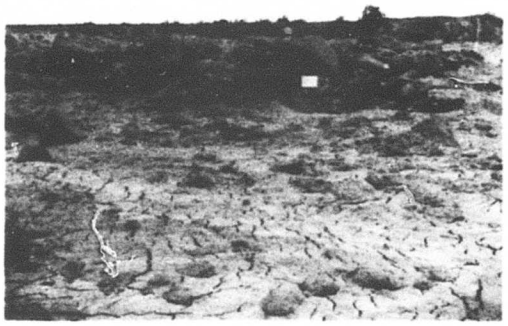

Figure 10. Debris-flow deposit with boulders two meters in diameter at Thompson Creek, Sevier County, Utah.

Figure 11. Head of the Thompson Creek Landslide, Sevier County, Utah. Arrow marks location of debris-flow source area shown in Fig. 12.

Figure 12. Debris-flow source area at Thompson Creek, Sevier County, Utah. Location shown in Fig. 11 and shown as JR106 in Fig. 8.

scars were initiation sites of debris flows during the rainstorm. Several of the initiation sites displayed a close association of small, freshly broken landslide blocks, bare earth scars, and the creek running below (Fig. 13).

One of the bare scars had small, active debris flows still mobilizing from its lower end near the creek. The scar was at the base of a thirty meter high, steeply sloping, bank of landslide debris. The debris had scattered, broken, volcanic clasts in a sandy-silt matrix. Its size distribution is shown in Fig. 14. The mobilization of the debris was occurring where a small spring bubbled out of the landslide debris. The water slowly oozed up and out of the debris, thoroughly wetting the surface. As the debris became soaked, a mass with a volume of about 30 liters slowly began to slump and slide downhill. The top of the sliding material moved downhill faster than the bottom so the debris dumped in front of the main mass was overrun and incorporated. This caterpillar-tractor-tread type of movement served to completely mix the debris with the included water until the material looked like a remolded mud with a consistancy similar to that of wet concrete. The flow moved a distance of about two meters until it reached a slope of a few degrees, where it stopped. The entire process from slumping to cessation of flow took place in about two minutes. The process of initiation apparently was self perpetuating because, as soon as several debris-flows had been mobilized, the undercut bank caved, producing a landslide of a few cubic meters that would fill up the bowl containing the spring and the process would begin again.

Figure 13. Debris-flow source area at Thompson Creek, Sevier County, Utah. Location shown as JR116 in Fig. 8.

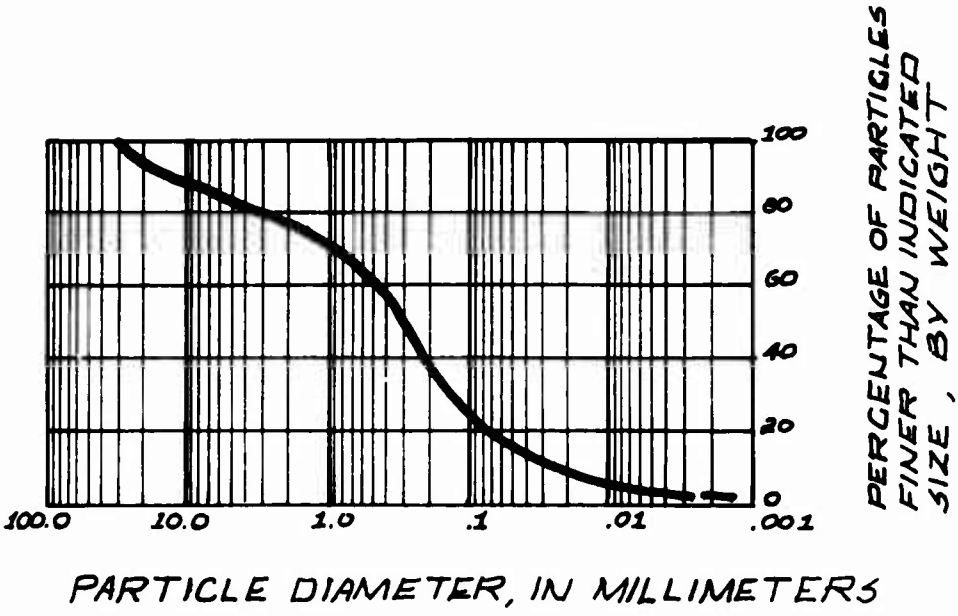

Figure 14. Size distribution of debris-flow source material collected from Thompson Creek, Sevier County, Utah.

Lead Canyon, Inyo County, California

Debris-flow deposits within and at the mouth of Lead Canyon indicate that the canyon has been the source of many debris flows, although the even distribution of shrubs suggests that no large flows have occurred for many years (Fig. 15a, 15b). Lead Canyon is cut into the east-facing slope of the Inyo Mountains, about 310 km north of Los Angeles, California (Fig. 1, Table 1).

An area was studied on unpatented mining claims about 5 km west of the mouth of Lead Canyon, in steep, rugged terrain with sparse vegation, typical in this area of an arid climate. The rocks are shales, siltstones, mudstones, sandstones, quartzite, marbles, and dolomitic carbonates of the Cambrian Mazourka Group that have been intruded locally by alaskite (Ross, 1967). Bedrock is prominately exposed between talus cones, alluvial fill, and soil (Fig. 15b). Debris-flow lateral ridges could be followed uphill to where they blended into slopes of alluvium and talus. The alluvium and talus slope up to the mouths of bedrock ravines or to the bases of high rocky cliffs. No arcuate scars or other evidence of a source for the debris in the quantity that would be required to build the lateral ridges below were found between the tops of the cliffs and the ridge crests. The debris-flow source material appeared to be a loose aggregate in steep bedrock gullies cutting through the cliffs and the debris in the upper ends of the talus and alluvial slopes. Apparently, rainwater is collected above the cliffs, funneled down the bedrock ravines, and dumped onto the talus and alluvial slopes. In order to investigate the mechanism of initiation an experimental site was chosen just below a

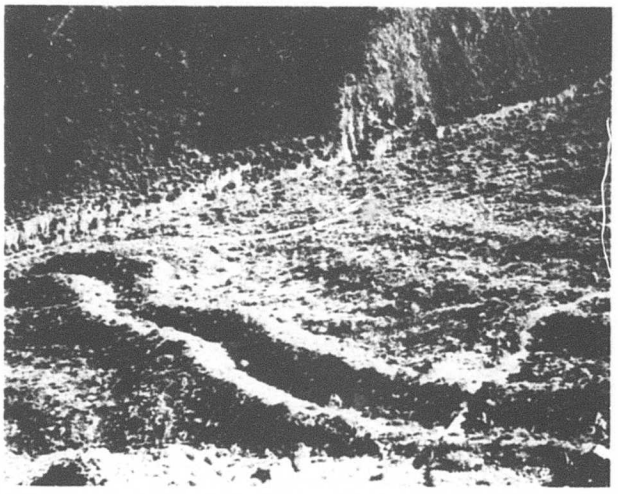

A

B

Figure 15. Debris-flow deposits and source area at Lead Canyon, Inyo County, California

A. Debris-flow lateral deposits leading from the source area.

B. Debris-flow source areas on north-facing slope. Arrow points to experimental site.

steep cliff face at the head of a small ravine (Fig. 15). The alluvium at the base of the cliff had recognizable snouts of old debris flows that contained blocks of material that could be traced headward toward the small ravine by following sinuous ridges that presumably represent traces of lateral ridges of debris flows. The ravine is about 10 to 15 meters wide at the top, 1 to 6 meters deep and has an average slope of 30 degrees. It is cut into weathered alaskite. Some sparse soil is developed at the head of the ravine where the slope approaches 40 degrees.

Water was concentrated in one area by pouring water from a ten liter container onto the slope. As the experiment began, the ground was soft and porous, sucking up water like a sponge. But, as the volume of water was increased, the ground became saturated and a mixture of water and soil began to run out of the hole where the water was impacting (Fig. 16a). The mixture flowed downhill, becoming more and more charged with fine to pebble-sized debris. It continued to pick up debris in its race downhill and eroded small channels (Fig. 16b, 16c). As the water continued to pour onto the slope the impact hole was eroded larger by the stream of water from the container (Fig. 16c). The mixture of water and soil eroded channels about 2 to 3 meters long and 2 to 3 cm deep. About three meters from the impact hole the mixture changed abruptly into a non-erosive, smooth-surfaced flow of debris (Fig. 16d). About 10 meters from the impact hole the debris began to form small lateral ridges along the sides of the debris stream. The flow moved downhill several tens of meters, gradually thinning until it stopped.

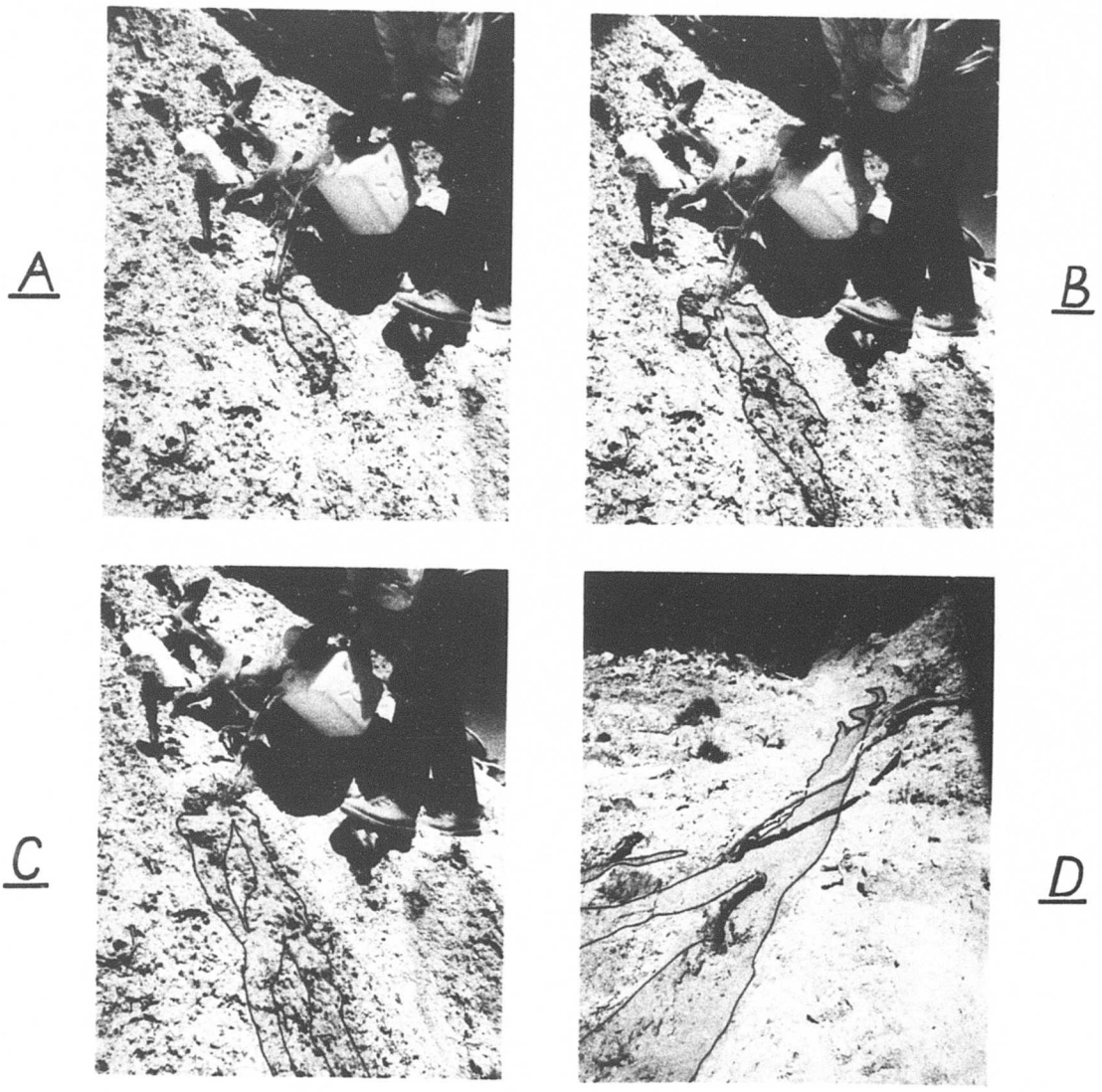

Figure 16. Initiation of a debris flow at Lead Canyon, Inyo County, California. Impacting water mobilized the debris.

A. Erosion at the impact hole initiating the turbulent debris wave which is eroding a channel.

B. Incorporation of debris during channel erosion.

C. Rapid initiation and removal of debris from the impact site is shown along with channel erosion.

D. Path of debris flow, showing lateral and terminal deposits. The impact site is about 2 to 3 meters to the left of edge of photograph.

The flow seemed to have four phases. The first was a tumbling flow of fluid debris that picked up dry materials and eroded a channel. The second was a smooth flow of debris that moved across the ravine bottom without eroding or depositing material. The third was a smooth debris flow which moved at about half the rate of that of the tumbling phase and which did not erode the channel, but rather deposited lateral ridges. The fourth was the cessation of flow recorded in lobate, debris-flow snouts.

An additional observation of the ability of debris flows to increase their proportion of granular material appears relevant. Jahns described a debris flow resulting from thundershowers in the Black Range of southwestern New Mexico (1949, p. 11). He notes that:

> "The waters ... formed a debris-laden front that traveled down the valley at a rate of about five miles per hour...., they coursed down a canyon whose bottom was marked by sun-cracked and hoof-printed mud, only partially dry. The front of the wave was distinctly higher and steeper on one side of the channel than on the other, apparently because the water there was more heavily freighted with stones, fragments of vegetation, and other detritus. As more and more solid matter was picked up from the bottom and from caving banks of the wash, the forward progress of the water in contact with the bottom was slowed distinctly. Relatively clear water, traveling faster at positions higher in the wave, constantly flowed over the debris-rich portion as a sort of waterfall, only to be in turn slowed by additional debris picked up from the dry stream bed. In this way an essential vertical wall of water was maintained to a height of about eight inches."

Other Active Debris-flow Source Areas

A debris flow occurred in the cirque headwall of Mayflower Gulch on the west side of Tenmile Range, Colorado, on 18 August 1961. The flow was observed by Curry (1966, p. 772) who reported the initiation as follows:

> "Direct observations of the mudflows were hampered by very intense rain and by the fact that the author was about 900 m (3000 feet) from the cirque headwall, at the rain guage, at the time the flows began. At about 4 p.m. on August 18 a loud roar became clearly audible above the thunder. A series of what appeared to be rockfall avalanches were noted in four different localities around the cirque headwall. These appeared confined to areas previously covered with talus cones and, even though the talus had been soaked by 48 hours of intense rain, large rock-dust or water-vapor clouds accompanied the disturbances."

In a discussion of Eliot Blackwelder's paper on mudflows Singewald describes a series of debris flows witnessed in the spring of 1924 in the Andes of central Peru (Blackwelder, 1928, p. 482). The flows occured during a period when thundershowers were raging on the high mountain slopes and are described thus:

> "The rain had saturated the soil and disintegrated black shale on a steep bench high up on the mountain until it became soft and plastic enough to flow down into the narrower and steeper ravine, which led into the Rupac River."

An informative account of debris-flow initiation in Kenogami, in the Province of Quebec, is given by Terzaghi (1950, p. 112-114). The flows occurred in the summer of 1924 at the head of a gully 23 meters deep.

". . . the walls of the canyon started to collapse. Slide after slice broke down, leaving vertical cliffs, probably representing the rear walls of tension cracks. . . . The collapse of the slices was probably preceded by settlement which in turn produced the steep fissures. If this assumption is correct the peculiar character of the slides was due to . . . creep in weak stratum below the level of the foot of the cliff . . . . The collapsing slices crumbled, and the fragments formed a mud flow which descended on the bottom of the canyon with a velocity of 8 to 10 miles per hour into the valley of the Au Sable River and further on to the Saguenay River."

Terzaghi's description is further enriched by the report of a person who was physically incorporated into a debris flow.

". . . after reaching the bottom I was thrown about in such a manner that at one time I found myself facing upstream toward what had been the top of the gully. . . The appearance of the stream was that of a huge, rapidly tumbling, and moving mass of moist clayey earth. . . . At no time was it smooth looking, evenly flowing or very liquid. Although I rode in and on the mass for some time my clothes afterwards did not show any serious signs of moisture or mudstains. . . . as I was carried further down the gully away from the immediate effect of the rapid succession of collapsing slices near its head. . . it became possible to make short scrambling dashes across its surface toward solid ground at the side without sinking much over the ankles."

Many debris flows occurred in Nelson County, Virginia, during an intense rainstorm precipitated by hurricane Camille in 1969 (Williams and Guy, 1973). An eyewitness reported: "the ground started oozing slowly downhill for a fraction of a second, and then the entire section of the hillside suddenly slid quickly down the slope accompanied by a loud noise." In addition, a witness to debris-flow initiation in West Virginia in 1949 testified: "the whole strip of hillside started moving at about the same instant." (Williams and Guy, 1973, p. 15).

Intense rains on June 26, 1960 were immediately followed by a series of sheet slides and debris flows at Ulvådal, western Norway (Rapp, 1963).

An observer to the phenomena stated (Rapp, 1963, p. 198, 200):

> "Suddenly we observed a new slide. A mass of earth, boulders, trees and water moves down the slope and a new slide track is formed . . . The river is filled with a porridge or earth which flows downstream, mixed with a crowd of naked birch stems, twisting and whirling . . . New slides are coming down. It looks like a wave of water that squeezes earth and trees out of the ground and back again. The trees fall down immediately (note by Rapp: they are tilted backwards. . .). Then they are pushed together with the earth and boulders on the way downslope, so they reach the river naked, without twigs and bark. Water sprays out in small cascades from the moving earth."

Conway was witness to some 150 debris-flow initiations in one day as they were occurring from a vast mountain slope about 10,000 feet in height (Conway, 1907, p. 501-502). The debris flows occurred in the Hispar Valley in what I believe to be the southern Himalaya Mountains. Melting snow in early July was the reported trigger for the initiation of the debris flows which were said to have:

> ". . . started at the top as a very little falls, and then by mixing of the water and the snow with the debris that they picked up on the way, and the rocks and rubbish that fell into them, formed a little dam in the gully, and behind that dam the stuff collected till it burst the dam. Then the thing fell further, and clogged and formed a dam lower down, so that there was a continual formation of dams and bursting through of them, and each time the stuff collected it was larger in amount in proportion as it was formed lower down. I saw one of these dams formed and burst quite low down, and the amount of stuff that was held back, and then the enormous discharge that came when the dam burst, enabled me to judge of what was possible in that way. The sides of the gullies in this case were constantly falling in, not falling out, and pieces of rocks, 6-feet cubes and larger, were carried down as though they were corks in this stuff. They rolled over and over, and fell at last into the bottom of the river below."

An intense rainstorm on 13 February 1970 was nearly immediately

followed by the mobilization of many debris flows in the Mgeta area, Western Uluguru Mountains, Tanzania (Temple and Rapp, 1972). Numerous local people witnessed the events and their testimonies are summarized as follows (Temple and Rapp, 1972, p. 187):

"1. All the slides were associated with a very rapid movement of material or a very sudden slope failure.

2. The moment of slide occurrence was accompanied by a considerable noise like thunder.

3. The air smelt as if quarry blasting had occurred for some time after slides moved (the local people are familiar with explosives as Mgeta is one of the most important collecting-centres for mica from tiny mines scattered all over the Mgeta area).

4. Individual slides and displacements were accompanied by a cloud of discoloured, usually brown coloured gas or dust.

5. When the slides occurred it was raining with extreme intensity.

6. Almost all the movements and slope failures occurred within a very limited period of time (1 hour)."

SUMMARY OF OBSERVATIONS OF THE INITIATION OF DEBRIS FLOWS

All of the observations of debris flows initiating have a unifying trait; every debris flow mobilized by mass movement of in-situ material. Where the debris was mobilized slowly enough for observation, as at Heath Canyon, Woodside, Thompson Creek, Kenogami, Nelson County, and Ulvådal, the movement began by the process of landsliding, which led to mobilization of the debris. With one exception, the other flows mobilized so fast that slopes appear instantaneously to turn into flowing masses of debris. The presence of discrete failure surfaces is the strongest evidence that incipient landsliding has occurred in these cases. The debris flow produced experimentally at Lead Canyon appears to be an exception because of the absence of surfaces of failure. However, the impacting water did erode in-situ debris evenly, without preferentially selecting certain sizes of material, and a fluid debris flow developed below the impact site.

Two ways of forming a debris flow come to mind: start with dry debris and add water or, start with water and add dry debris. Both ways conceivably would result in debris flows of similar composition. However, the observations recorded here suggest that most debris flows originate by the application of water to a mass of in-situ debris. Then, once the debris flow has been initiated, increases in contents of either debris or water are accomplished under the proper conditions.

SELECTED SOURCE AREAS THAT HAVE RECENTLY PRODUCED DEBRIS FLOWS

During the period 1970 to 1973 I visited source areas that had recently produced debris flows, primarily in California. The source areas were quite different, ranging from a dump of a marble quarry, through burned off slopes in metamorphic rocks, to natural slopes in soft claystones and sandstones, and observations in some of them provide further insights into processes of mobilization of debris flows.

Roofing Granule Quarry, San Bernardino County, California

In August of 1971 a thundershower precipitated a debris flow from an abandoned waste dump of a quarry for marble used as roofing granules (Fig. 17) 2 1/2 km north of the town of Wrightwood, about 65 km northeast of Los Angeles, California (Fig. 1, Table 1).* The marble is surrounded by Mesozoic tonalite and diorite (San Bernardino Sheet, Geol. Map of Calif., 1969). The waste dump slopes at an angle of about 35 degrees and has a height of 170 meters. The base of the dump is at an elevation of 1800 meters. The upper two thirds of the dump contains marble blocks up to ten cm in diameter in a matrix consisting of weathered carbonate detritus and soil. The lower third of the dump contains larger clasts of marble, with blocks up to 1/2 meter in diameter not uncommon. The dump has virtually no vegetative cover and the adjacent natural slopes are sparsely vegetated, a situation indicative of the semi-arid to arid climate (Fig. 18).

---

*I wish to thank Professor Perry Ehlig, California State University at Los Angeles, for showing the waste dump and debris-flow deposits predating those of August, 1971.

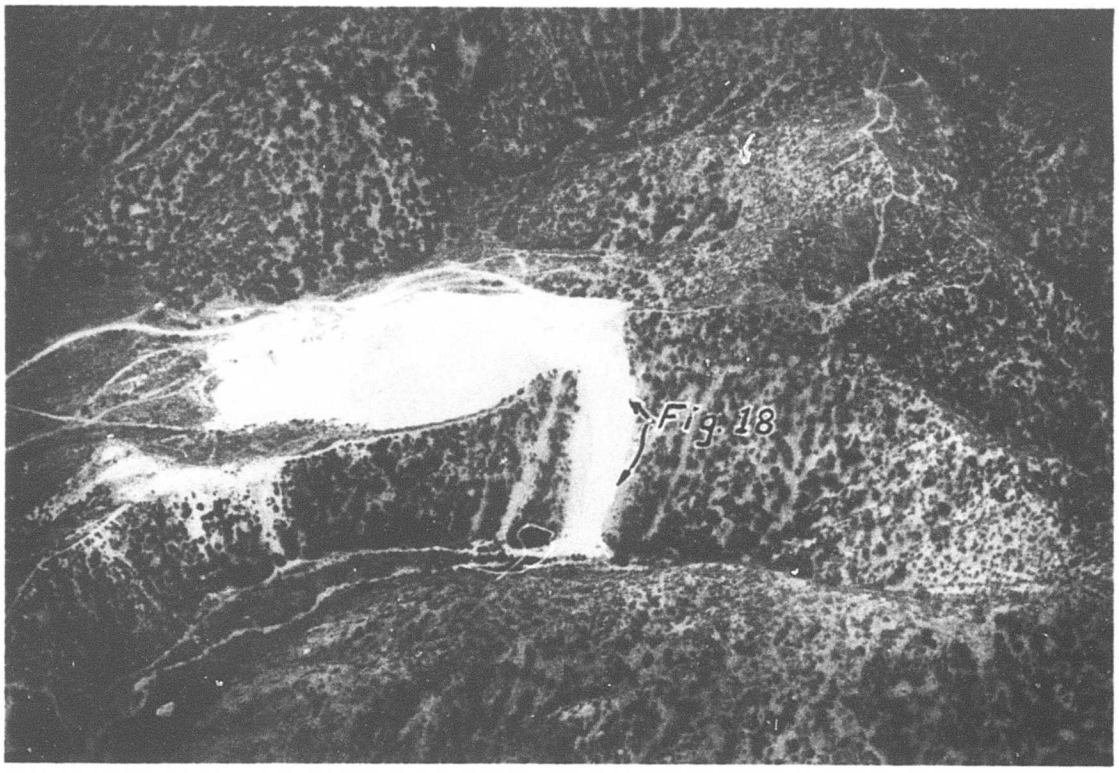

Figure 17. Roofing Granule Quarry, San Bernardino County, California. Debris-flow source area is the light-toned area extending down into the canyon.

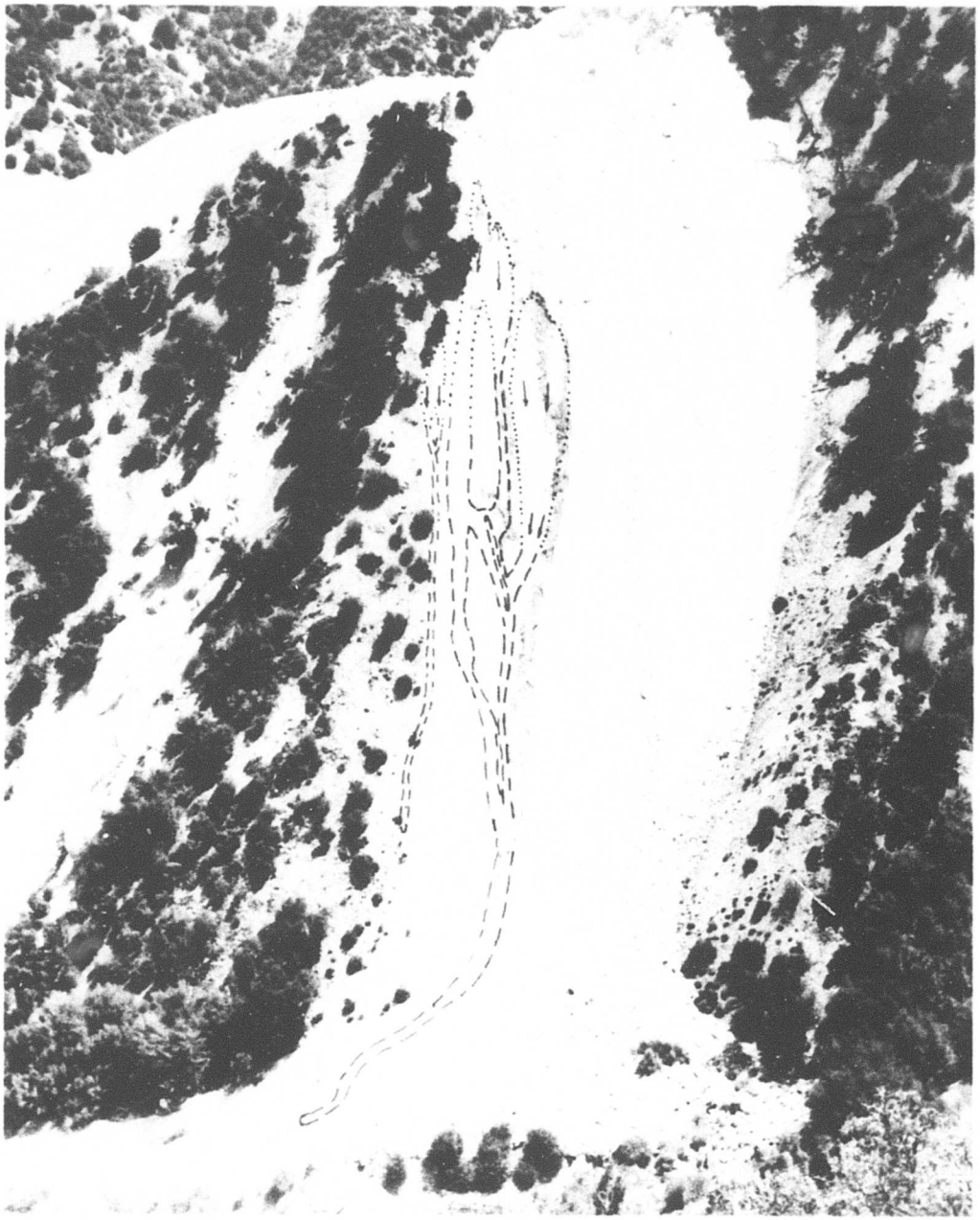

Figure 18. Debris-flow source area at the Roofing Granule Quarry, San Bernardino County, California. Debris-flow scars, flow paths, and deposits of August 1971 are outlined in black. The arrows indicate areas of rills which were the sites of initiation via landsliding.

The debris flow of August 1971 started near the top of the quarry dump, at a slope angle of 35 degrees, and stopped near the canyon floor, at a slope angle of about ten degrees. The flow path (Fig. 18) is about 240 meters long. The debris flow carried only a few cubic meters of material. The rainstorm apparently stopped just after the debris flow mobilized, leaving the medial and lateral deposits, source area, and attendant features in an excellent state of preservation. The debris appeared to mobilize from small rills one to twelve cm in width, which at first glance seemed to be a style of initiation different from that reported earlied, until detailed examination proved otherwise.

The source area was recognized by following the lateral ridges of debris sourceward. Farther uphill the debris had moved across several meters of the slope with a width of one to three meters without forming levees or channels -- a situation comparible to sheetflow. Above this area were small, rill-like channels, at the tops of which were arcuate scars surrounding spoon-shaped depressions (Fig. 19). The small channels ranged in width from one to twelve cm with depths up to six cm. The smaller channels were cut into larger older channels. Inside the small channels (e.g., Fig. 19) were spoon-shaped bowls, one to three cm deep and up to eight cm wide. In places small pebble-sized rocks were lying loose inside the spoon-shaped bowls, otherwise, the channels were clean and smooth. The small spoon-shaped bowls are interpreted as miniature landslide scars within the larger channel. Thus the channels probably represent sites of landslide activity that propagated uphill as the debris was mobilized.

Because of the distinctive character of the carbonate dump debris, compared to the natural slope debris, the older debris-flow deposits

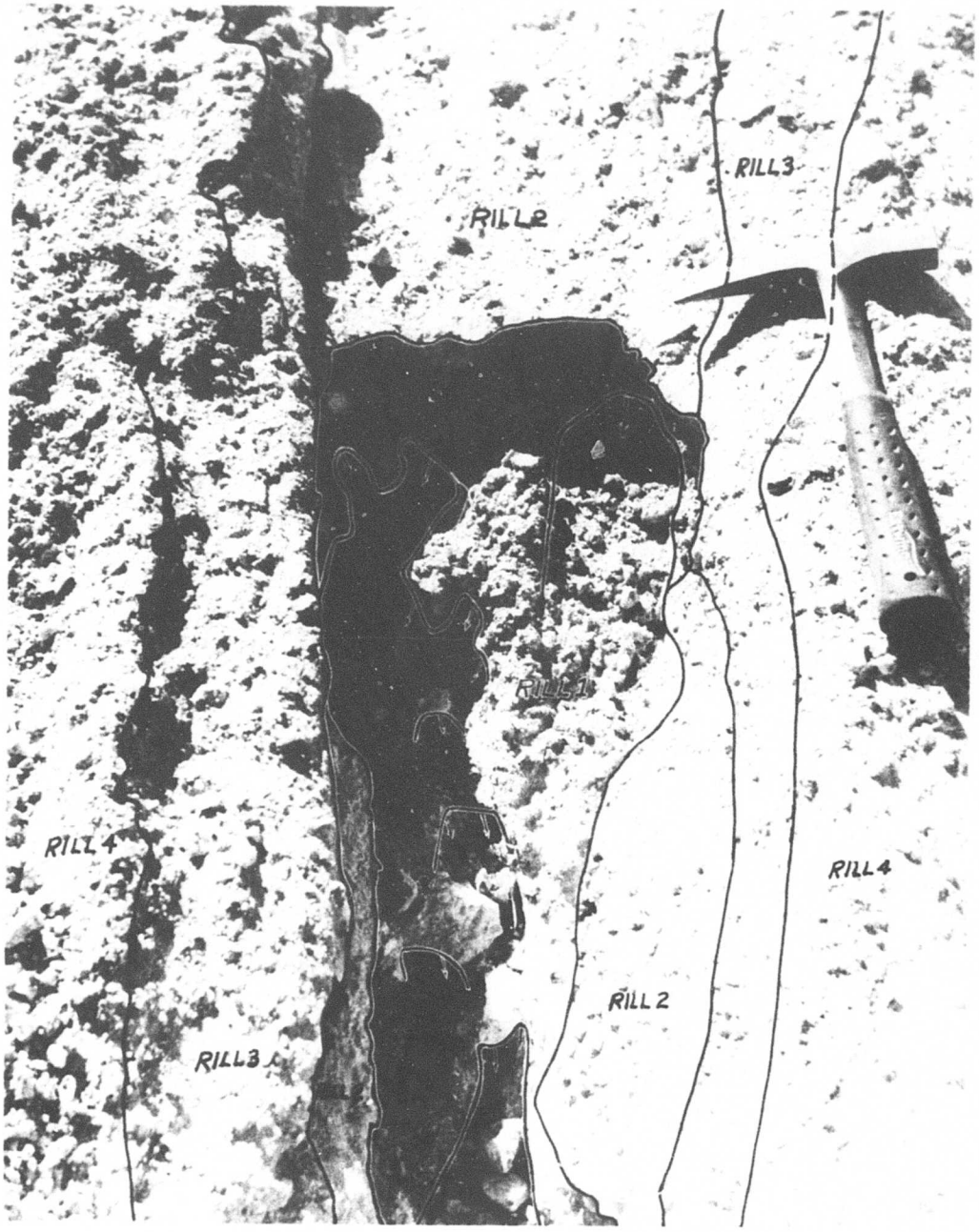

Figure 19. Debris-flow source rill at the Roofing Granule Quarry, San Bernardino County, California. A series of older rills is labelled R1 to R4. Small landslide scars are outlined inside the prominent rill.

from the dump were easily recognized on the canyon floor and at the mouth of the canyon. One flow, which stopped about one km from the dump at the mouth of the canyon, was studied to test the hypothesis based on indirect field observations that the debris mobilized en masse. Comparison of size distribution data for source and deposit materials (Fig. 20) indicates little, if any, sorting has occurred, providing further indirect evidence that the debris from the waste dump mobilized en masse and flowed to the point of deposition with little, if any, sorting of the particles during transport.

Arroyo Hondo, Fresno County, California

Debris flows originated in Arroyo Hondo during the summer of 1971. The source area is about 40 km north of the town of Coalinga and about 220 km southeast of San Francisco, California (Fig. 1, Table 1). Most of the source area lies within the boundaries of the Lillis-Christie Ranch and is about 8 km west of Interstate Highway 5.* The topography is gently rolling with moderately steep ground sloping into dry arroyos (Fig. 21). Arroyo Hondo generally cuts across the strike of the bedrock whereas the lesser drainages tend to follow weak layers. The drainages carry water only during periods of high precipitation. Semi-arid climatic conditions, with 20 to 37 cm of annual rainfall and high summer temperatures, severely restrict the vegetation (Bull, 1964).

The source area is involved in extensive landsliding and soil creep (Fig. 22). The landslides range in scale from one meter thick soil-slides to large block slides 100 meters wide and 50 meters thick.

---

*The courtesies extended by Mr. Wm. Crossland and Mr. Jay Jones during the fieldwork are gratefully acknowledged.

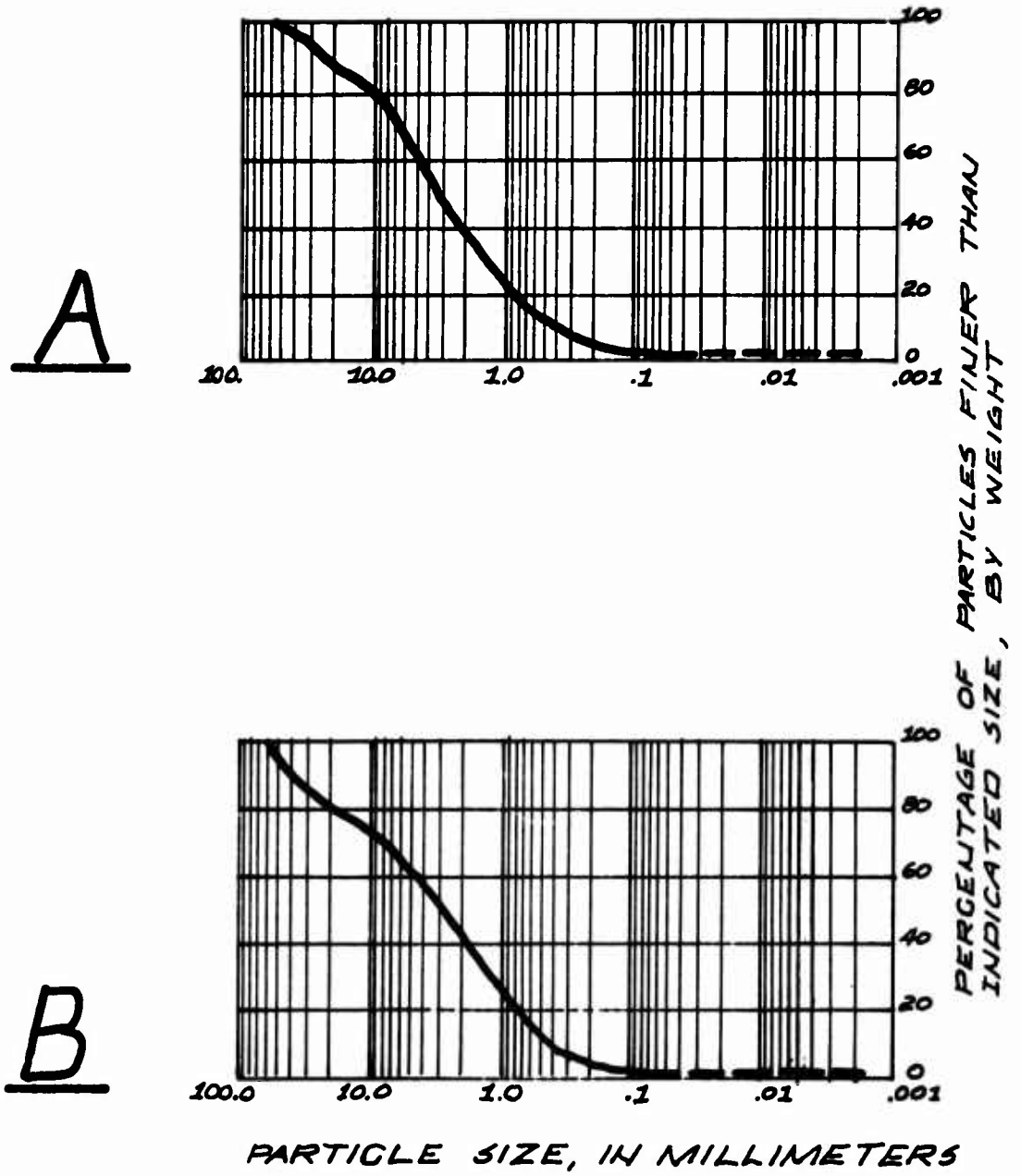

Figure 20. Roofing Granule Quarry, San Bernardino County, California. Size distribution curves.

A. Debris-flow source material.

B. Debris-flow deposit.

Figure 21. A source area at Arroyo Hondo, Fresno County, California. The material for the debris flows came from about the middle of the slope.

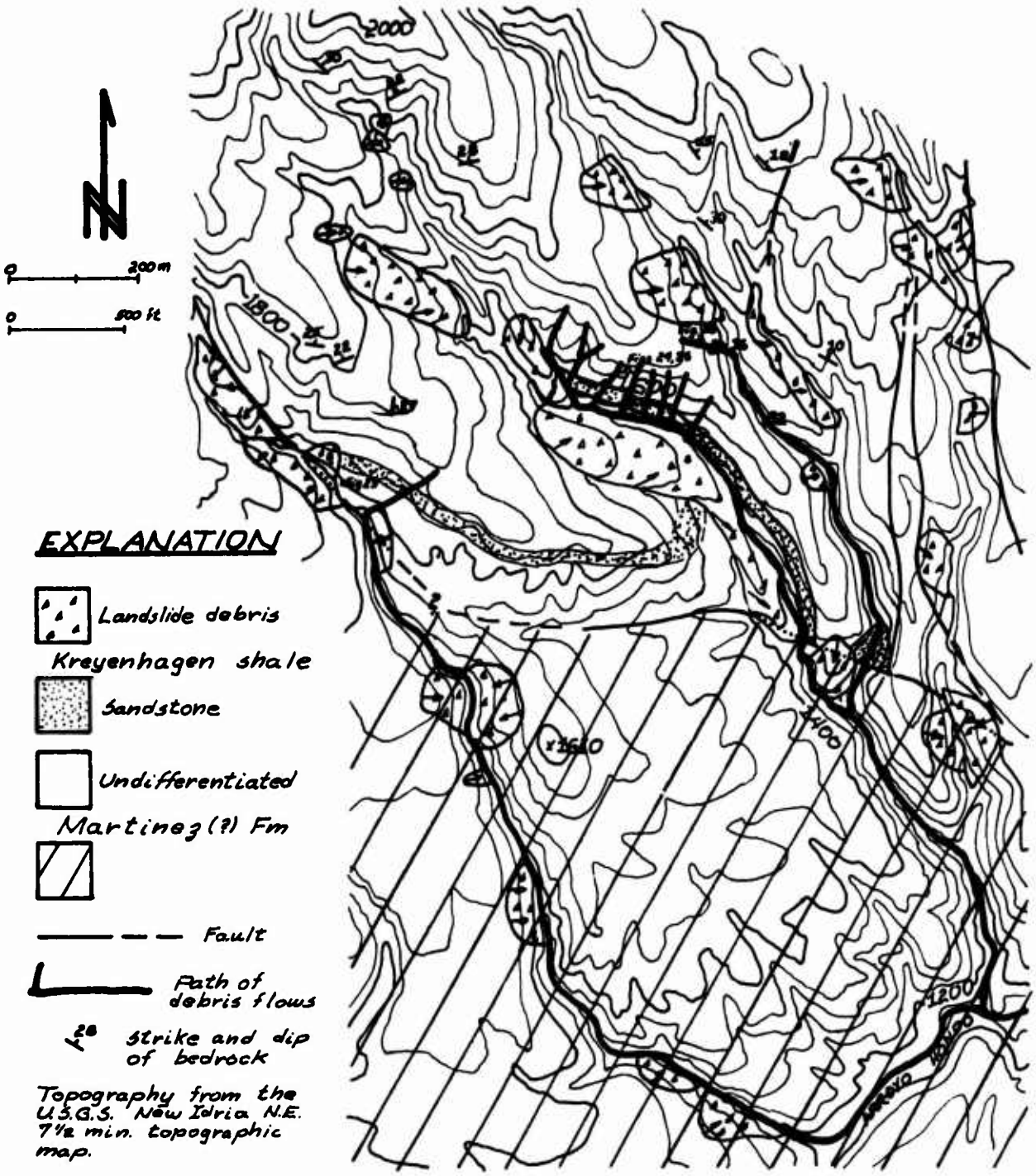

Figure 22. Geologic map of the source area of the debris flows of 1971 in Arroyo Hondo, Fresno County, California.

Soil creep is active along the sides of the arroyo where, in some places, wide cracks and wobbly blocks of soil make walking hazardous.

During 1971 debris flowed about 9 km from the source area to the mouth of Arroyo Hondo and carried about 120 cubic meters of material. The debris was deposited in the channel of Arroyo Hondo on a slope of less than one degree and was about four to eight cm thick. The debris deposit was clay-rich with clasts of low density claystone up to six cm in diameter.

The debris flow was quite fluid during flow, as indicated by the small sizes of particles, by the thinness of the deposits, by the low slopes and by the slop marks at bends in the channels. Thus, a method of incorporating large amounts of water was operating during either the initiation or the flow. Examination of the flow channels indicates no falls or other steep gradients that would allow strong mixing of debris during transport. The absence of granular debris larger than a few cm in diameter and inspection of the channel deposits suggest that damming of the channel and mixing, as described by Conway, probably did not occur. Thus much of the water probably was incorporated in-situ by clay-rich debris during initiation.

The bedrock in the source area is the Kreyenhagen Shale of Eocene age (Anderson and Pack, 1915). The formation at Arroyo Hondo is interbedded silty claystone and friable sandstone. The sandstone is fine to coarse-grained and light tan. The claystone has blocky fracturing and is light gray-brown. At places the claystone has a pronounced shale-like parting. The claystone weathers to a depth of several feet and upon drying the weathered claystone develops "popcorn-like" appearance

of the surface and wide shrinkage cracks -- conditions suggestive of a high content of montmorillonite clay (Fig. 23). Indeed, X-ray diffraction studies indicate that montmorillonite is the dominant clay mineral (John Baltierra, Pers. Comm.).

The Kreyenhagen Shale is folded in the north of the study area (Fig. 22). In the southern part of the area it strikes northwest and dips northeast. It is crossed by faults north, south, and west of the area. One fault displaces a montmorillonite-clay horizon and establishes the southerly limit of sources for the 1971 debris flows.

A map (Fig. 22) of the debris-flow source area indicates that the majority of the 1971 flows mobilized from a single stratigraphic horizon, about 35 meters thick, of montmorillonite-rich claystone within the Kreyenhagen Shale. The upper part of this horizon is coarser grained, grading into a fine-grained sandstone over a thickness of about 70 meters. The rock unit under the montmorillonitic claystone is fine to medium-grained, tan sandstone (Fig. 24).

A small pit, about 1/2 meter wide, one meter long, and one meter deep was dug into the claystone horizon a few meters above the sandstone layer (Fig. 25). There were about 10 to 15 cm of clay-rich soil over a similar thickness of weathered claystone. Many small rills were eroded into the soil. The surface of the soil was covered with a thin crust about one cm thick that was intensely cracked. Under the crust the soil was dry and finely powdered. A handfull of the surface material would sift quickly through the fingers and the thin crust was easily powdered by rubbing between the hands. Water poured on the ground surface was immediately soaked up.

Figure 23. Popcorn-like appearance of clay-rich soil at Arroyo Hondo, Fresno County, California.

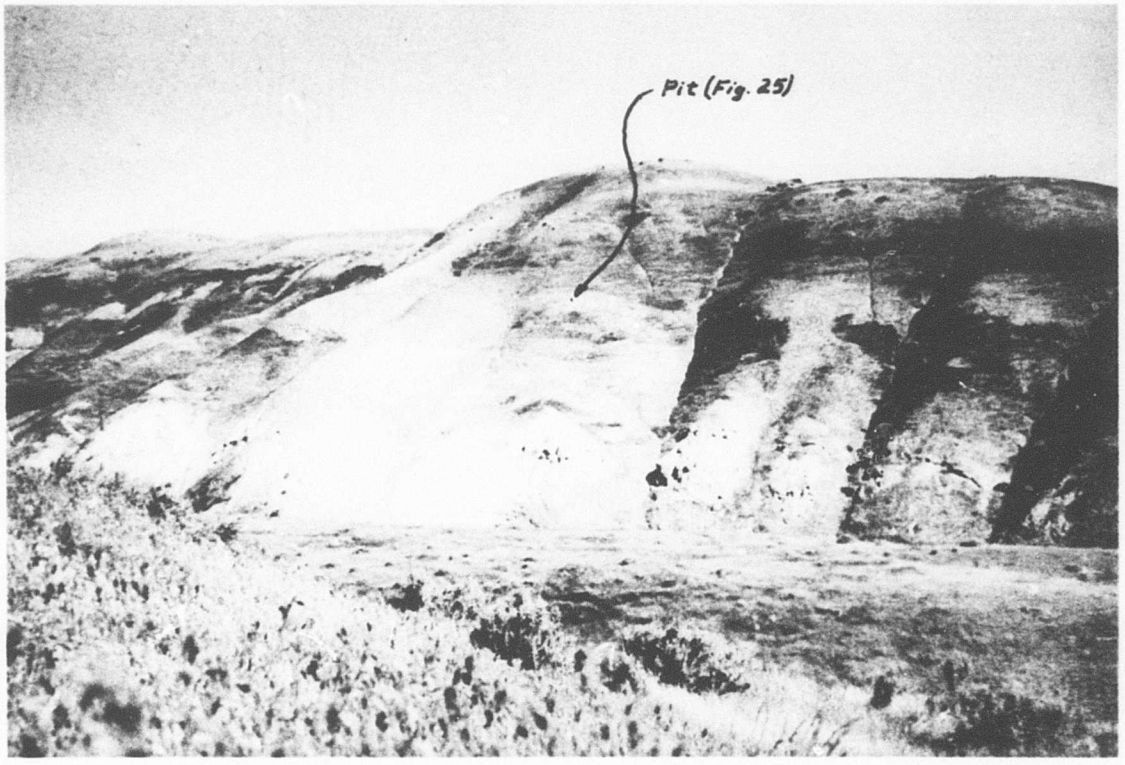

Figure 24. Debris-flow producing horizon above lighter-toned, sandy horizon at Arroyo Hondo, Fresno County, California.

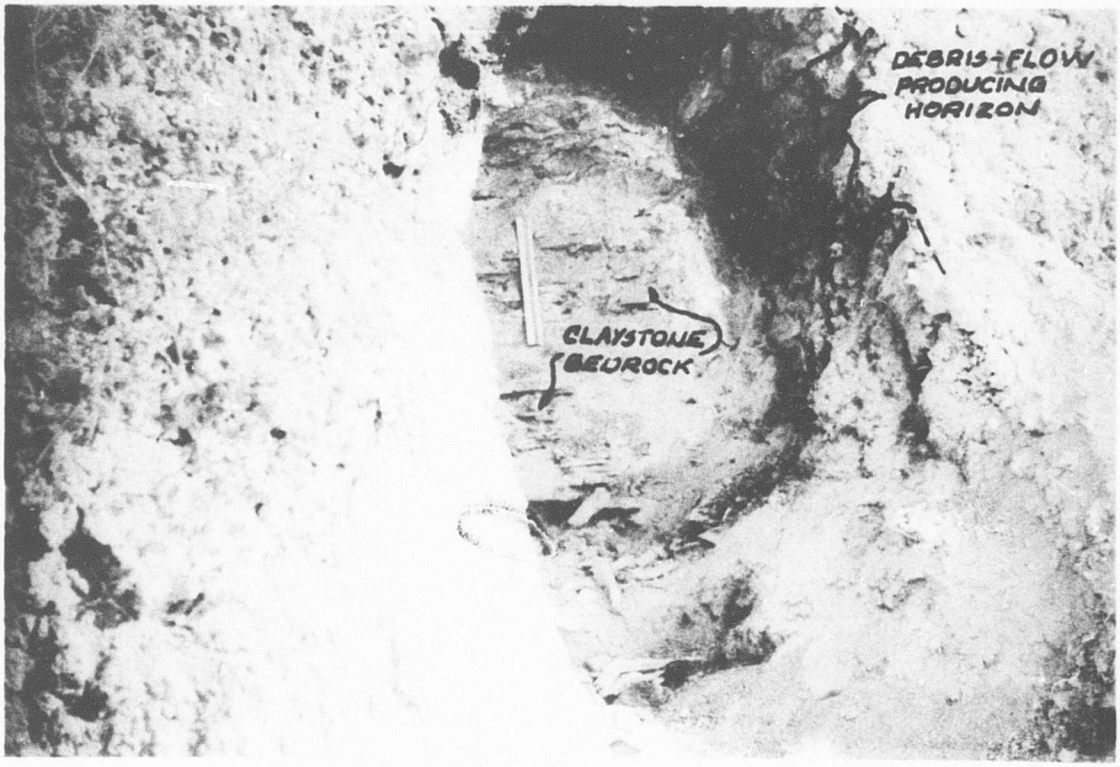

Figure 25. Pit exposure of the debris-flow producing horizon, showing clay-rich soil over claystone bedrock, at Arroyo Hondo, Fresno County, California.

The debris mobilized within small rills up to 8 cm wide and 3 to 4 cm deep in the clay-rich soil. They mobilized from small landslides up to one meter wide and 250 cm deep where the soil contained some sand and claystone chips. The rills were on relatively smooth slopes between small swales and the landslides generally occupied axes of swales. At one location a sheet of weathered claystone and clay-rich soil, averaging 6 to 8 cm in thickness, mobilized from the face of a large landslide block (Fig. 26). One landslide, about 40 cm thick, 12 meters long and 4 to 5 meters wide partly mobilized leaving scattered blocks of disturbed but intact soil (Fig. 27).

Although the rills were slightly washed, subdued arcuate head scars with spoon-shaped, semi-enclosed basins similar to those at the roofing granule quarry were plainly visible. The rills are interpreted to have been caused by the process of small-scale landsliding and mobilization of debris flows en mass during high intensity rains. Where the source material is more sandy the landslides are larger and the width to length ratio increases until the channel-like appearance is lost. However, both the rills and the landslides apparently were formed by the same initiation process, differing only in scale.

Big Sur, Monterey County, California

On the first of August 1972 a wildfire started north of the village of Big Sur, about 175 km south of San Francisco, California, near Big Sur State Park (Fig. 1, Table 1). The fire was contained on 6 August 1972 after burning an estimated 175 square kilometers of chapparal, grass, and timber. Most of the drainages of Pfeneger, Juan Higuera,

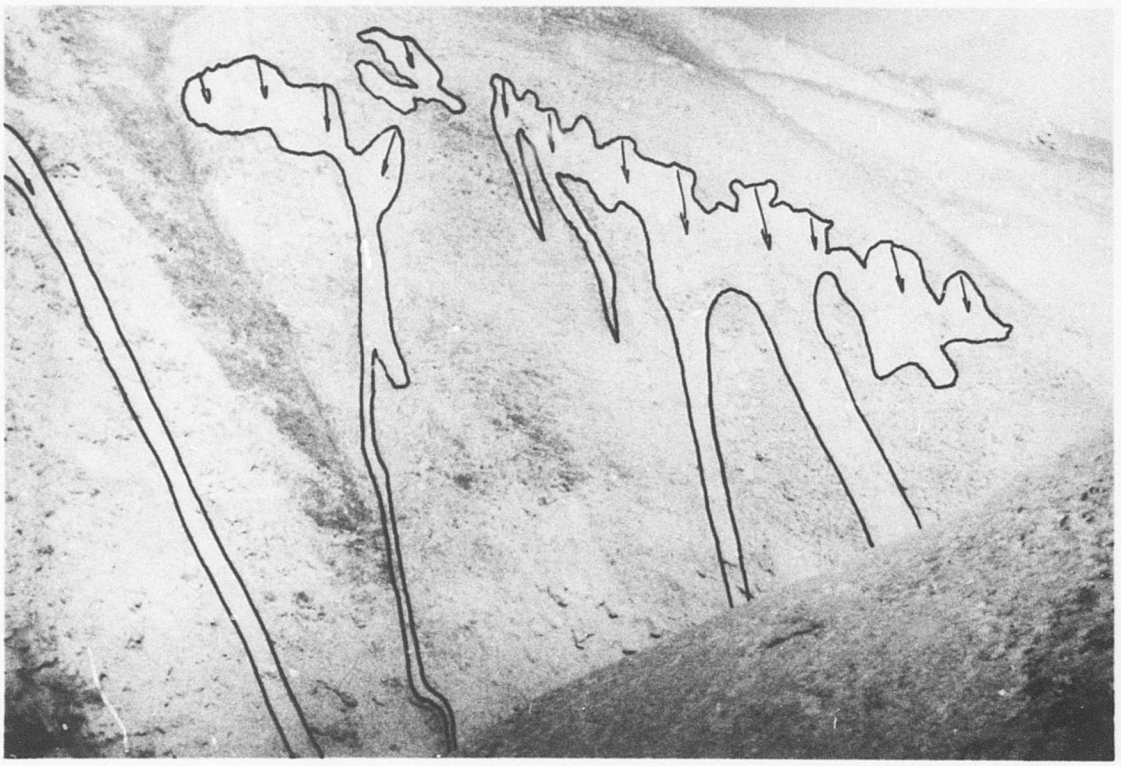

Figure 26. Mobilization sites of a series of debris flows from a single horizon at Arroyo Hondo, Fresno County, California.

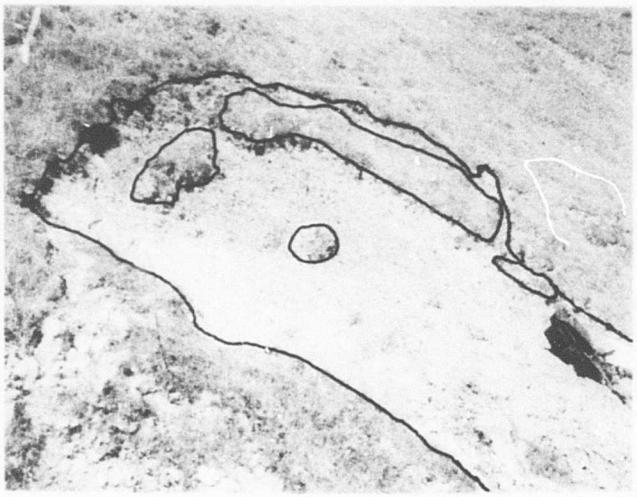

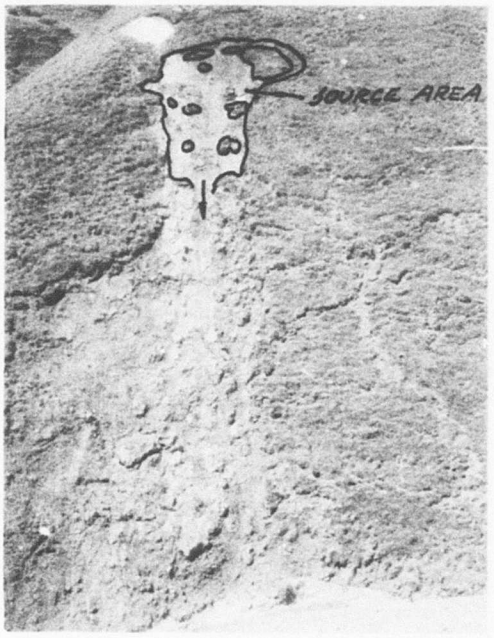

A

B

Figure 27. Mobilization site of a debris flow initiated by landsliding at Arroyo Hondo, Fresno County, California.

A. Initiation site of debris flow with flat bottomed scar and remnants of blocks of material.

B. Debris-flow source area and channel.

and Pfeiffer-Redwood Creeks, up to the top of Cabezo Prieto Ridge, were included in the holocast (Fig. 28). Even before the ashes cooled the U. S. Forest Service had begun planning emergency measures for the additional water and debris runoff expected when the winter rainy season set in (Erwin, et al., 1972). In mid-October, and again, in mid-November, intense, short-duration rainfall, following a longer period of steady rainfall, was almost immediately followed by debris flows that left a path of destruction on inhabited alluvial fans at the mouths of Pfeneger Creek, Juan Higuera Creek, and Pfeiffer-Redwood Creek (Cleveland, 1973).

The debris flows of 12 October and 15 November 1972 appeared to mobilize only from drainages affected by the fire of August 1972. No fresh debris-flow deposits were noted in the nearby drainage basins. Debris flows from Pfeiffer-Redwood Creek carried fine-grained debris, whereas debris flows from Pfeneger Creek carried coarse-grained debris with blocks up to 2 2/3 meters in diameter (Cleveland, 1973). Juan Higuera Creek drains an area substantially larger than either Pfeneger Creek or Pfeiffer-Redwood Creek and lies between the two creeks, yet it produced the lowest amount of debris (Cleveland, 1973).

Source areas of the Big Sur debris flows are quite steep and rugged. Over a horizontal distance of about three km the Cabezo Prieto Ridge rises about one km above the village of Big Sur, at the mouth of Pfeneger Creek. Average precipitation along the Big Sur River is 100 to 125 cm annually. The debris-flow source area probably receives more rainfall because of its height and placement in the paths of storm fronts. The vegetation where unburnt in the source area,

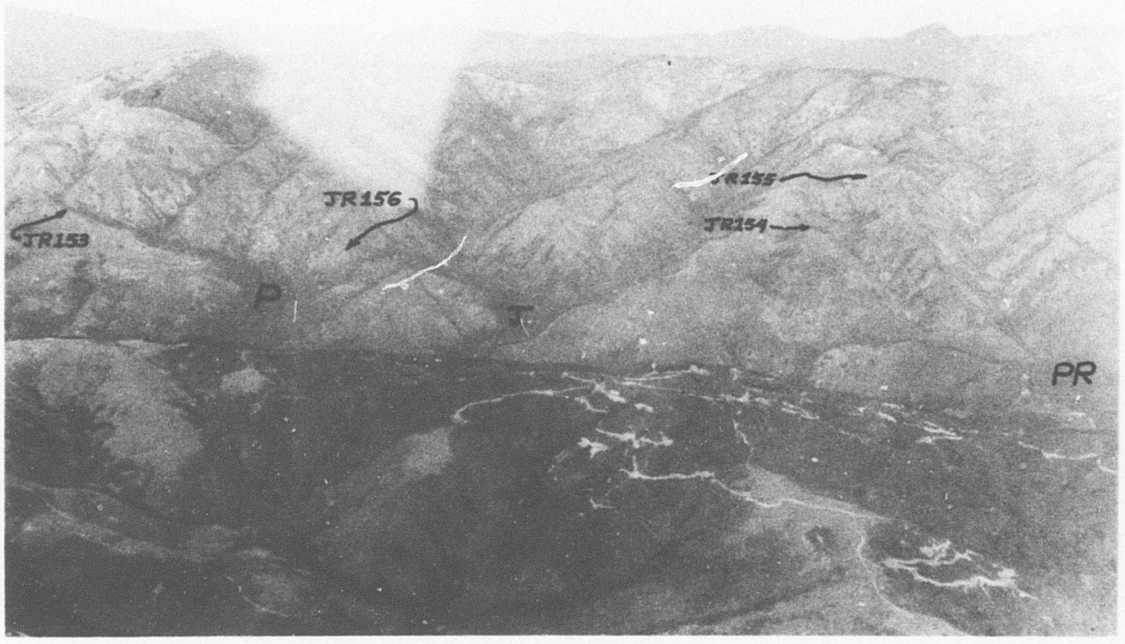

Figure 28. Oblique easterly view of the three major drainages, Pheneger Creek, (P), Juan Higuera Creek, (J), and Pfeiffer-Redwood Creek (PR) that were the sites of debris flow activity in October and November, 1972, at Big Sur, Monterey County, California.

varies from grassland and chapparal along the ridges to timber including coast redwoods nestled in the valleys.

The geology of the Big Sur Area has been studied in some detail (Oakeshott, 1951; Gilbert, 1972). The bedrock underlying most of the debris-flow source area is composed of resistant metamorphic rocks, largely gneiss, quartzite, and marble of the Sur Series (Fig. 29). Where the slopes become gentle, as along ridge crests, the bedrock is covered by one to two meters of soil, but elsewhere the bedrock is generally blockily fractured, slightly weathered, with less than 30 cm of soil cover.

I examined the drainage basins of Pfeneger, Juan Higuera, and Pfeiffer-Redwood Creeks only in a reconnaissance manner. Field examinations and sample collections were limited to areas within one day traverses of the main highway.* Two aerial surveys were made, one after each major episode of debris-flow activity. Three geologists and a pilot studied the source area during the reconnaissance flights. No evidence of landsliding was visible from the air, however, some areas looked bare, rough, and streaked in a downslope direction. Some slopes up to 100 meters wide and 300 meters long were covered with parallel, streak marks that resembled rills cut into a thin soil cover -- which indeed the field reconnaissance proved them to be (Fig. 30). In one instance debris-flow deposits could be traced directly upslope through small gullies, and into a series of rills.

The rills were up to 15 cm wide and 10 cm deep. Samples of the soil adjacent to the rills contained only minor amounts of clay and showed a

---

*Access across the Curtis and Ewoldsen properties is gratefully acknowledged.

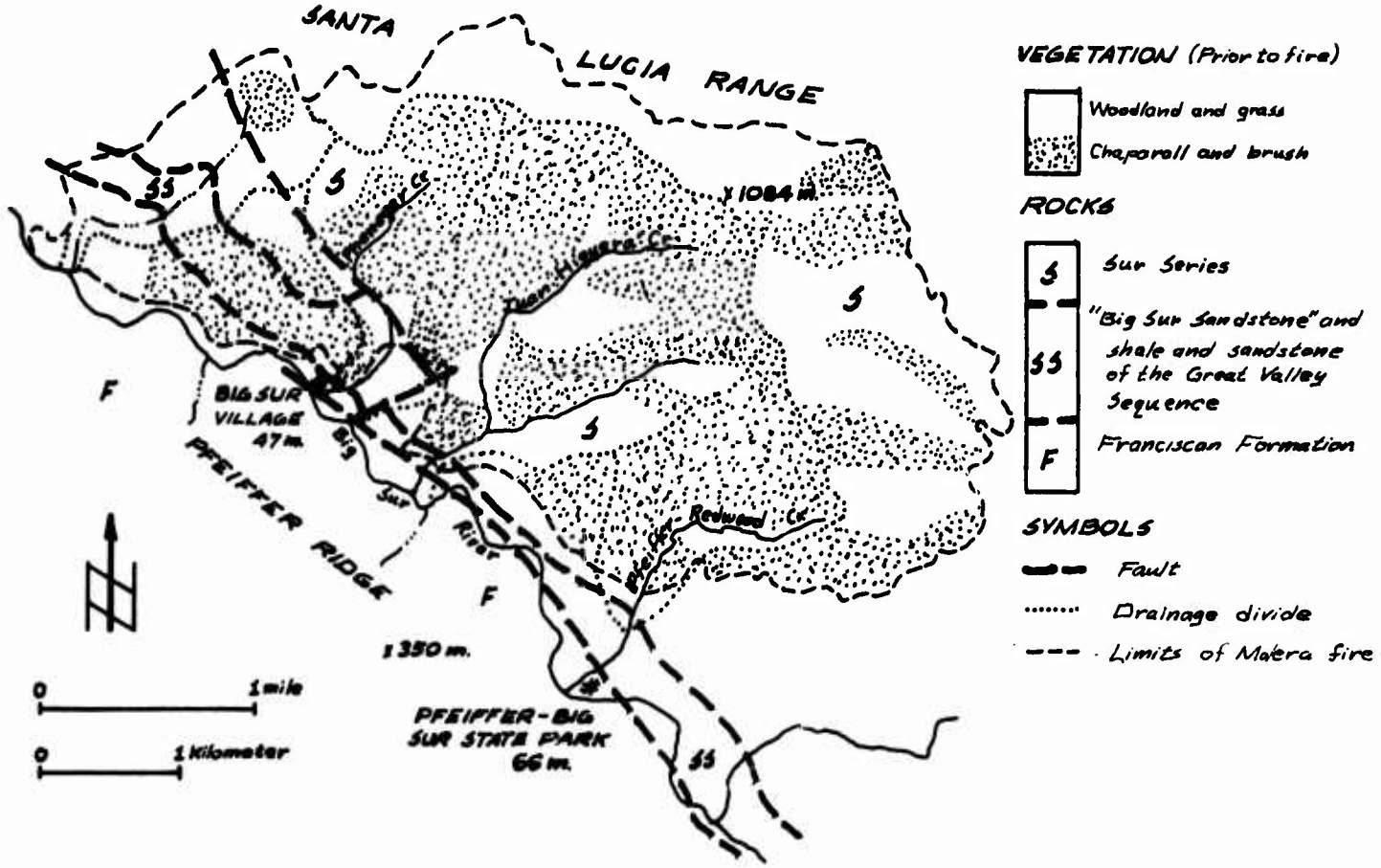

Figure 29. Generalized geologic map of the Big Sur area, Monterey County, California (after Cleveland, 1973, p. 128).

Figure 30. Rill-like debris-flow source area at Big Sur, Monterey County, California.

wide range of particle sizes (Fig. 31). The rills were subdued and only part preserved, presumably due to the rains following the debris mobilization. There were arcuate-shaped scars and spoon-shaped depressions at the heads of the rills (Fig. 30). Thus it appears that the debris was mobilized en masse from rills as at the Roofing Granule Quarry and at Arroyo Hondo.

The debris flows that issued from the mouths of the major canyons contained blocks of rock much larger than the widths of rills in the source areas I visited. Presumably, coarse debris in the floors of major canyons was picked up by the finer-grained debris flows because the canyons had been swept clean of coarse debris and vegetation. Debris had been accumulating in the canyons since the fire of 1907 and the resulting debris flows of 1907 to 1910 (L. Jackson, Pers. Comm.). Rock waterfalls several meters high are common in the canyons, providing large amounts of kinetic energy to mix the debris in the canyons.

After the mid-October rainstorms, forest service personnel noticed in some of the burned area that if the damp surface of the ground was kicked the ground was dry at a depth of a few cm. This phenomenon has been attributed to a chemically formed, non-wettable horizon developed during intense brush fires (De Bano, 1969). Perhaps the rill formation and the potential for debris-flow mobilization were encouraged by non-wettable zones formed during the fire.

San Rafael, Marin County, California

During an intense rainstorm of 13 February 1973 a debris flow mobilized within the city limits of San Rafael, northeast of San Francisco

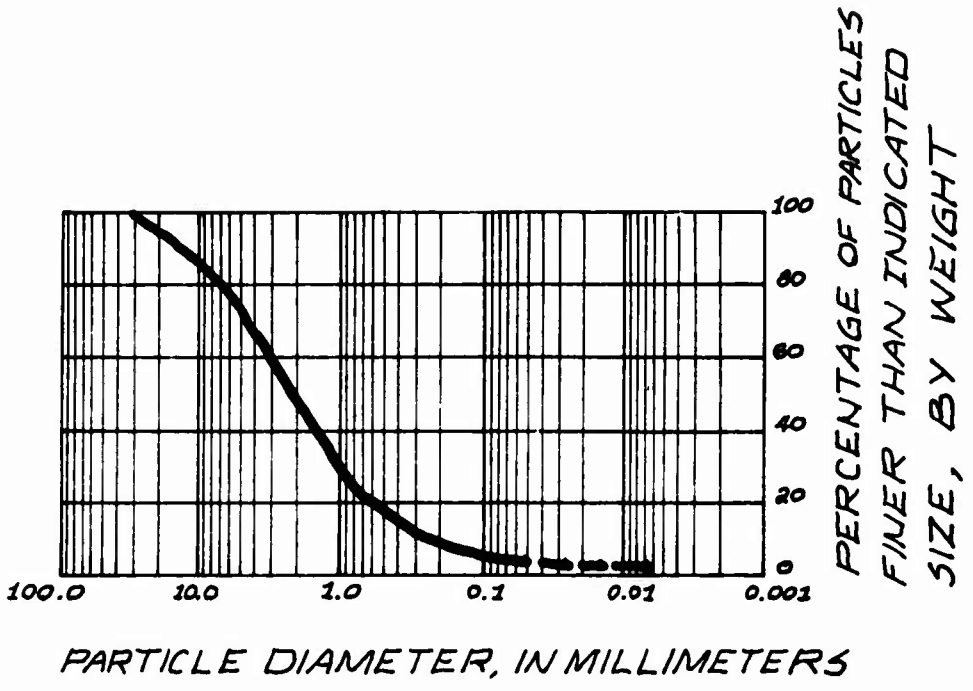

Figure 31. Size distribution of debris-flow source material from Big Sur, Monterey County, California.

California (Fig. 1, Table 1, Fig. 32a). The debris-flow initiated from a moderately steep, mountainous area near the top of a ridge, careened down a small canyon while dropping 200 meters over a 700 meter horizontal distance, and stopped in the back yard of a residence recently built across the natural drainage (Fig. 32b). About 400 cubic meters of debris was initiated, although, luckily for the occupants of the house, only about 20 to 40 cubic meters of debris was deposited at the terminal end of the debris flow, the balance being left as lateral ridges pastered along the canyon walls.

The debris flow mobilized in a grass-covered swale surrounded by a moderately dense growth of chapparal and small trees. The average annual rainfall for this area is 53 cm. The rocks exposed in the source area are weathered, fine-grained, tan sandstones and mudstones of the Franciscan Assemblage (San Francisco Sheet of the Geologic Map of California, 1961). The debris flows initiated from a mass about one meter thick, twelve meters wide, and 30 to 40 meters long. Initiation involved silty to sandy loam soil and weathered bedrock, and occurred along the soil-bedrock interface (Fig. 33a, 33b).

The source area slopes about 30 degrees. No water was visible when I visited the source on 15 February 1973, two days after the flow. The source area had been swept clean of debris leaving bare rock exposed. Several cubic meters of homogeneous debris was deposited at the base of the source area where the slope is reduced to about 15 degrees and where the canyon bends nearly 90 degrees (Fig. 35a). Additional debris was deposited for another 50 to 75 meters downstream from the 90-degree bend. Farther downstream the canyon slope abruptly

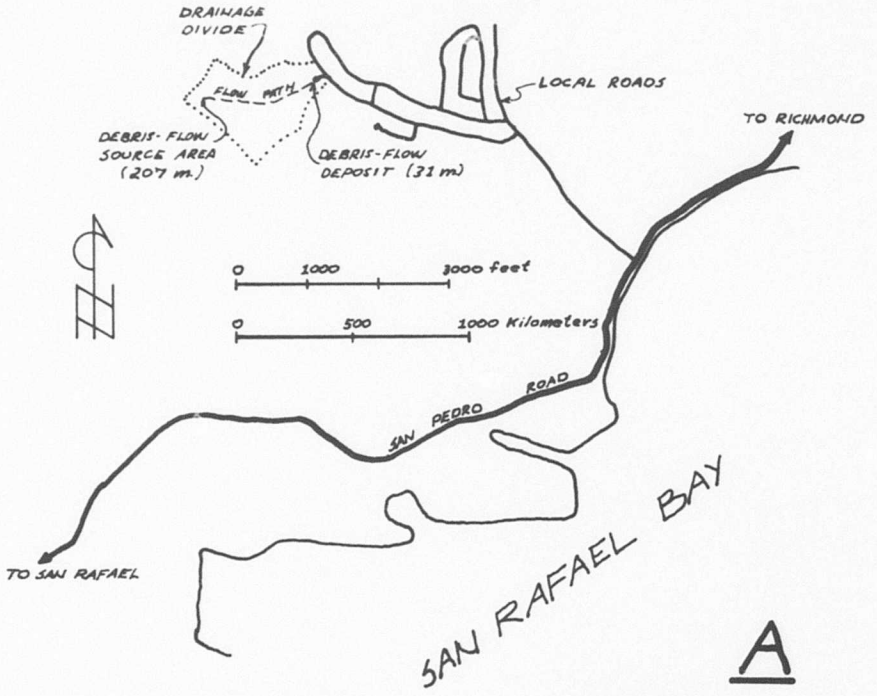

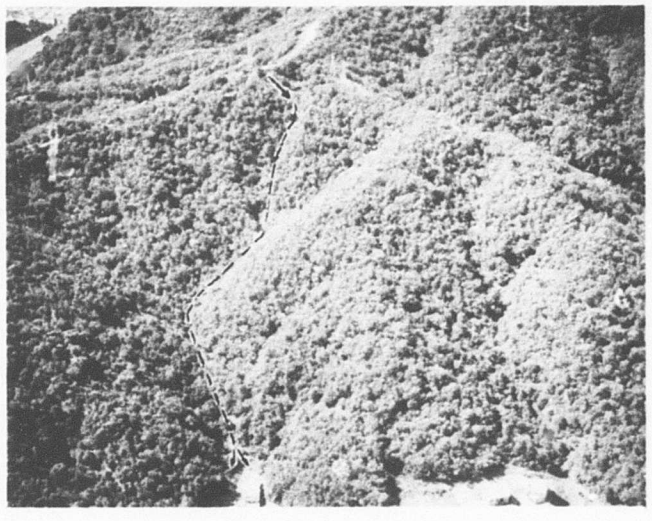

Figure 32. San Rafael, Marin County, California, debris-flow source area.

A. Location of debris-flow source area and path of flow.

B. Oblique westerly view of debris-flow source area, flow path, and site of deposition behind, and slightly around, the home straddling the gully.

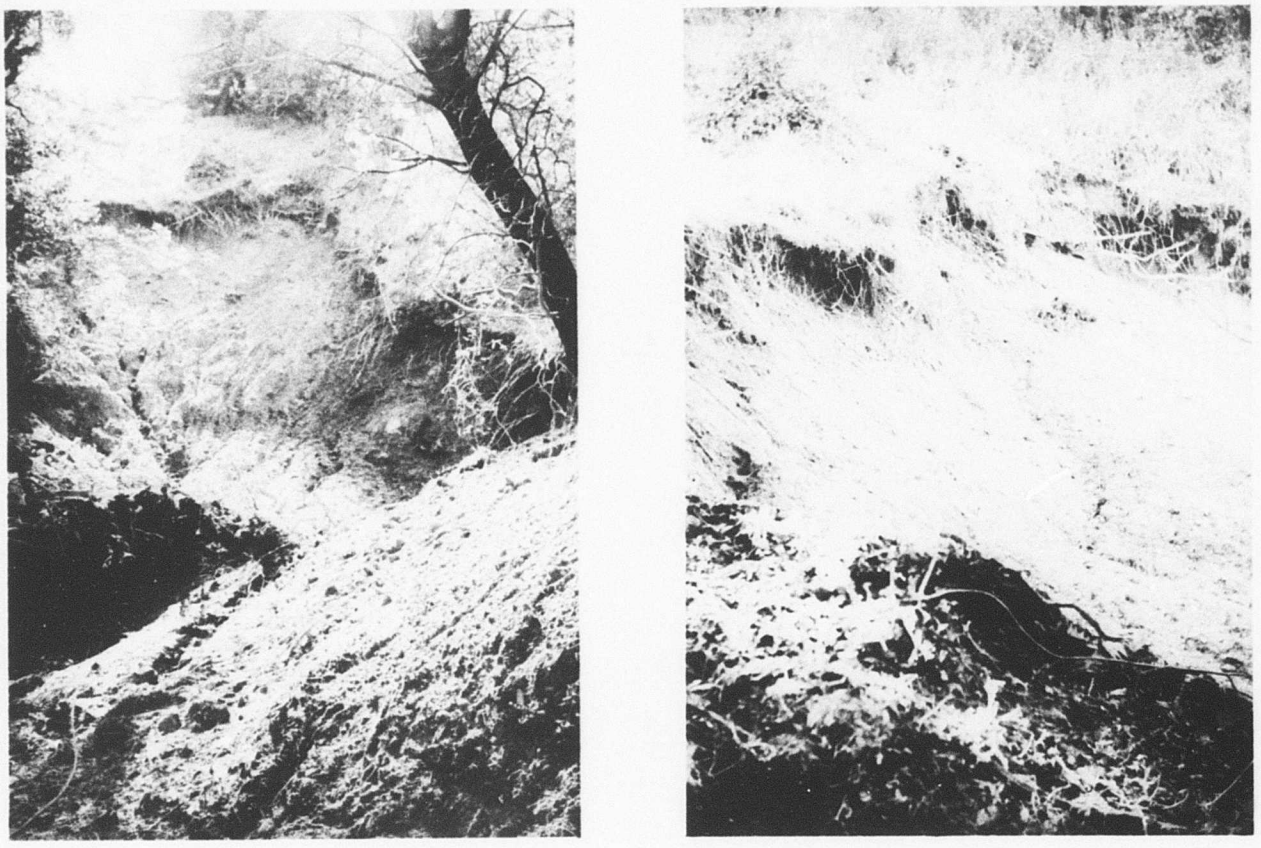

A

B

Figure 33. Debris-flow source area at San Rafael, Marin County, California.

A. View upstream of source area. The width of the head scarp is about 12 meters.

B. One meter deep pull-away scar marking the head of the landslide.

steepens and part of the debris flowed down the steppened slope towards the residence.

The appearance of the source area suggests that the debris began to slide en masse, becoming a mobile flow within a few meters. The debris was mobile by the time the 90-degree bend near the base of the initiation site was encountered by the mass.

Other Source Areas That Have Recently Produced Debris Flows

Three descriptions of source areas that have recently produced debris flows deserve special mention. They were written by students who recognized an initiation process similar to that observed at Lead Canyon described herein which does not rely on initiation via landsliding.

Matthes discussed fans formed by debris flows in Yosemite National Park, California (Matthes, 1930, p. 108-109). One source area, between the Three Brothers and El Capitan, is described as being in a recess:

> ". . . only 1 1/4 miles long and received no drainage from any hanging upland valley but heads abruptly against the rim, not far back of Eagle Peak. Its entire drainage area is considerably less than 1 square mile. However, the upper funnel-shaped part of the recess is enclosed almost wholly by steep slopes of bare, smooth granite from which the storm waters run off with amazing speed; and the principal drainage lines converge to one point and are so nearly of equal length and equal steepness that the waters reach the point of confluence almost simultaneously. The conditions, therefore, all operate to intensify torrential action. Finally, the recess contains, in addition to the rock waste derived from its own walls, a large body of morainal debris that was left in it by the ancient glaciers. This unconsolidated material gives way readily before the rushing waters and makes up a considerable part of the fan."

Johnson studied a series of debris-flow deposits near Klare Springs in Death Valley National Monument, California (Johnson, 1970, p. 436-437). He wrote that the debris flows were initiated (Johnson and Hampton, 1969, p. 4.7):

> ". . . near the top of a talus slope, where water traveling at high speeds apparently impacted the talus and dissipated its energy by dispersing large masses of talus. Very steep channels carved in bedrock above the talus provide ideal chutes for high speed flow of water during unusually intense rainstorms. The water apparently rushes out of the channels much as water from a firehose and strikes the talus. The erosive power of water issuing from a firehose or even from a garden hose is quite familiar. Natural debris flows initiated by this "firehose effect" are restricted to special conditions, usually very steep talus slopes."

Fryxell and Horberg visited sites of debris-flow initiation in Grand Teton National Park, Wyoming, that occurred in 1941 following a series of torrential rains. Impressive and well preserved debris-flow deposits were found in Upper Leigh Canyon which were interpreted to have formed in the following manner (Fryxell and Horberg, 1943, p. 466):

> "The heavy rain which provided the 'trigger effect,' initiating the mudflows, was carried off Mount Moran and its west ridge. . . by couloirs which thus were swept by short-lived torrential streams. Because the couloirs narrow and steepen below, these streams converged into torrents of tremendous volume and force which, directed diagonally downward upon the talus slopes beneath, acted like huge hydraulic hoses. Already unstable because near saturation, the talus was churned into a mixture of debris and water which gave way and flowed downslope. In its wake was left the flat trench out of which material had issued; lower the stream of debris came to rest as a mudflow. Some of the debris may have been swept out of the couloir, but probably most of it was derived from the talus."

SUMMARY OF CONDITIONS FAVORABLE TO THE INITIATION OF DEBRIS FLOWS

The conditions favorable for the initiation of debris flows in Turkestan have been summarized by Rickmers (Rickmers, 1913, p. 195-196):

> "Intermittent water supply owing to a dry climate, absence of strong vegetation and barren mountain flanks reaching up to the snowline are the conditions which favor the mudspate as a habitual and periodic phenomenon. Slopes of soft grit . . . covered with snow are the best starting ground. During spring the snow melts evenly over a large surface thus soaking a top layer of the friable stuff up to a bursting point. In this manner large quantities of half liquid rubbish are suddenly set free, initiating the process."

Blackwelder outlined the conditions that favor the development of debris flows as follows (Blackwelder, 1923, p. 478):

> "(1) unconsolidated material that becomes slippery when wet;
> (2) slopes steep enough to induce flowage in such viscous material;
> (3) abundant water;
> (4) insufficient protection of the ground by forest."

Water required for the initiation of debris flows is supplied in at least five ways. First, direct intense rainfall on debris slopes has provided the triggering effect for debris flows at: Thompson Creek, Utah, Lead Canyon, California, Mayflower Gulch, Colorado (Curry, 1966), the Andes of central Peru (Singewald, in Blackwelder, 1928), Nelson County, Virginia (Williams and Guy, 1971, 1973), Ulvådal, Norway (Rapp, 1963), Mgeta, Tanzania (Temple and Rapp, 1972), Roofing Granule Quarry, California, Arroyo Hondo, California, Big Sur, California (Cleveland, 1973), San Rafael, California, Yosemite National Park, California (Matthes, 1930, Klare Springs, California (Johnson and

Hampton, 1969), Grand Teton National Park, Wyoming, (Fryxell and Horberg, 1943), and in the European Alps (Bonney, 1902). Second, melting snow provided the water necessary for the initiation of debris flows at: Heath Canyon, California (Sharp and Nobles, 1953), and Hispar Valley, Himalayas (Conway, 1907). Third, ground water movement emerging in springs in the debris slopes initiated debris flows at: Woodside, California (Johnson and Rahn, 1972), and at Thompson Creek, Utah. Fourth, the mobilization of debris flows was allowed by sufficient interstitial water as recorded by Terzaghi (1950). Fifth, a catastrophic supply of water was provided by a volcanic eruption which ejected the contents of a crater lake forming debris flows in Java (Scrivenor, 1929).

Although lack of vegetation is considered by Rickmers, Blackwelder, and others to be a critical condition for the development of debris flows, observations in several debris-flow source areas suggest that its role is secondary. Observations of debris-flow source areas in heavily vegetated topography have been made in Nelson County, Virginia (Williams and Guy, 1971, 1973), Ulvådal, Norway (Rapp, 1963), Centre County Pennsylvania (Johnson and Rahn, 1972), and on Oahu, Hawaii (Wentworth, 1943). Studies in the Mgeta area, Tanzania (Temple and Rapp, 1972), showed that debris flows occurred more readily in areas that had been cultivated by man than in a nearby forest preserve. Debris flows occurred only in a Big Sur, California, area where the native vegetation had been recently burned, although chemical alteration of the soil during the fire could have been a more important factor than the lack of vegetation.

All the debris-flow source areas described here are in unconsolidated materials, including alluvium, talus, weathered bedrock or soil. Although the size distributions of material from most source areas are not known, the materials typically are poorly sorted, are polymodally distributed among the size classes, and contain small proportions of clay-sized material (e.g., Sharp and Nobles, 1953; Curry, 1966; Figs. 3, 14, 20, 31). The presence of clay even in small amounts appears to be necessary for the initiation of most debris flows. Perhaps this is because clay mixed with water posesses strength which supports the granular material (Hampton, 1970). Indeed, as little clay as 10 percent of the total weight of solids theoretically can completely support sand-sized material in a debris flow (Hampton, 1972).

None of the debris flows observed during this study initiated from slopes with angles of less than 20 degrees, and slopes of 30 to 50 degrees are typical (e.g.: Heath Canyon, Woodside, Thompson Creek, Roofing Granule Quarry, Arroyo Hondo, Big Sur, San Rafael, Lead Canyon, Mgeta (Temple and Rapp, 1972), and Oahu (Wentworth, 1943)).

Debris tends to form U-shaped channels in some cases bounded by debris-flow lateral deposits or levees (Johnson, 1970, Ch. 15; Sharp, 1942; and Blackwelder, 1928). Flow containment appears to be a necessary condition for continued flow of debris flows. Debris flows stop if they spread out laterally and thin, as though the thickness of the debris becomes in critical equilibrium with the strength and unit weight of the debris and the slope angle (Johnson, 1970, p. 488).

IDEALIZATION OF THE MOBILIZATION PROCESS

A conceptual model of the mobilization of debris has been beautifully cast into words by Rickmers who writes (1913, p. 194-195):

> "When a gentle slope of grit and shingle has been soaked like a sponge by rain or melting snows there may come a time when it bulges out and slides off in the manner of a bog-burst on Irish Moors. Slipping into channels and gullies this mass is mixed with more water, attains a higher speed and carries away soft material as well as rocks which it finds on its way. It is during this descent that the mudspate generally acquires its characteristic composition, for only by movement can an even mixture of liquid and solids be maintained. It is neither dry nor is there much free water, but the whole mass appears like a rapid flush of mud, although frequently the rock waste is so rough as not to suggest what is popularly called mud. Enormous boulders will float in this thick porridge like cork on water or iron on quicksilver. A mudspate may also be caused by the sudden bursting of a reservoir of water in the bed of a torrent (or the glacier above) which thus may be enabled to charge itself, for a short time, with an inordinate amount of loose material from the higher banks beyond the reach of normal floods.
>
> The typical mudspate-track does not, however, readily associate itself with the ravine of a permanent or powerful mountain stream, for the simple reason that the catchment area and bed of a torrent at work throughout the year are already deprived of the bulk of easily shifted material. Operating with a minimum of water the mudspate liquifies itself automatically when, during its descent, it has become too thick. Stopping for a while it dams up the water runlet in the gully and then proceeds again, repeating if needs be, the process several times."

The debris-flows at Ulvådal, western Norway were inferred to have formed in the following manner (Rapp, 1963, p. 200):

> "The main moving mass was probably a large frontal lobe, gliding and rolling, heavily laden and lubricated by the surface water from the new slide track behind it, growing by incorporating frontal slabs. The removal of the superficial ground layer in a widening path along the whole slide course was probably caused in this way. In my opinion

> the almost equal depth of erosion along the whole path proves that the main type of movement was that of a slide, not of a flow. In the experience of the present writer mudflows (debris flows) usually move in relatively narrow paths and often only transport earth, not actively erode their substratum, due to their viscosity and low friction on the ground."

Johnson and Rahn conceptualized the mobilization of debris flows as follows (1970, p. 179):

> ". . . a complete transition can be visualized: from the slip of some landslide masses along thin shear zones at their bases, to more nearly general deformation as the masses move into channels, and finally to the plastico-viscous type of flow . . . . . recognized in channelized debris flows."

Thus, the mobilization process can be idealized by considering first a block of debris at critical equilibrium on a slope (Fig. 34a). Enough water has been incorporated by the debris such that incipient failure has been induced along a shear zone at the base of the debris. Progressive failure in the debris mass is started at the base of the landslide, allowing small landslide blocks to rotate, to dilate, to incorporate water and to slide downhill (Fig. 34b). As landsliding and remolding progress, succeeding debris overrides the snout and flow is begun (Fig. 34c). When most of the debris has rotated, slid and jostled, the mass looses coherency and begins to flow (Fig. 34d). The flowing debris can incorporate loose material in its path by overrunning, it or material can fall onto the flow from the channel sides (Fig. 34e). If the flow is sluggish relatively clear water may be incorporated by flowing over the snout, wetting the channel and being overrun by the moving mass (Fig. 34f). In this way a debris flow can be mobilized.

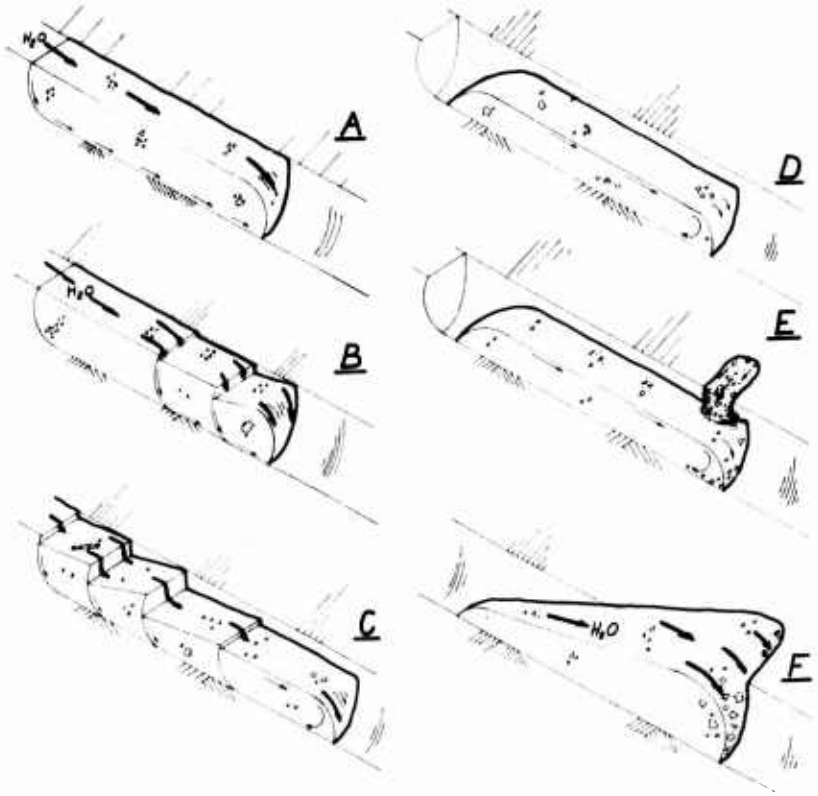

Figure 34. Conceptual model of the mobilization of debris flows.

A. Mass of soil at incipient failure by landsliding along a discrete shear zone.

B. Blocks of soil rotate, jostle, and incorporate water as they slide downhill.

C. Distal blocks rotate forward and are overridden by succeeding debris as landsliding proceeds uphill.

D. Debris has incorporated enough water to allow flow of most of the mass.

E. Debris may be incorporated into the debris flow through mixing at the snout along the channel or by the falling in of debris.

F. Sluggish debris flows can liquify themselves by temporarily clogging the channel until relatively clear water runs over the snout, wetting the channel. The debris flow can then override and incorporate the water and water-soaked debris lining the channel, until mobility is restored.

Mobilization of debris by the firehose method sidesteps the landslide phase by substituting churning, tossing and mixing of the debris by the impacting water for the incipient landsliding, but the remainder of the model of mobilization applies.

BIBLIOGRAPHY

Anderson, R., and Pack, R. W., 1915, Geology and oil resources of the west border of the San Joaquin Valley north of Coalinga, California: United States Geological Survey Bulletin 603, 220 pp.

Blackwelder, E., 1928, Mudflow as a geologic agent in semiarid mountains: Geological Society of America Bulletin, Volume 39, pp. 465-484.

Bull, W. B., 1964, Alluvial fans and near-surface subsidence in western Fresno County, California: United States Geological Survey Professional Paper 437A, 71 pp.

Callaghan, E., and Parker, R. L., 1961, Geology of the Monroe Quadrangle, Utah: United States Geological Survey Map GQ155.

Cleveland, G. B., 1973, Fire + rain = mudflows, Big Sur: California Division of Mines and Geology, California Geology, pp. 127-135.

Conway, M., 1907, The Fan Mountains in the Daub of Turkestan--discussion: Geological Journal, Volume 30, pp. 501-502.

Curry, R. R., 1966, Observation of alpine mudflows in the Tenmile Range, Central Colorado: Geological Society of America Bulletin, Volume 77, pp. 771-776.

De Bano, L. F., 1969, Water repellent soils. A worldwide concern in management of soil and vegetation: Agricultural Science Review, Volume 7, Number 2, pp. 11-18.

Erwin, R.; Dalen, R.; Taylor, M; and Franklin, F., 1972, Report on flood hazards and emergency measures needed as a result of the Molera Fire 8/1/72: United States Forest Service unpublished report, 24 p.

Fryxell, F. M., and Horberg, L., 1943, Alpine mudflows in Grand Teton National Park, Wyoming: Geological Society of America Bulletin, Volume 54, pp. 457-472.

Gilbert, W. G., 1972, Sur Fault Zone, Monterey County, California: Stanford University, Unpublished Ph.D. dissertation, Branner Library, Stanford, California.

Hampton, M. A., 1970, Subaqueous debris flow and generation of turbidity currents: Stanford University, Unpublished Ph.D. dissertation, Branner Library, Stanford, California.

_____, 1972, The role of subaqueous debris flow in generating turbidity currents: Journal of Sedimentary Petrology, Volume 42, Number 4, pp. 775-793.

Jahns, R. H., 1949, Desert floods: Engineering and Science Monthly, California Institute of Technology Contribution Number 499, pp. 10-15.

Johnson, A. M., 1967, A model for debris flow: Pennsylvania State University Unpublished Ph.D. dissertation, State College, Pennsylvania.

_____, 1970, Physical processes in geology: Freeman, Cooper and Company, 577 p.

_____, and Rahn, P. H., 1970, Mobilization of debris flows: Zeitschrift für Geomorphologie, Supplementband 9, pp. 168-186.

_____, and Hampton, M. A., 1968, Subaerial and subaqueous flow of slurries: unpublished progress report, United States Geological Survey Contract number 14-08-0001-10884.

_____, _____, 1969, Subaerial and subaqueous flow of slurries, unpublished final report, United States Geological Survey Contract number 14-08-0001-10884.

Krumbein, W. C., 1942, Flood deposits of Arroyo Seco, Los Angeles County, California: Geological Society of America Bulletin, Volume 53, pp. 1355-1402.

Matthes, F. E., 1930, Geologic history of the Yosemite Valley: United States Geological Survey Professional Paper 160.

Morton, D. M., and Cambell, R. H., 1973, Mudflows at Wrightwood, southern California, spring 1969 (abs): Geological Society, Engineering Group, Symposium on Mudflows 13 November 1973.

Oakeshott, G. B., 1951, Guide to the geology of Pfeiffer Big Sur State Park, Monterey County, California: California Division of Mines and Geology Special Report 11, 16 p.

Rapp, A., 1963, The debris slides at Ulvådal, Western Norway, An example of catastrophic slope processes in Scandinavia: Nachrichten der Academie der Wissenschaften in Göttingen, II, Mathematisch-Physikalische Klasse, Number 13, pp. 195-210.

Rickmers, W. R., 1913, The Duab of Turkestan: Cambridge Press.

Ross, D. C., 1967, Geologic map of the Waucoba Wash Quadrangle, Inyo County, California: United States Geological Survey Map GQ 612.

Scrivenor, J. B., 1929, The mudstreams ("Lahars") of Gunong Keloet in Java: The Geological Magazine, Volume LXVI, pp. 433-434.

Sharp, R. P., 1942, Mudflow levees: Journal of Geomorphology, Volume 5, pp. 222-227.

_____, and Nobles, L. H., 1953, Mudflow of 1941 at Wrightwood, southern California: Geological Society of America Bulletin, Volume 64, pp. 547-560.

Temple, P. H., and Rapp, A., 1972, Landslides in the Mgeta area, Western Uluguru Mountains, Tanzania: Geografiska Annaler, 54 A, p. 157-193.

Terzaghi, K., 1950, Mechanism of landslides: IN, Application of geology to engineering practice, Berkey volume, Geological Society of America, pp. 83-123.

Troxell, H. C., and Peterson, J. Q., 1937, Flood in La Cañada Valley, California: United States Geological Survey Water Supply Paper 796C, pp. 53-98.

Wentworth, C. K., 1943, Soil avalanches on Oahu, Hawaii: Geological Society of America Bulletin, Volume 54, pp. 53-64.

Williams, G. P., and Guy, H. P., 1971, Debris avalanches - a geomorphic hazard: IN, Coates, D., editor, Environmental Geomorphology, State University, New York, Binghampton, pp. 25-46.

_____ _____, 1973, Erosional and depositional aspects of Hurricane Camille in Virginia, 1969: United States Geological Survey Professional Paper 804, 80 p.

ANALYSIS OF MOBILIZATION OF DEBRIS FLOWS

PART II. A METHOD OF DETERMINING COULOMB STRENGTH PROPERTIES OF SOFT, REMOLDED DEBRIS USING PAIRED CONICAL PENETROMETERS

ABSTRACT

Theoretical, experimental and field analyses of processes of debris flow have indicated that a rapid but accurate method of determining Coulomb properties of soft, reconstituted debris is necessary for predicting conditions of initiation and flow of debris. Standard methods of soils testing are not useful for soft debris, primarily because of relatively high friction in standard test apparatuses.

The method we have developed for the testing of debris samples consists of measuring relations between applied loads and depths of penetration into debris for cones with apical angles of 15 and 30 degrees. These measurements, and the density of the debris, can be used to determine both apparent cohesion and apparent friction angle of the debris. Theoretical analysis, based on plasticity theory, indicates that the difference in angles between the two cones should be as large as possible in order to maximize differences in normal stresses applied by the cones to the debris, but that the cone apical angle should not exceed 30 degrees for debris with friction angles greater than 30 degrees.

The method has proved to be useful for understanding high susceptibilities to debris flow of granular materials in some source areas and low susceptibilities in others. It might be useful for determining apparent Coulomb properties of other soft materials, such as sediment on the sea floor.

INTRODUCTION

Some of our most recent research into flow of debris, consisting of mixtures of clay and water plus granular solids, has focused on mechanisms of initiation of flows under a variety of field conditions (Rodine, Part I, in prep.). Previous studies of debris flow, variously called mudflow, debris avalanche, or debris slide, have suggested that flowing debris can be characterized rheologically by a combination of ideal Coulomb strength and ideal Newtonian viscosity (Johnson, 1965, 1970). The adoption of such a Coulomb-viscous model can explain many features of flowing debris and debris-flow deposits, such as the ability of granular debris to flow on low slopes and yet transport large clasts, the development of a plug of non-deforming debris in the center of a moving flow, the formation of lateral deposits or levees, the transformation of some subaqueous debris flows into turbidity currents, and even the tendency for debris flows to form "U"-shaped channels (Johnson, 1965, 1970; Johnson and Hampton, 1969; Hampton, 1972; Rodine, Part III, in prep.). Furthermore, the Coulomb model for debris seems to explain effects of size distributions of granular constituents on strength parameters, as well as the tendency for granular materials in some source areas to be more susceptible to debris flow than in others (Rodine, Part III, in prep.; Rodine and Johnson, Part IV, in prep.).

The application of much of the previous research to the prediction of the susceptibility of debris to mobilization in possible source areas depends on the ability to measure both Coulomb strength parameters -- apparent cohesion, C, and apparent angle of internal friction, ϕ. The

Coulomb model, with tensile stresses positive, is:

$$\tau = C - \sigma_n \tan \phi \qquad (1)$$

where:

τ = shear stress at failure

σ_n = normal stress on failure surface (tension is positive)

Each of the two strength parameters is dominant in different situations. For example, the critical thickness, T_c, of Coulomb debris beginning to flow or stopping flowage on an infinite slope is (e.g., Johnson, 1970, eq. (12.14)):

$$T_c = \frac{C}{\gamma} \left(\frac{1}{\sin \delta - \cos \delta \tan \phi} \right) \qquad (2)$$

where:

γ = unit weight of debris

δ = slope angle

The maximum radius, R_m, of a completely submerged spherical particle that can be supported by the strength of Coulomb debris is approximately (Johnson, 1970, eqs. (13.40, 13.41)):

$$R_m = \frac{C}{\gamma} \left(\frac{f(\phi)}{\frac{\gamma_b}{\gamma} - 1} \right) ; \; f(\phi) = \bar{p}/C \qquad (3)$$

where:

$f(\phi)$ is a function of ϕ equal to $\bar{p}/C$ shown in Figure 8

and

γ_b = unit weight of particle

Eq. (2) and (3) are plotted in Fig. 1 for various friction values.

The upper part of Fig. 1 indicates relations among critical thickness, friction angle and cohesion for an assumed slope angle of 20 degrees and it shows that an increase in friction, $\underline{\phi}$, markedly increases the critical thickness, especially as the friction angle approaches the slope angle. Flow is impossible if the friction angle is greater than or equal to the slope angle, that is, if $\underline{\phi} \geq \underline{\delta}$. Comparison of the upper and lower graphs indicates that, for small friction angles, a small change in $\underline{C}$ will have a much larger effect on the maximum size of particle that can be transported than on the minimum thickness of a long, wide debris flow. Accordingly, both friction and cohesion are critical parameters to analyses of debris flow.

This paper is concerned with a method we have developed to measure Coulomb strength parameters of remolded debris, with consistencies generally softer and more fluid than most soils. Testing of low-strength soils using standard, direct-shear or triaxial tests (e.g., Lambe, 1951) is most difficult, primarily because instrumental errors, notably friction, are of the same order of magnitude as the strengths. Previously, we developed a test procedure which used spherical penetrometers (Johnson, 1970), but we could determine only the Tresca strength parameter of debris. Russian investigators (e.g., Rebinder, 1967) use conical penetrometers for strength testing of drilling muds and Swedish investigators have developed a dynamic cone penetrometer test for clay samples (e.g., Hansho, 1957), but again, only a single strength parameter can be determined. There are many other methods of determining the single strength, or Tresca, parameter of soils by means of

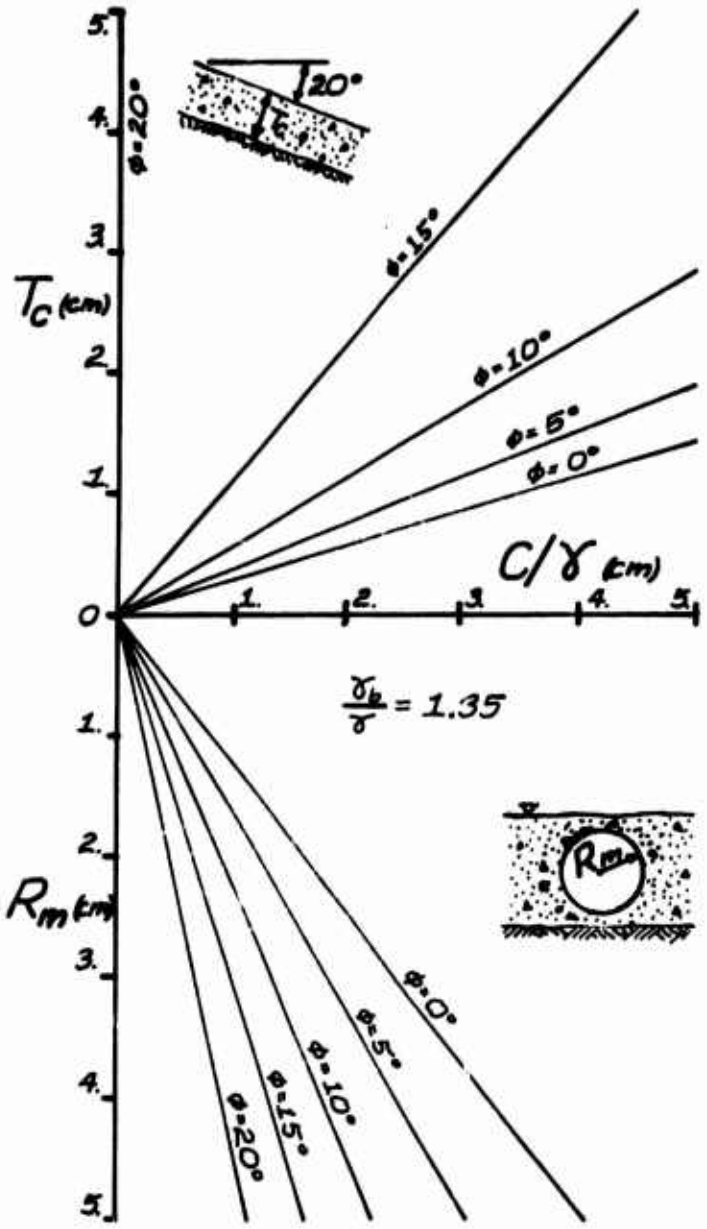

Figure 1. Relations among friction angle, cohesion and either the critical thickness of a debris flow or the radius of largest spherical particle that can be transported by a debris flow.

penetrometer tests, both in the field and in the laboratory (e.g., Lambe and Whitman, 1969; Sanglerat, 1972). The strength testing method we have developed employs two conical penetrometers with different apical angles. Our method avoids most of the problems with apparatus friction as well as allows the separation of both Coulomb parameters, apparent cohesion and apparent friction angle. The method is based on the solution of equations developed using plasticity theory, as explained in the Appendix. A graphical solution to the plasticity equations is included which allows the strength parameters to be determined quickly, with minimal computation.

The research reported here has been supported by the Army Research Office, grant number AROD-31-124-G158. We wish to thank Finn Bronner, of AROD, for constructive criticism and encouragement of our research. We are grateful to Dr. Robert W. Fleming, University of Cincinnati, and Dr. Monty A. Hampton, University of Rhode Island, for reviewing the manuscript and criticizing its content.

THE CONICAL PENETROMETERS

The conical penetrometers we use are shown in Fig. 2. The sides of one cone are inclined at an angle of 60 degrees to each other and of the other at an angle of 30 degrees. Each cone and frame is aluminum, except for steel bolts, teflon bearings, and a stainless steel tube between the cones and loading platform. The cones are counterbalanced in order to allow testing of very low-strength debris, with the consistency of soupy mud. A dial caliper attached to each cone measures the indentation of the cone into the debris after application of a weight to the loading platform. A third dial caliper is mounted on an aluminum stand so that it projects over the top of the debris container in order to measure the change in height of the surface of the debris as the cone is pushed into the debris.

Each cone was machined from solid cylindrical aluminum stock with care taken to maintain a constant wall thickness of approximately 1.3 mm. Each was designed to remain bouyant in water without counterbalancing. This design requirement resulted in a height of 8.4 cm for the 60-degree cone and 16.8 cm for the 30-degree cone. The stainless steel tube, with a diameter of 4.76 mm, was designed so that loads up to 10 kgm could be transmitted from the loading platform to the cone without buckling. Machinist time for both cone assemblies was about 24 hours. Total construction cost for both conical penetrometers, the third dial caliper mount, plus the cost of the 3 dial calipers was about $400 in 1972.

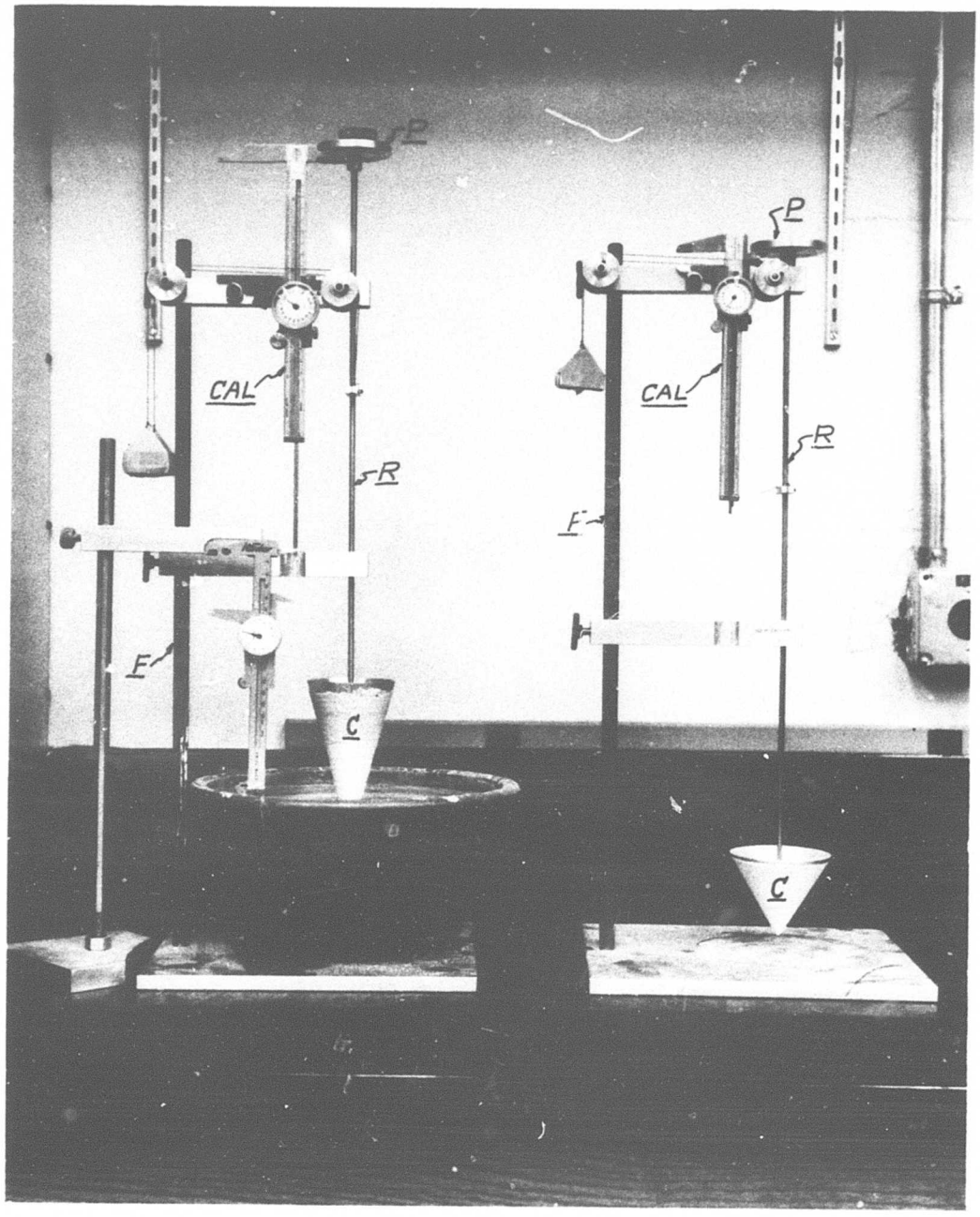

Figure 2. The paired conical penetrometers used for testing debris. Each penetrometer consists of a frame (F), cone (C), dial caliper (CAL), pan for weights (P), and stainless steel rod (R).

THEORY OF PENETROMETERS

Principle of the Apparatus

The essential principle of the penetrometer apparatus is that cones with different apical angles apply different average normal stresses to the debris during testing. These differences theoretically allow the separation of apparent cohesion from apparent friction angle of debris, because, according to eq. (1), apparent friction angle depends upon the average normal stress whereas apparent cohesion does not.

The theoretical relationship among debris strength, density, cone apical angle, and depth and force of penetration are derived in the Appendix. The theory presupposes that cone penetration results in symmetric plastic flow throughout a zone, the shape of which is determined by the angle of the cone and the properties of the debris. In order to determine the theoretical pattern of slip lines within the zone, a computer program was written to integrate along slip lines, following a method similar to that used by Cox, Eason, and Hopkins (1961). One half of the theoretical pattern of slip lines for $\phi = 20°$ and $C/H\gamma = 0.10$ is shown in Fig. 3, where H is the depth of penetration. The other half of the pattern is a mirror image of the pattern shown in Fig. 3.

The pattern derived with the approximate solution suggests that the cone surface is an envelope of slip lines, that is, a limiting line (Prager and Hodge, 1951, p. 149), and our exact solution (Appendix) assumes that it is. The debris within area ABCD has yielded plastically, in accordance with eq. (1), with the slip line BCD forming the boundary

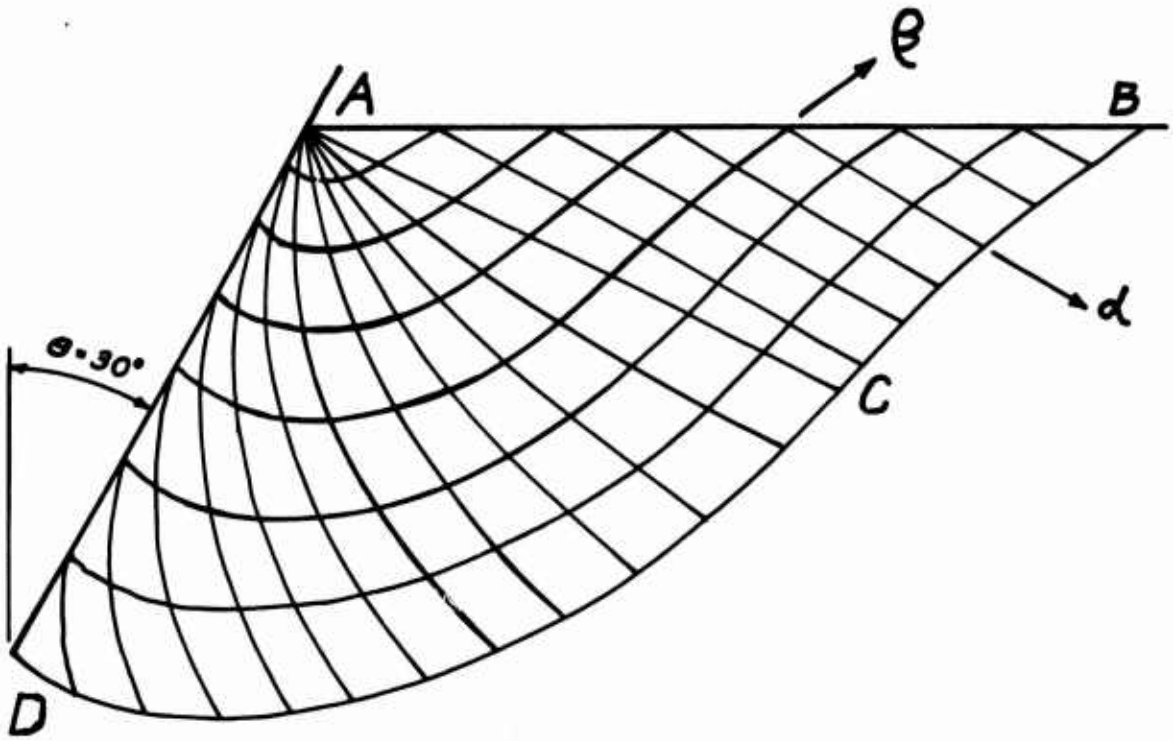

Figure 3. Cross section showing half of cone and theoretical pattern of slip lines adjacent to cone in Coulomb material with properties $\phi = 20°$, $C/H\gamma = 0.1$.

between material at and material below the yield strength. The physical analog of the intersection of the slip line BCD with the surface at B is shown clearly in experiments with dry, silt-sized glass beads (Fig. 4).

Operating Restrictions

The pattern of slip lines surrounding the cone, as shown in Fig. 3, places theoretical restrictions on the maximum cone angle, on the nature of the cone surface, and on the size of the container used for testing of debris. The apical angle, θ, of the cone, which is defined as one-half the included angle between the sides of the cone, must be less than $\pi/4-\phi/2$, because ω, the angle between the slip lines radiating from the tip of the cone, cannot be less than $\pi/2-\phi$ (Fig. 5A). If the apical angle were greater than this limit a region of no flow, or a plug, would form around the cone, as shown in Fig. 5B. Strength determinations are complicated considerably if a plug forms because in this case indentation depth cannot be measured directly. Thus, the cone angles were selected to avoid the formation of a plug. We selected one cone with a 30-degree apical angle. The friction angle for remolded silts and uniform fine- to medium-grained sand ranges from 26-30 degrees (Hough, 1957, ref. in Lambe and Whitman, 1969) so that we would not expect debris samples to have friction angles in excess of 30 degrees. Choice of the second cone, with a smaller apical angle, was dictated by the desire for a large difference in average normal stress between the two cones and for a durable cone. A difference in average normal force F_n, of about 42 percent was determined theoretically, using formulae derived in the appendix, for cones with apical angles of 30 and 15 degrees (Fig. 6). This difference seems to be adequate and all our measurements have been made

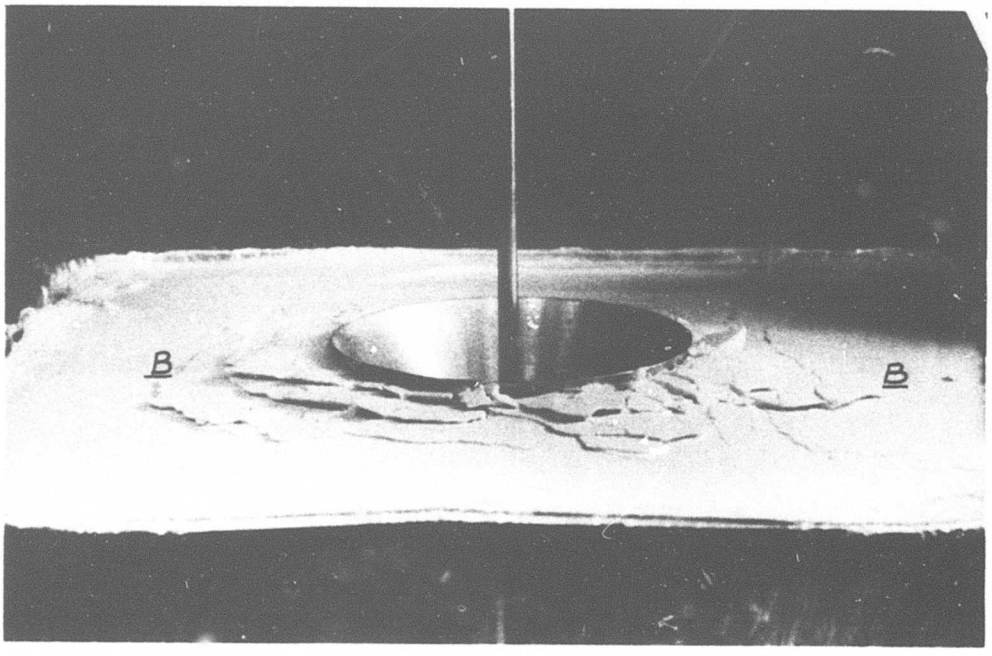

Figure 4. Trace of slip surface, B, between deforming debris, near cone, and rigid debris, distant from cone.

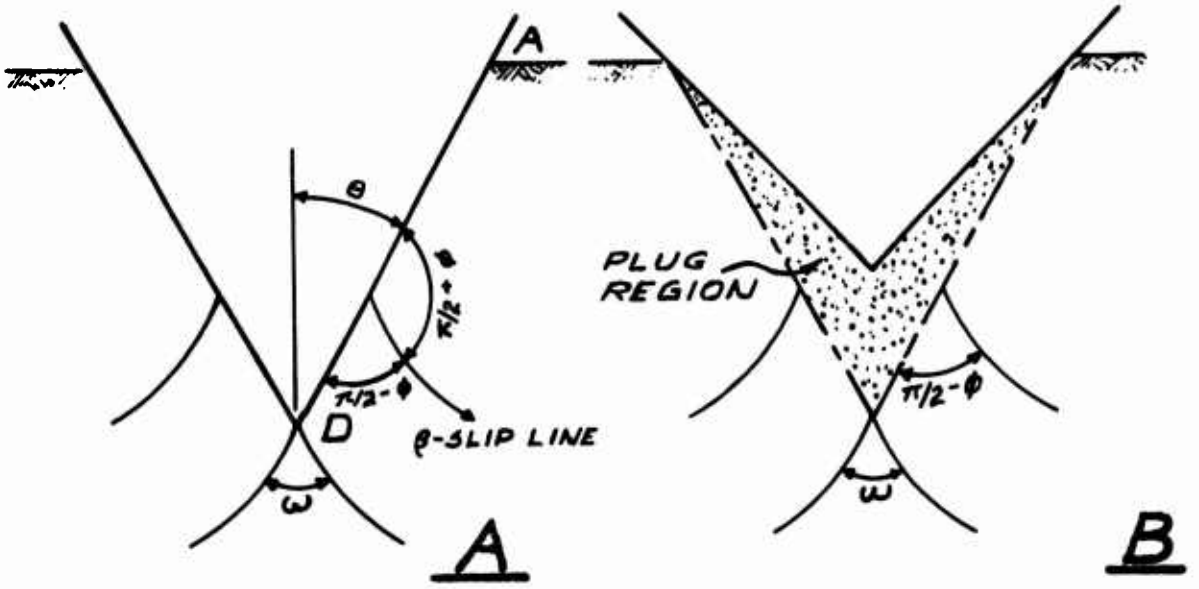

Figure 5. Theoretical relations between slip lines and surface of frictional cone.

A. Apical angle, $\underline{\Theta}$, less than critical value -- no plug forms and surface of cone is a slip line.

B. Apical angle, $\underline{\Theta}$, greater than critical value -- plug, or non-deforming region of no flow, develops near the cone, acting much as part of the cone.

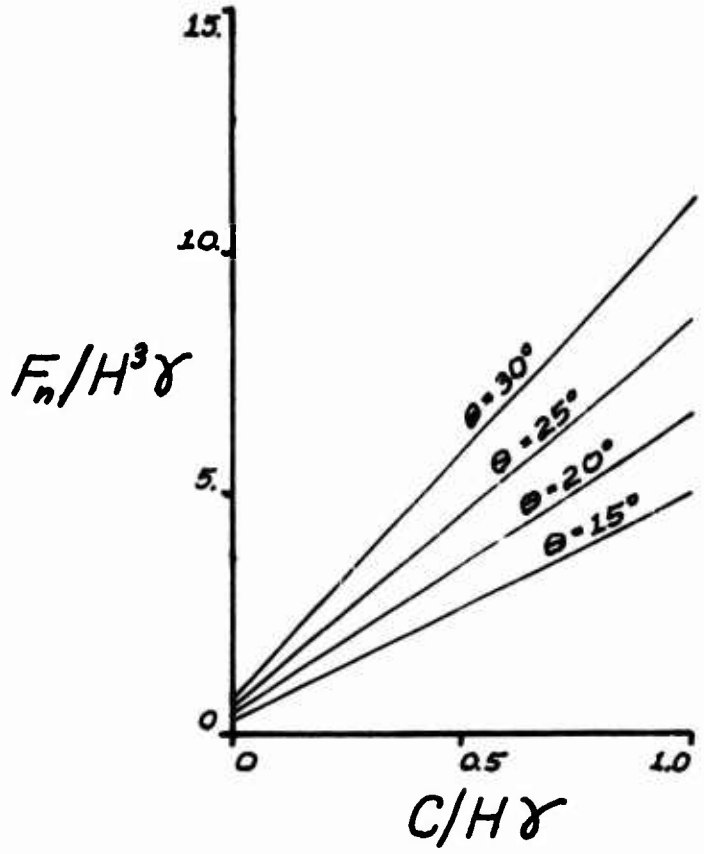

Figure 6. Theoretical relations among normal force on cone F_n, apical angle, θ, and cohesion, C, of debris. The wider the spread of the curves, the more sensitive the paired penetrometers are to differences in the friction angles of debris.

with the pair of cones with apical angles of 15 and 30 degrees shown in Fig. 2.

One of the fundamental assumptions of our theoretical solutions (e.g., Fig. 3) is that the boundary between the cone and the debris is a limiting line, along which the shear stress is equal to the shear strength of the debris. Thus, in designing the cones it was important to insure that all shear would occur within the debris without any slippage along the cone. Otherwise, one would have to incorporate in the solution a variable coefficient of friction for debris sliding on the cone surface, which would introduce another complication. Because our test procedure excludes debris with abundant particles larger than coarse sand we forced the slippage to occur within the debris by gluing coarse sand to the cones.

The container used for the debris must be large enough to avoid interferring with the slip-lines formed as the cone penetrates the debris, yet small enough so that the sample is of a manageable size. In order to obtain a first estimate of the radius of interference, $\underline{R}_I$, and of the depth of interference, $\underline{Z}_I$, Fig. 7A was derived by simplifying the slip-line geometry. The equations derived from Fig. 7 are plotted in Fig. 7B for various $\underline{\phi}$ values, and for cones with 15- and 30-degree apical angles, $\underline{\theta}$. For example, $\underline{\phi}$ = 30 degrees, with a hemispherical container filled with debris to a depth of 20 cm, radial interference using the 30-degree cone would begin at an indentation depth, $\underline{H}$, of about 5 cm and bottom interference at about 10 cm. We use a crudely hemispherical container with a radius of approximately 11 cm. During the testing of weak debris, $\underline{\phi} \simeq 0$ and $\underline{C} \simeq 100$ dn/cm^2, the 30-degree cone penetrates as deep as 7 cm with a 200 gm weight. Using Fig. 7B

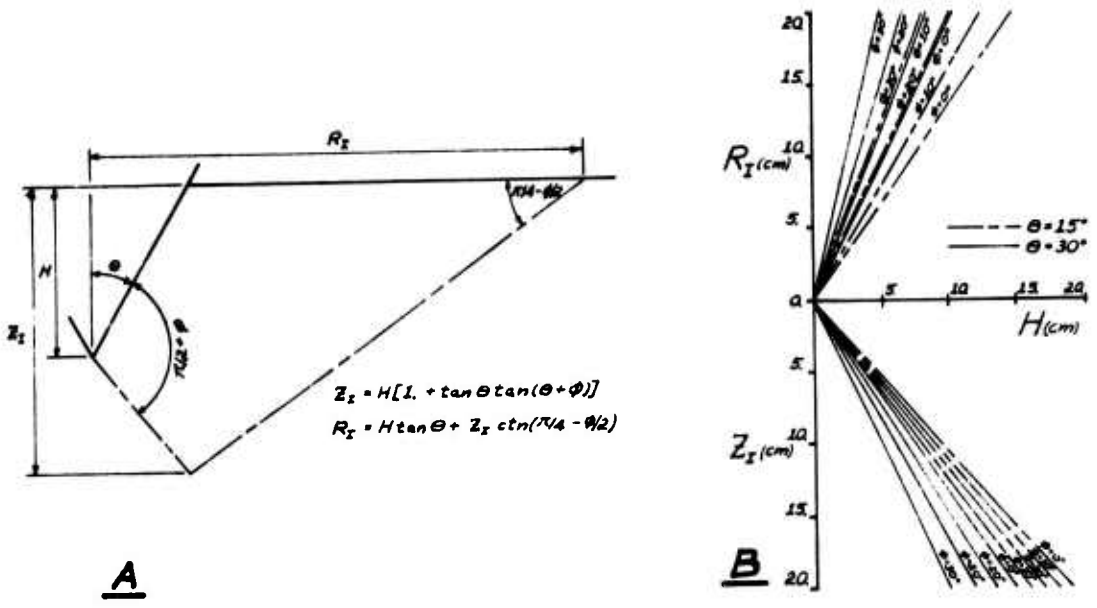

Figure 7. Limiting dimensions of container used for testing of debris samples.

A. Simplification of slip-line pattern, indicating minimum radius, $\underline{R}_I$, and minimum depth, $\underline{Z}_I$, of container of deforming debris.

B. Relations among $\underline{R}_I$, $\underline{Z}_I$, friction angle, $\underline{\phi}$, and depth of penetration of cone, $\underline{H}$, for cones with apical angles of $\underline{\Theta}$ = 15° and 30°.

we note that no radial interference nor depth interference will occur at $\underline{H}$ = 7 cm and $\underline{\phi}$ = 0. If, however, our test sample had high friction, $\underline{\phi}$ = 30 degrees, bottom interference would have begun at an indentation depth of about 5.5 cm. Selection of container size, then, depends upon the expected depth of penetration and the range of internal friction angles of samples. Large containers allow larger penetration depths before slip-line interference begins but they require large samples of debris. If apparatus friction and operating errors can be kept low, small containers, such as the bowl of 11 cm diameter, and small samples of debris can be used without introducing significant errors.

Comparison of Theoretical Results

To the best of our knowledge there have been no other theoretical solutions for the force required to drive a cone into Coulomb material. We have thoroughly checked the literature and have asked experts in plasticity theory (E.H. Lee, Pers. Comm.; M.J. Hvorslev, Written Comm.; and R.T. Shield, Written Comm.) in search for other solutions. Numerical checks of our solution must, therefore, rely heavily upon comparisons with those for penetration loads for flat, frictionless punches. An approximate solution for the indentation of a circular punch into weightless Coulomb material was derived by Cox, Eason and Hopkins (1961). Their results are shown in Fig. 8, in terms of mean penetration pressure, $\overline{\underline{p}}$, apparent cohesion, $\underline{C}$, and angle of internal friction, $\underline{\phi}$. Ishlinsky (ref. in Hill, 1950, p. 281) assumed a Tresca model and computed a $\overline{\underline{p}}/\underline{C}$ value of 5.70 for a frictionless spherical punch. Shield (1953) derived a lower bound solution for a flat, frictionless, rectangular punch on weightless Coulomb material; his results are also shown on

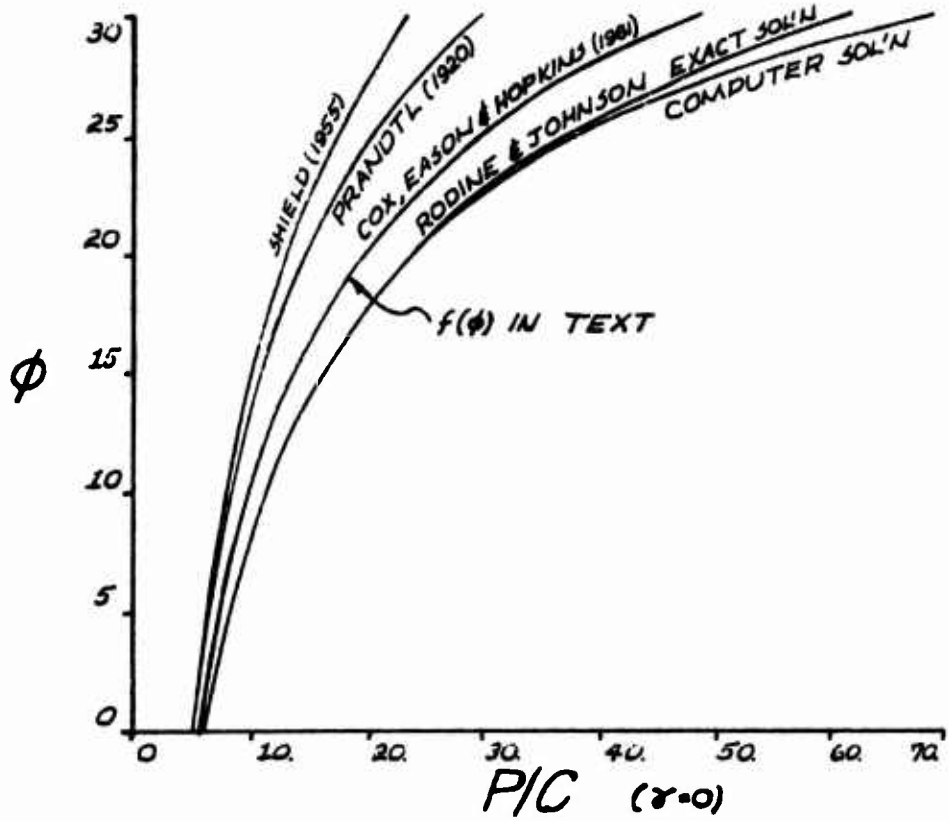

Figure 8. Theoretical relations between angle of internal friction, $\underline{\phi}$, and mean vertical force per unit area, $\underline{\bar{p}}$, according to various investigators. Relations derived by Shield, by Prandtl, and by Cox et al., are for flat smooth punches. Relations derived here are for frictional cones.

Fig. 8. Prandtl (1920, ref. in Shield, 1953) derived a plane-strain solution for a flat, frictionless punch on weightless Coulomb material (Fig. 8). Finally we solved for stresses on the surface of a frictional cone by finite-difference methods, and a computer, by integrating along slip-lines from the free surface of the debris to the cone surface. The results are approximate, but they correspond closely to those of our exact solution (Fig. 8). The three other solutions for Coulomb material, those of Shield, of Prandtl, and of Cox, Eason and Hopkins, predict smaller mean pressure values than our two solutions. But this difference is reasonable because, whereas the other solutions allow the slip lines to be curved throughout the zone of flow (Fig. 3), ours requires that the slip lines straighten out at the surface of the cone.

OPERATING PROCEDURE

For our study of debris strength, the first step is to add deionized water to an air-dried sample and to stir and remold the sample in order to insure homogeneity. A small portion is removed for the determination of bulk density and water content. The unit weight, γ, of the sample is computed by multiplying the density of the debris by the acceleration of gravity. When the sample of debris has been thoroughly remolded, it is placed beneath one of the penetrometers. The cone is lowered until the tip touches the surface of the sample, and the dial caliper is read. Then a weight, L, is placed on the pan above the cone, the cone penetrates into the sample, and the dial caliper is read again. We have found it necessary, particularly when testing weak debris, to add a correction for the rise of the surface of the debris as the cone penetrates the debris. The rise of the surface is measured with a second dial caliper set over the rim of the container (see Fig. 2). Finally, the indentation depth, H, is the difference between the dial caliper readings before and after loading, plus the increase in height of the debris surface. This process of loading and measurement of penetration depth is repeated by increasing the load and measuring the resulting penetation depth at least five or six times, in order to determine a load-penetration curve for each cone (Fig. 9).

After a weight is applied it is necessary to jostle the cones slightly until a meniscus-like depression in the debris surface near the cone disappears before reading the indentation depth on the dial caliper. If the debris is stiff, slight horizontal tapping on the rod connecting the load pan to the cone usually dissipates the depression. Also

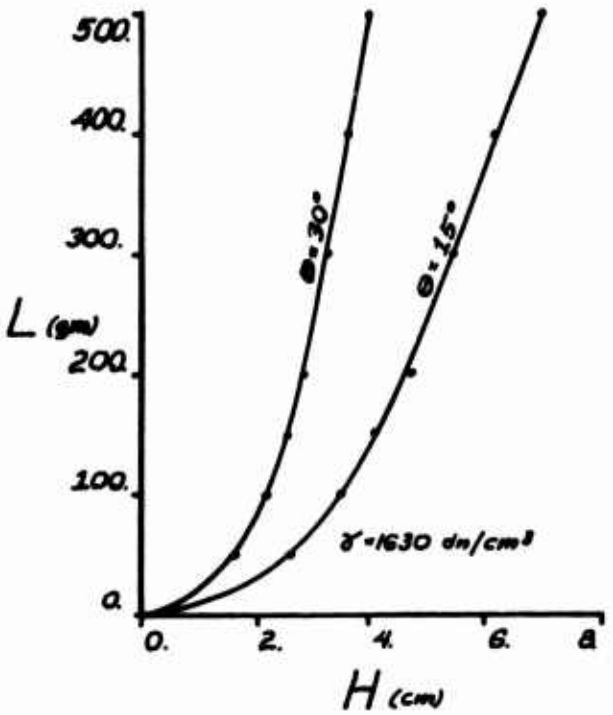

Figure 9. Relations between weight applied to cone, L, and depth of penetration of cone, H, for a remolded sample of material from the source of a debris flow.

coarse particles in relatively fluid, low-strength debris tend to settle during the penetrometer tests so fluid debris must be remolded after each depth measurement, and before applying more weight, in order to obtain reproducible results.

After several loads have been applied and the resulting indentation depths measured, the data are plotted for each cone, as shown in Fig. 9. The next step is to calculate the apparent Coulomb properties. According to eq. (A13b), in the Appendix, the depth of penetration, $\underline{H}_{30}$, of a 30-degree cone is a function of applied force $\underline{F}_{30}$, and of unit weight $\underline{\gamma}$, apparent cohesion, $\underline{C}$, and apparent friction angle, $\underline{\phi}$, of the debris,

$$F_{30}/H_{30}^{3}\gamma = (C/H_{30}\gamma)\ \{\pi \tan^2\theta\ [(2D/(2-A))\ (Q_o/C) - \text{ctn}\ \phi]\ \}$$

$$+ 2\ \pi\tan^3\theta\ DB/[3(2-A)], \qquad (4)$$

where $\underline{A}$, $\underline{B}$, $\underline{D}$, and $(\underline{Q_o/C})$ are constants defined in eqs. (A11), (A14), and (A15b), with the apical angle, $\underline{\theta}$, equal to 30-degrees, and $\underline{H} = \underline{R}$ ctn $\underline{\theta}$. A similar equation can be written for the 15-degree cone by replacing the subscript 30 with the subscript 15 in eq. (4), and setting $\underline{\theta}$ = 15 degrees. Now, there are two unknowns, $\underline{C}$ and $\underline{\phi}$, and two independent equations, so that one can solve the equations simultaneously for $\underline{C}$ and $\underline{\phi}$. The equations are complicated, but, by equating the forces, $\underline{F}_{15}$ and $\underline{F}_{30}$, apparent cohesion, $\underline{C}$, can be eliminated. Then an indentation ratio, $\underline{H}_{15}/\underline{H}_{30}$, can be introduced, to reduce the depths to a single variable, and the resulting equation solved for $\underline{\phi}$ by iterative methods. Fig. 10A represents the solutions for various $\underline{\phi}$ values. Finally, once $\underline{\phi}$ has been determined from Fig. 10A, $\underline{C}$ can be determined

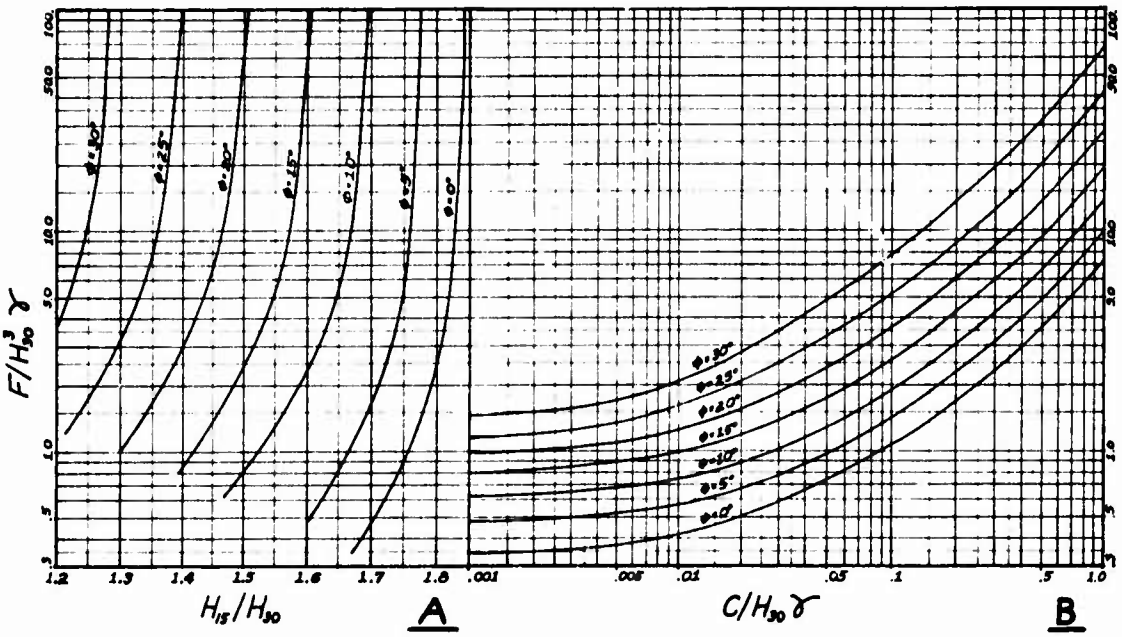

Figure 10. Graphs used to compute apparent values of Coulomb cohesion and friction angle.

A. Experimental measurements provide values for ratio of depths of penetration of 15-degree, $\underline{H}_{15}$, and 30-degree, $\underline{H}_{30}$, cones and force parameter, $F/H_{30}{}^3\gamma$, for 30-degree cone. With these values as coordinates, the apparent angle of internal friction, $\underline{\phi}$, is determined by interpolation between graphs.

B. Then the values of the force parameter and of the apparent angle of internal friction are used to determine the cohesion parameter, $C/H_{30}\gamma$, with the second set of graphs.

from Fig. 10B, which is the graphical solution to eq. (4). Thus, Figs. 10A and 10B can be used with the experimental data to determine values of apparent cohesion and apparent friction angle for a sample of debris.

Let us consider an example of the use of the graphs for determining $\underline{\phi}$ and $\underline{C}$ by analyzing test data for debris-flow source material collected from Arroyo Hondo, Fresno County, California (Rodine, Part I, in prep.). The water content of the test sample was 37.11 weight percent of the total solids and fluid. According to the load-penetration curves for this sample, Fig. 9, a load of 300 gm corresponds to penetration depths of $\underline{H}_{15}$ = 5.42 cm and $\underline{H}_{30}$ = 3.21 cm. The load is recorded in column a, and the indentation depths in columns c and d, of Table 1. The force, $\underline{F}$, on the cones is the weight, $\underline{L}$, times the acceleration of gravity, as recorded in column b of Table 1. Next, the depth ratio, $\underline{H}_{15}/\underline{H}_{30}$, and the force term, $F/H_{30}^3\gamma$, are calculated and entered in columns e and f, respectively, of Table 1. The apparent friction angle, $\underline{\phi}$, is determined from Fig. 10A by finding the point with coordinates equal to the depth ratio and force term. The apparent friction angle, about 8.6 degrees, is recorded in column g, Table 1. The cohesion term, $C/H_{30}\gamma$, is located at the coordinate intersection of the determined value of $\underline{\phi}$ and the force term, by means of Fig. 10B, and recorded in column h. Finally, cohesion is equal to the value of the cohesion term times the unit weight, γ, and the depth, $\underline{H}_{30}$, and is about 2140 dn/cm^2, as indicated in column i of Table 1.

In general, $\underline{\phi}$ and $\underline{C}$ are determined for several values of load and corresponding penetration depth, and are then averaged to determine $\underline{\phi}$ and $\underline{C}$ for the sample. We have found that a complete test sequence,

including graphical solutions for ϕ and C, takes between 30 and 60 minutes. Thus, our method allows many rapid determinations of Coulomb strength parameters for remolded debris samples to be made in one day.

TABLE 1

a Applied Load L (gm)	b Applied Force F (dynes)	c Indentation 15°cone H_{15} (cm)	d Depths 30°cone H_{30} (cm)	e Depth Ratio H_{15}/H_{30}	f Force Term $F/H_{30}^3\gamma$	g Apparent Friction Angle ϕ (deg)	h Cohesion Term $C/H_{30}\gamma$	i Apparent Cohesion C (dynes/cm^2)
300	$2.94*10^5$	5.42	3.21	1.69	5.46	8.6 ± 1.0	0.410	2140 ± 160
290				1.69		8.5		2130
310				1.69		8.7		2150
300				1.66		9.6		2300
300				1.72		7.6		1980

SOURCES OF ERROR

Besides errors introduced by the operator, and by discrepancies between real and theoretical behaviors of debris, there are several sources of error in the procedure we use for determining $\underline{\phi}$ and $\underline{C}$. The errors are introduced through measurement errors of density, penetration force, and penetration depth, plus an error introducted by neglect of surface slope of the debris near the cone. Our equipment allows us to determine penetration force to within $\pm$ 9.8 x 10^3 dn (10 gm) and penetration depths to within $\pm$ 0.05 cm. Uncertainties in values of apparent Coulomb constants as a result of errors in measurement of density are negligible compared to errors in penetration force and penetration depth.

Errors due to variations in penetration force are reduced greatly as the total force is increased. The error in determining the apparent friction angle due to force uncertainties, according to Fig. 10A, is negligible if the force term exceeds 5 or 10, depending on the depth ratio of the sample. Our debris samples had apparent cohesion values ranging from thousands to less than one hundred dn/cm^2. Apparent cohesion is directly related to the applied force, eq. (4), such that deviations up to 30 percent for low values of apparent cohesion say $C \simeq 100$ dn/cm^2, are found when the weight varies by 10 gm. Fortunately, as the apparent cohesion increases, the deviations decrease rapidly.

Error introduced due to penetration depth variations can strongly affect calculations of apparent friction angle. An error of $\pm$ 0.02 in the depth ratio will commonly result in a difference of 1 degree in $\underline{\phi}$, according to Fig. 10A. Apparent cohesion calculations are more strongly

affected by depth variations at low $\underline{C}$ values. For example, a value of $C = 100 \pm 30$ dn/cm^2 is possible if the depth varies by $\pm$ 0.05 cm.

As an indication of potential ranges of error, the lower part of Table 1 shows the deviation of $\underline{\phi}$ and $\underline{C}$ for variations in applied weight and indentation depth for one example. It is important, especially when working with low-strength, soupy debris, to keep the apparatus friction as low as possible and to exercise extreme care in reading the dial calipers.

One source of error that has been ignored thus far is that caused by a sloping surface of the debris being tested. During our testing of a wide range of debris types we have found that the slope of the debris surface near the cones generally is negligible - except in debris containing high proportions of sand-sized particles. Thus, for nearly all our tests we have ignored the surface slope. However, the correction for surface slope can be made readily by modifying merely two equations, eqs. (A16a) and (A16b) in the Appendix:

$$\left.\begin{aligned} P_o &= C(1 + \pi/2 + 2\theta - 2\,\delta), \\ Q_o &= C \tan(\pi/4 + \phi/2) \exp[\tan\phi\,(\pi/2 + 2\theta - 2\,\delta + \phi] \end{aligned}\right\} \quad (5)$$

where $\underline{\delta}$ is the surface slope of the debris next to the cone. Thus, where surface slopes are significant, it will be necessary to construct new sets of graphs to replace those in Figs. 10A and 10B, using eqs. (4) and (5), with appropriate subscripts for $\theta = 15$, and $\theta = 30$ degrees. We have found such graphs to be unnecessary for the types of debris we have tested. Computations indicate that errors in estimating apparent friction angles can be significant if the friction angle is greater than 15 degrees and if the surface slope exceeds one degree

whereas most of the tests of debris indicated friction angles less than ten degrees.

Our experimental work has been confined to determinations of strengths of relatively weak, completely remolded debris samples - for which the results appear quite reasonable. The method has been used to determine Coulomb strength parameters of debris-flow source materials for prediction of susceptibility of several areas to erosion by the process of debris-flow (Rodine and Johnson, Part IV, in prep.). Single conical penetrometers have been used with success to determine single strength parameters of deep ocean sediments (e.g., Hirst, Richards, and Inderbitzen, 1972) , so the method should enable the determination of both Coulomb strength parameters of the same materials.

APPENDIX

Our solution for the penetration of a frictional cone into an ideal Coulomb plastic is based primarily on a theory developed by Cox, Eason, and Hopkins (1961) for soil plasticity problems with radial symmetry. We refer the reader to this paper for most details of the theory, merely indicating novel derivations in following pages. Our solution also is based on the theory of limiting lines and discontinuities which are not clearly explained anywhere, in our opinions, but which can be understood by studying papers by Cox, Eason, and Hopkins (1961), Hill, Lee and Tupper (1951), Hill (1961), Prager (1954), and a textbook by Prager and Hodge (1951).

As mentioned in the text, we assume that the interface between the cone and the Coulomb material is a limiting line, or an envelope of slip lines, in fact, an envelope of $\underline{\alpha}$-slip lines in the terminology of Cox, Eason, and Hopkins (1961). In one of our abortive attempts at a solution we assumed that the cone surface was composed of straight $\underline{\alpha}$-slip lines. However, the solution gave anomalous results for the mean stress, $\underline{p}$, on the surface of the cone. We also tried a computer solution, integrating along the slip lines from the free surface to the cone surface. The computer solution would converge only if the $\underline{\alpha}$-slip lines were allowed to become asymptotic with the cone surface, that is, if the cone surface became an ideal limiting line (e.g., Prager and Hodge, 1951, p. 149-154). A plot of the computer generated slip-line pattern for $\underline{\phi}$ = 20 degrees is shown in Fig. 3. The limiting line concept provided the clue to the solution presented in following paragraphs. Furthermore, a rather thorough investigation of solutions

of closely related problems indicates to us that the following solution is correct.

The problem is to calculate the static force required to push a frictional cone to a certain depth in a dense, Coulomb material. We ignore pore water pressure for several reasons explained in Part III (Rodine, in press). We assume that movements are so slow that accelerative and viscous effects can be ignored. The weight of the loaded cone must equal the integral of the normal and shear stresses applied to the cone by dense Coulomb material. Now we will calculate these stresses. The stresses within the Coulomb material, at some distance from the cone, are of no interest so we will focus on an element of material in direct contact with the cone (Fig. A1). The element, coordinate system, and the stress components are shown in Fig. A1. First, we will derive equations of equilibrium for the element and then substitute expressions for stresses in a Coulomb material into these equations.

The areas of the sides of the element, shown in Fig. A1, are:

$$\begin{aligned} A_\Gamma &= [r + (dN/2)\cos\Theta - ds\sin\Theta]\, dN\, d\eta \\ A_B &= [r + (dN/2)\cos\Theta]\, dN\, d\eta \\ A_F &= [r + dN\cos\Theta - (dS/2)\sin\Theta]\, dS\, d\eta \\ A_R &= [r - (dS/2)\sin\Theta]\, dS\, d\eta \\ A_S &= dN\, dS, \end{aligned} \tag{A1}$$

and the volume of the element is:

$$V = [r + (dN/2)\cos\Theta - (dS/2)\sin\Theta]\, dN\, dS\, d\eta \tag{A2}$$

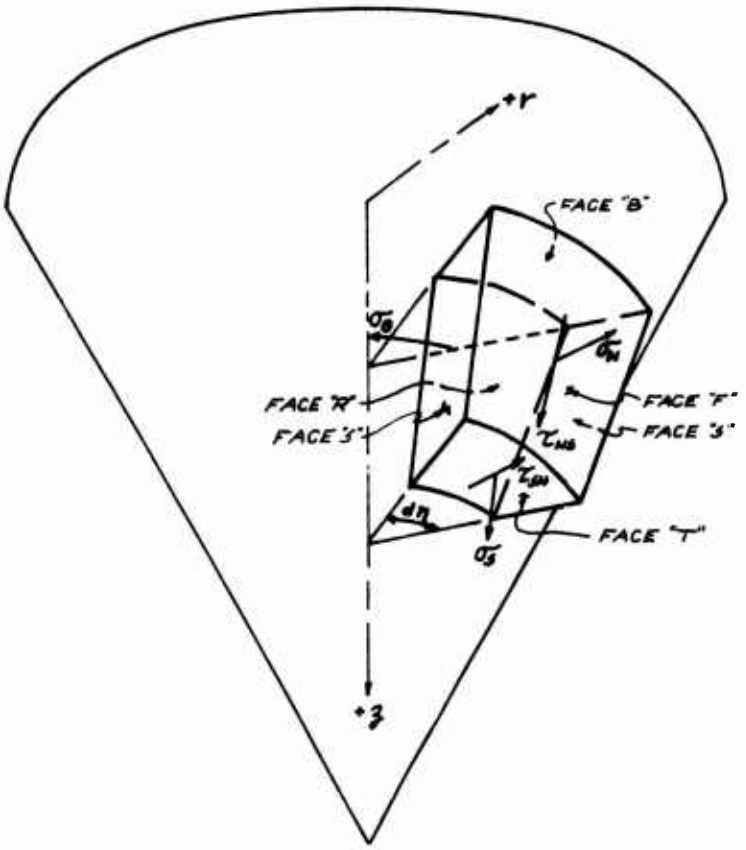

Figure A1. An element of debris on the surface of a conical penetrometer, indicating components of stress and identifying faces, coordinates, and angles.

Radial symmetry requires that σ_Θ, Figs. A1, A2, be a principal stress, and that: $\tau_{N\Theta} = \tau_{\Theta N} = \tau_{S\Theta} = \tau_{\Theta S} = 0$.

Allowing the stress components to vary in space leads to the equations of equilibrium in the S and N directions (Fig. A2):

$$\left.\begin{aligned}
&(\sigma_S + \frac{\partial \sigma_S}{\partial S}\, dS)\, A_T - \sigma_S A_B + (\tau_{NS} + \frac{\partial \tau_{NS}}{\partial N}\, dN)\, A_F - \tau_{NS} A_R \\
&\qquad + W \cos\Theta + 2\sigma_\Theta A_S\, (\tfrac{d\eta}{2}) \sin\Theta = 0 \\
&(\sigma_N + \frac{\partial \sigma_N}{\partial N}\, dN)\, A_F - \sigma_N A_R + (\tau_{SN} + \frac{\partial \tau_{SN}}{\partial S}\, dS)\, A_T - \tau_{SN} A_B \\
&\qquad + W \sin\Theta - 2\sigma_\Theta A_S\, (\tfrac{d\eta}{2}) \cos\Theta = 0
\end{aligned}\right\} \quad (A3)$$

where: $W = \rho g V = \gamma V$; ρ is density; g is acceleration of gravity; and γ is unit weight.

Substituting expressions for the areas from Eq. (A1) and the volume from eq. (A2) into eqs. (A3) yields the differential equations of equilibrium:

$$\left.\begin{aligned}
&\frac{\partial \sigma_S}{\partial S} + \frac{\partial \tau_{NS}}{\partial N} + \frac{\tau_{NS}}{r} \cos\Theta + \frac{\sigma_\Theta - \sigma_S}{r} \sin\Theta + \gamma \cos\Theta = 0 \\
&\frac{\partial \sigma_N}{\partial N} + \frac{\partial \tau_{SN}}{\partial S} - \frac{\tau_{SN}}{r} \sin\Theta + \frac{\sigma_N - \sigma_\Theta}{r} \cos\Theta + \gamma \sin\Theta = 0
\end{aligned}\right\} \quad (A4)$$

Moment equilibrium requires that: $\tau_{NS} = \tau_{SN}$.

There are four stress components in the two equilibrium eqs. (A4). The number of variables can be reduced from four to two by means of the Coulomb theory of plasticity, eq. (1), and by making a special

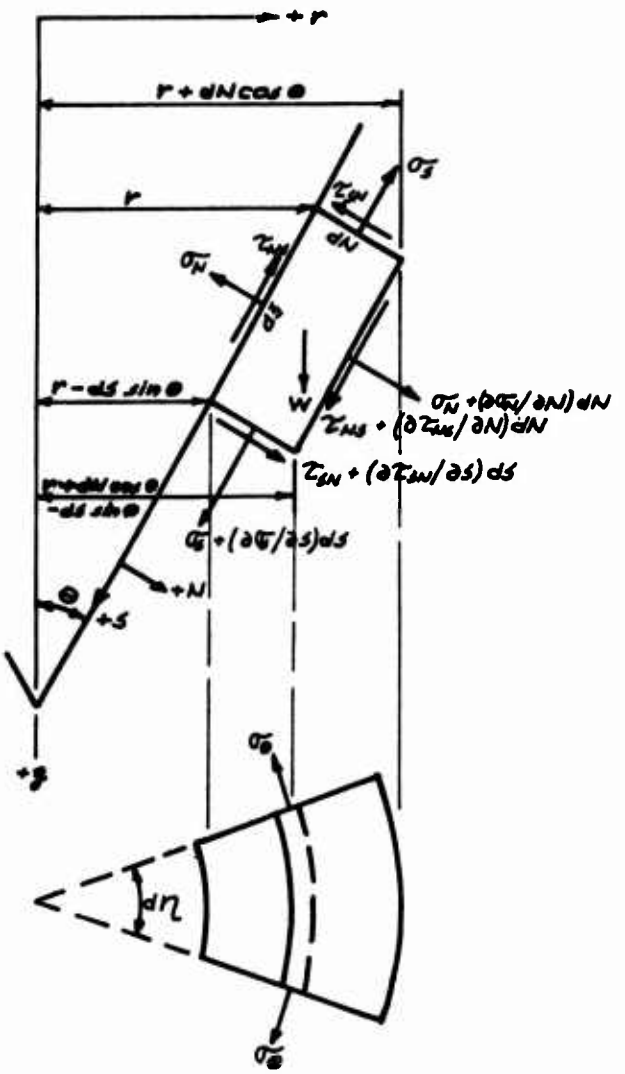

Figure A2. Cross sections of an element of debris on the surface of a cone, indicating variations in stress components and coordinates of key points.

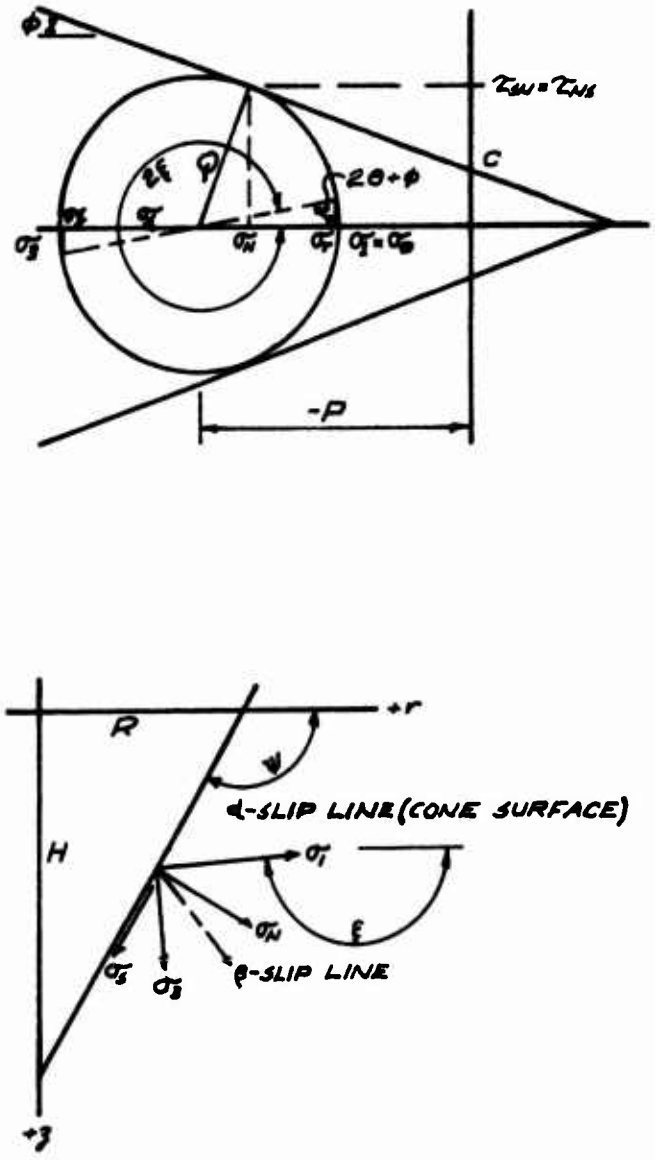

Figure A3. Mohr-Coulomb diagram for an element of material in contact with a cone and definitions of angles used in theoretical analysis.

assumption about the circumferential stress, σ_θ. Three of the stress components can be related to a variable mean stress, p, and a variable angle, ψ, by analysis of the Mohr-Coulomb diagram shown in Fig. A3. The angle ψ, shown in Fig. A3, is the angle between the horizontal and the α-slip line. Now, the surface of the cone is an α-slip line so that the angle ψ is constant along the cone. Accordingly, Fig. A3 shows that the mean stress along the cone boundary is:

$$p = -(1/2)(\sigma_1 + \sigma_2) = (Q - C\cos\phi)/\sin\phi, \tag{A5}$$

where Q is defined in Fig. A3. The components of normal and shear stresses along the cone are:

$$\left.\begin{aligned} \sigma_S &= -p - Q\sin\phi \\ \sigma_N &= -p + Q\sin\phi \\ \tau_{SN} &= Q\cos\phi \end{aligned}\right\} \tag{A6}$$

Either p or Q could be eliminated from eqs. (A6) with the use of eq. (A5).

Finally, we adopt the Haar-von Karmen hypothesis (e.g., Cox, Eason, and Hopkins, 1961), which states that the circumferential stress, σ_θ, is equal to one of the other two principal stresses. At the free surface, $\sigma_1 = 0$, and the maximum compressive stress, σ_3, is directed in a radial direction, so it appears most reasonable to select

$$\sigma_\theta = \sigma_2 = \sigma_1 = -p + Q, \tag{A7}$$

throughout the Coulomb material.

Now, using the assumption that the cone surface is a limiting line, the change in orientation of the principal stresses, relative to the

normal, N, and tangential, S, directions is zero (e.g., see fig. 49, Prager and Hodge, 1951, p. 150). That is, both $d\psi = 0$ and $d\xi = 0$. Accordingly, for the entire element near the boundary, we merely substitute eqs. (A6) and (A7) into the equilibrium eqs. (A4).

$$\left.\begin{aligned} -\frac{\partial p}{\partial S}(1+\sin^2\phi) + \frac{\partial p}{\partial N}(\sin\phi\cos\phi) + \frac{Q}{r}(\cos(\Theta-\phi)+\sin\Theta) + \gamma\cos\Theta = 0 \\ \frac{\partial p}{\partial S}(\sin\phi\cos\phi) - \frac{\partial p}{\partial N}\cos^2\phi - \frac{Q}{r}(\sin(\Theta-\phi)+\cos\Theta) + \gamma\sin\Theta = 0 \end{aligned}\right\} \quad (A8)$$

Now the equilibrium equations contain only one dependent variable, p (or Q), instead of four.

Solving eqs. (A8) for $\partial p/\partial S$ we have

$$\frac{\partial p}{\partial S} = \frac{Q}{r}\{\cos(\Theta-\phi)+\sin\Theta-[\sin(\Theta-\phi)+\cos\Theta]\tan\phi\} + \gamma[\cos\Theta+\sin\Theta\tan\phi] \quad (A9)$$

The next step is to integrate eq. (A9) along the cone boundary in order to determine the mean stress distribution. Skipping all the intermediate steps eq. (A9) integrates to

$$p = C(\operatorname{ctn}\Theta + 1)\,\ell n\left(\frac{R}{r}\right) + \gamma\operatorname{ctn}\Theta\,(R - r) + p_o \quad (A10a)$$

for $\phi = 0$, and

$$Q = Q_o(R/r)^A + [\gamma B/(1 + A)]\,[R(R/r)^A - r] \quad (A10b)$$

for $\phi > 0$. Here R is the radius of the cone (Fig. A3b), p_o and Q_o are constants of integration, and

$$\left.\begin{aligned} A &= [\cos(\Theta-\phi)+\sin\Theta-\tan\phi(\sin(\Theta-\phi)+\cos\Theta]\,(\sin\phi/\sin\Theta) \\ B &= [\cos\Theta+\tan\phi\sin\Theta]\,(\sin\phi/\sin\Theta) \end{aligned}\right\} \quad (A11)$$

Equations (A10) define the relations between the mean stress and the radial distance along the cone; thus, if these equations are substituted into eqs. (A6), the stresses along the cone are completely defined. The force required to push the cone into the Coulomb material is

$$F = \int_0^R (-\sigma_N \sin\Theta + \tau_{SN} \cos\Theta)\ (2\pi r/\sin\Theta)\ dr. \qquad (A12)$$

Substituting eqs. (A10) into the second and third of eq. (A6), thence into eq. (A12), and performing the integration yields

$$F = C\ \pi R^2\ [0.5 + 1.5\ \mathrm{ctn}\ \Theta + p_o] + \gamma\ \pi R^3\ \mathrm{ctn}\ \Theta/3 \qquad (A13a)$$

for $\underline{\phi} = 0$, and

$$F = C\ \pi R^2\ [(2D(Q_o/C))/(2-A) - \mathrm{ctn}\ \phi] + \gamma\ \pi R^3\ 2DB/(3(2-A)), \qquad (A13b)$$

or with $H = R\ \mathrm{ctn}\ \phi$,

$$F = C\ \pi H^2\ \tan^2\phi\ [(2D(Q_o/C))/(2-A) - \mathrm{ctn}\phi] + \gamma\pi H^3\tan^3\phi\ 2DB/(3(2-A)) \qquad (A13c)$$

for $\underline{\phi} > 0$, where

$$D = (\mathrm{ctn}\ \phi + \mathrm{ctn}\ \Theta)\ \cos\ \phi \qquad (A14)$$

In order to evaluate the constants of integration, $\underline{Q_o}$ and $\underline{p_o}$ in eqs. (A13), we use the slip-line, or characteristic, equations (Cox, Eason, and Hopkins, 1961, p. 20, eqs. (4.3.11)). At the singular boundary point, $\underline{A}$ in Fig. 3, the $\underline{\beta}$- characteristic line degenerates to a line which has zero arc length, but changes direction. Thus, at the singular point:

$$dp = 2C\, d\psi \tag{A15a}$$

for $\underline{\phi} = 0$, and:

$$dQ = 2Q \tan \phi \; d\psi \tag{A15b}$$

for $\underline{\phi} > 0$. Where $\underline{\psi}$ is a variable angle between the horizontal $\underline{R}$-direction and the direction of the $\underline{\alpha}$-characteristic, or slip, line. Integrating eq. (A15), from the free surface of the Coulomb material to the cone surface yields:

$$p_o = C(1 + \pi/2 + 2\Theta) \tag{A16a}$$

for $\underline{\phi} = 0$, because at the free surface $\underline{p} = \underline{C}$, and $\underline{\psi} = \pi/4$, and at the cone boundary $\underline{\psi} = \pi/2 + \underline{\Theta}$ and

$$Q_o = C \tan (\pi/4 + \phi/2) \exp [\tan \phi \, (\pi/2 + 2\Theta + \phi)] \tag{A16b}$$

for $\underline{\phi} > 0$, because at the free surface $Q = C \tan (\pi/4 + \phi/2)$, and $\underline{\psi} = \pi/4 - \phi/2$, and at the cone boundary $\underline{\psi} = \pi/2 + \underline{\Theta}$.

Thus eqs. (A13), with constants defined in eqs. (A11), (A14), and (A16) are expressions for the forces required to push cones into Coulomb plastic material. The solution is based on the assumption that the surface of the Coulomb plastic is flat. If the surface slopes, one uses eqs. (5) in the text, instead of eqs. (A16), for p_o and Q_o. The other equations are unchanged.

BIBLIOGRAPHY

Cox, A. D., Eason, G., and Hopkins, H. G., 1961, Axially symmetric plastic deformation in soils: Philosophical Transactions of the Royal Society of London, Series A, Volume 254, p. 1-45.

Hampton, M. A., 1972, The role of subaqueous debris flow in generating turbidity currents: Journal of Sedimentary Petrology, Volume 42, Number 4, p. 775-793.

Hansbo, S., 1957, A new approach to the determination of the shear strength of clay by the fall-cone test: Royal Swedish Geotechnical Institute Proceedings Number 14, 47 p.

Hill, R., The mathematical theory of plasticity: Oxford University Press, 355 p.

_____, 1961, Discontinuity relations in mechanics of solids: in: Progress in Solid Mechanics, Volume 2, North-Holland Publishing Co., p. 247-276.

_____, Lee, E. H., and Tupper, S. J., 1951, A method of numerical analysis of plastic flow in plane strain and its application to the compression of a ductile material between rough plates: American Society of Mechanical Engineers, Journal of Applied Mechanics, Volume 18, p. 46-52.

Hirst, T. J., Richards, A. F., and Inderbitzen, A. L., 1972, A static cone penetrometer for ocean sediments: American Society for Testing and Materials, Special Technical Publication 501, p. 69-80.

Johnson, A. M., 1965, A model for debris flow: Ph.D. Dissertation, The Pennsylvania State University, University Park, Pennsylvania.

_____, 1970, Physical processes in geology: Freeman, Cooper and Co., 577 p.

_____, and Hampton, M. A., 1969, Subaerial and subaqueous flow of slurries: Final Report, U. S. Geological Survey; Branner Library, Stanford University, Stanford, California.

Lambe, T. W., 1951, Soil testing for engineers: John Wiley and Sons, New York.

_____, and Whitman, R. V., 1969, Soil mechanics: John Wiley and Sons, New York, 553 p.

Prager, W., 1954, Discontinuity fields of plastic stress and flow: American Society of Mechanical Engineers, Proceedings of the Second U. S. National Congress of Applied Mechanics, p. 21-32.

_____, and Hodge, P. G., 1951, Theory of perfectly plastic solids: John Wiley and Sons, New York, 263 p.

Rebinder, P. A., 1967, Investigation of the physicochemical mechanics of clay-mineral dispersions: Israel Program for Scientific Translations, Jerusalem, 146 p.

Rodine, J. D., (in prep.), Analysis of mobilization of debris flows: Part I, Processes of initiation of debris flows.

_____, (in prep.), Analysis of mobilization of debris flows: Part III, The ability of debris heavily freighted with coarse clastic materials to flow in gentle slopes.

Rodine, J. D., and Johnson, A. M., (in prep.), Analysis of mobilization of debris flows: Part IV, Mobility index - A measure of the potential for debris flow.

Sanglerat, G., 1972, The penetrometer and soil exploration: Elsevier Publishing Co., New York, 464 p.

Shield, R. T., 1953, Mixed boundary value problems in soil mechanics: Quarterly of Applied Mathematics, Volume 11, p. 61-75.

ANALYSIS OF THE MOBILIZATION OF DEBRIS FLOWS

PART III: THE ABILITY OF DEBRIS, HEAVILY FREIGHTED WITH COARSE CLASTIC MATERIALS, TO FLOW ON GENTLE SLOPES

ABSTRACT

Observations of many debris-flow deposits on gently-sloping alluvial fans have disclosed that debris commonly is heavily loaded with coarse clastic material and contains large isolated blocks. This paper describes how debris charged with coarse granular material can transport large blocks and flow on gentle slopes.

The ability of debris flows to support large blocks can be understood in terms of the high unit weight of the displaced debris plus the strength of the fluid phase; that is, the blocks float in the debris as the result of a small density difference between the blocks and the debris, plus the cohesive strength of the clay-water slurry.

The ability of coarse clastic debris to flow on gentle slopes probably is a result of poor sorting of debris-flow materials which contain minor amounts of clay. The poor sorting allows the debris to have a high density, yet have essentially no interlocking of clasts. The high density of the debris reduces effective normal stresses between clasts, thereby reducing apparent friction of the mixture.

The clay fraction, even if minor, plays a critical role in determining strength properties of debris. The mixture of clay plus water provides a cohesive slurry that supports fine-grained particles within the debris, as well as reducing the effective normal stresses between the particles. The increased unit weight of the clay plus water plus fine-grained particles allows the support of coarser grained particles. The pyramiding upon the clay-water slurry continues until the entire debris mass is supported in a virtually frictionless position because of the reduced effective normal stress and lack of particle interlocking.

Experimental results of mixing sand-sized particles with a slurry of clay plus water indicate that 45 to 55 volume percent of a single size, and up to 64 percent of two selected sizes, can be added before interlocking occurs. Theoretical analysis of multi-size classes suggest that 89 to more than 95 volume percent debris can be clastic material without significant particle interlocking.

INTRODUCTION

In the summer of 1917 a thundershower set a large debris flow in motion near the mining camp of Panamint City, in the Panamint Mountains near Death Valley, California (Johnson, 1965). The debris flow, charged with cobbles and boulders, coursed down Surprise Canyon and across a gently sloping alluvial fan. In one place, where the fan slopes at five degrees, stream activity on the alluvial fan has since exposed the debris-flow deposit and two large rock blocks (Fig. 1). Other examples of abundant coarse debris in debris-flow deposits on gentle slopes have been reported by Krumbein (1940, 1942), Troxell and Peterson (1937), Sharp and Nobles (1953), Mullineaux and Crandell (1962), Bull (1964), Bonney (1902), and Fryxell and Horberg (1943). The abundance of coarse clastic material transported by debris flows suggests high strength, yet, the ability to flow on gentle slopes suggests low strength.

This study is an inquiry into the ability of debris heavily freighted with coarse clastic materials to flow on gentle slopes and into the effect of grain-size distributions on the Coulomb strength parameters and on the unit weight of the debris. A series of experiments were made to determine Coulomb strengths of artificial debris consisting of mixtures of clay-water slurry and various concentrations of single-sized or two-sized spherical particles. Packing theory is used to analyse the experimental results as well as to evaluate interlocking of granular materials with wide ranges of sizes.

Experimental studies closely related to that reported here have been made by Seed et al. (1964A, 1964B), Trask (1959), Johnson (1969),

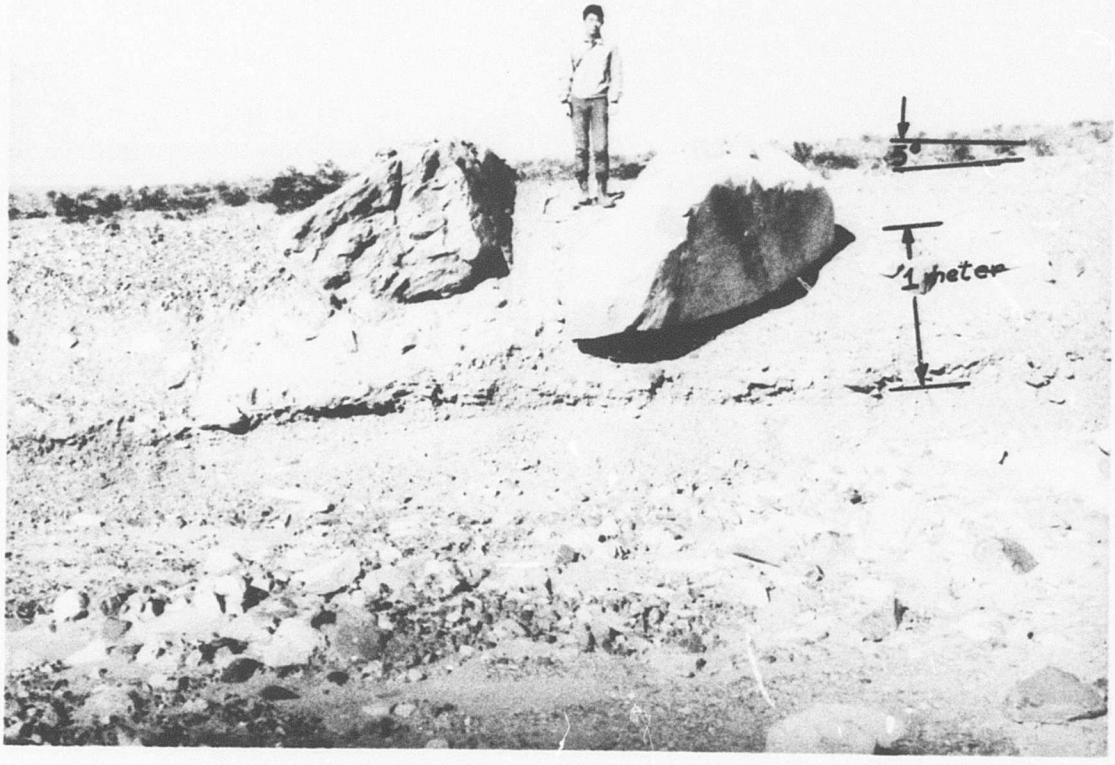

Figure 1. Debris-flow deposit of 1917 at Surprise Canyon near Death Valley, California. The deposit is about 1 m thick and slopes 5 degrees. The boulder on the right is about 3 m wide, 1 m deep and 2 m high. The boulder on the left is about 1.6 m wide, 2.6 m deep and 1.6 m high.

and Hampton (1972). Seed et al. determined Atterberg limits for mixtures of water and kaolinite, illite and bentonite and for mixtures of water, clay and sand or silt. Among other things, they determined that Atterberg limits for mixtures of clay minerals can be predicted if one knows the composition of the mixture, and that sand behaves as an inert filler if widely dispersed. Trask determined forces required to shear mixtures of clay, water and sand or silt using a vane shear apparatus, as a function of grain size, water content, clay type and weight ratio of clay to sand. Johnson made a similar but less comprehensive study, using one type of clay mixed with tap water and various proportions of sand and a sphere strength-meter, to measure Tresca strength, and concluded that the clay-water mixture largely controls the apparent strength of the artificial debris unless the sand comprises more than about 50 weight percent of the dry clay in the debris. Hampton made similar experiments also, using kaolinite or montmorillonite, sand or silt and tap water or artificial sea water to estimate whether some relatively well-sorted marine sands might have been transported by subaqueous debris flows.

Early stages of the research were supported by the U. S. Geological Survey, Contract no. 14-08-0001-10884, under the direction of Parke D. Snavely, Jr. Most of the research has been supported by the U. S. Army Research Office, Durham, North Carolina, Grant no. DA-ARO-D-31-124-71-G158, under the supervision of Dr. Finn Bronner.

A THEORY OF DEBRIS STRENGTH

A combination of Coulomb strength and Newtonian viscosity was proposed by Johnson to model the flow of debris (1965). The model has been used to explain the steep terminal margins of debris-flow deposits, the tendency of debris to form U-shaped channels, and even the transformation of subaqueous debris flows into turbidity currents (Johnson, 1970; Johnson and Hampton, 1968, 1969; Hampton, 1970, 1972). The Coulomb strength model is:

$$\tau = C - \sigma_n \tan \phi \qquad (1)$$

where τ is shear stress at failure, C is apparent cohesion, σ_n is normal stress at failure, and ϕ is apparent friction angle. Equation (1) shows the dependence of frictional strength and the independence of cohesive strength on the normal stress. If a debris-flow deposit is wide and long compared to its thickness, equilibrium requirements and eq. (1) lead to the critical thickness T_c, at which flow ceases:

$$T_c = C/[\gamma \cos \delta \ (\tan \delta - \tan \phi)] \qquad (2)$$

where γ is unit weight (density times acceleration of gravity), and δ is slope angle (Johnson, 1965). Equation (2) predicts that flow is impossible for a finite thickness of debris if the apparent friction angle equals or exceeds the slope angle. Thus, the effective friction angle of the debris at Surprise Canyon, Fig. 1, must have been less than the slope angle, that is, less than 5 degrees.

Although eq. (2) predicts that the apparent friction angle of debris-flow material must be less than the slope angle, it provides no

clues as to why the debris should have low frictional strength. In order to gain some insight into the strength of debris let us first consider a sample of ideal debris composed of water, clay and sand. The mixture of water and clay will be called the fluid phase and the sand particles the granular phase (e.g., Mead, 1925; Hampton, 1972). We have tested strengths of many kaolinite clay-water slurries with the conical penetrometers described by Rodine and Johnson (Part II, in press) and have found them to possess virtually no frictional strength even when apparent cohesion was several thousand dynes/cm^2. Thus, we will describe the fluid phase in terms of cohesion and unit weight. Now, suppose that we add the sand to the fluid phase, and that the strength and density of the fluid phase are sufficient to completely support the sand particles. If the volume percentage of sand is low, and the sample homogeneous, the strength will be provided by the fluid phase, and the unit weight will increase in proportion to the volume of sand. As more sand is added to the slurry, it will occupy a larger share of the total volume, and the strength will remain constant, equal to the cohesion of the fluid phase, until enough sand has been added to cause significant particle interactions. Let us consider these particle interactions.

Rowe (1962) has thoroughly analyzed interactions among rods and spheres packed in various ways and has developed a rather convincing explanation for the applicability of Coulomb's law to the description of the effective strength of granular materials. Here we will briefly review part of his theory. The resistance to horizontal movement of a circular rod nestled between two other rods, Fig. 3, is a combination

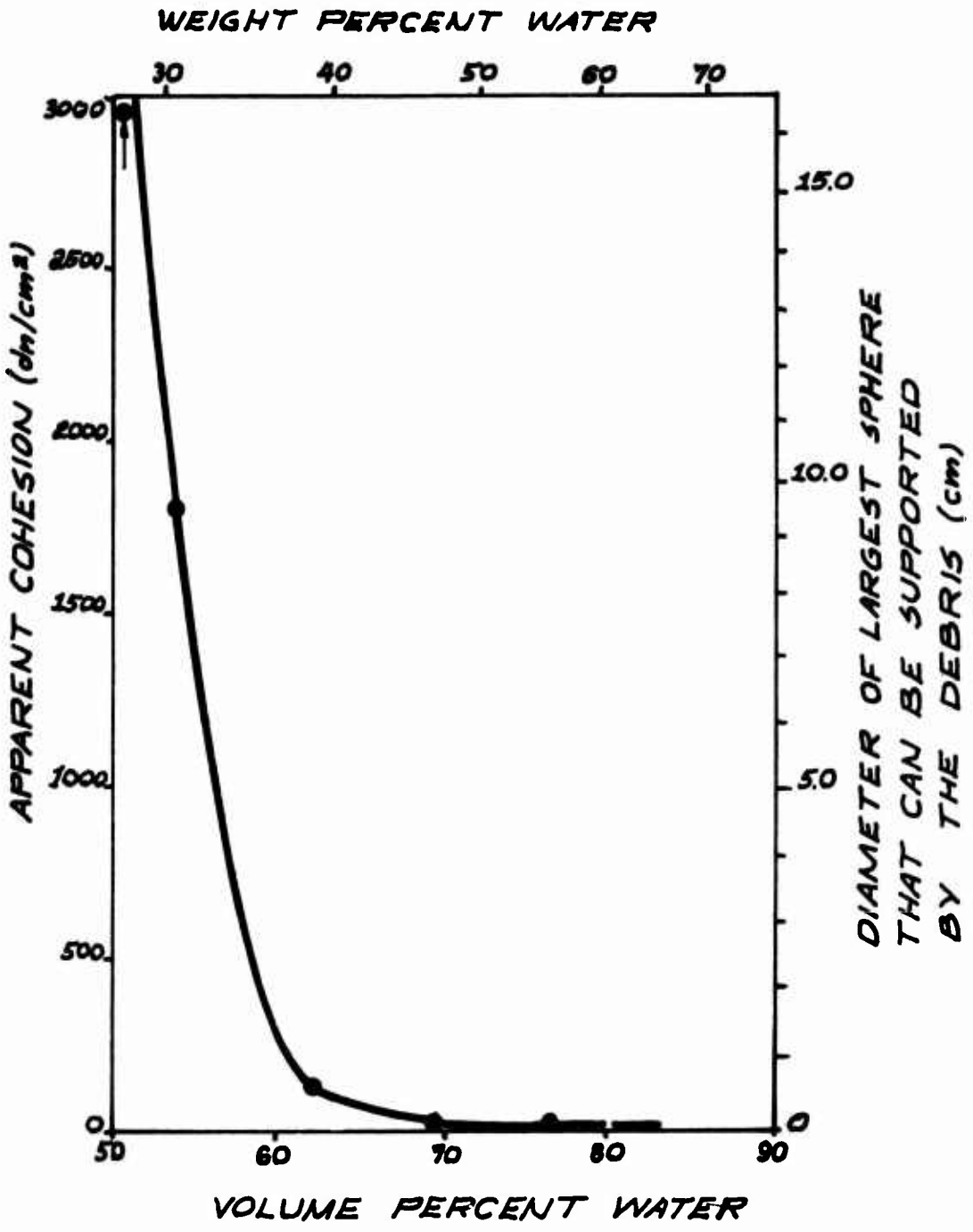

Figure 2. Volume and weight percent of water, mixed with kaolinite clay plus 1% calgon by weight of clay, as a function of the cohesive strength and theoretical diameter of the largest sphere that can be supported.

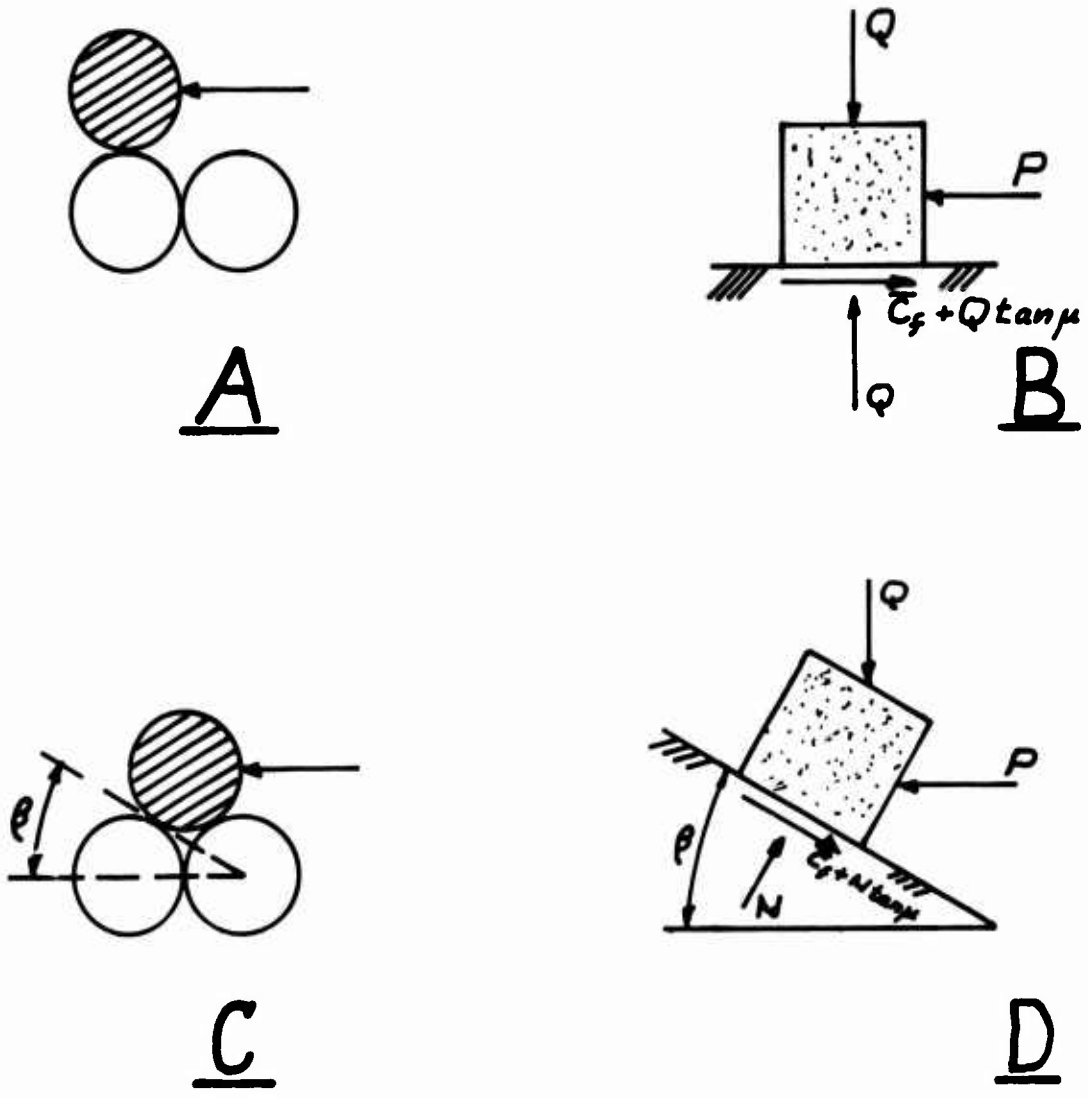

Figure 3. Two-dimensional friction models.

A. Rods packed cubically without interlocking.

B. Block on horizontal surface, situation analogous to A. Tan μ is the coefficient of sliding friction.

C. Interlocking rods.

D. Block on inclined surface, situation analogous to C.

of the sliding friction of the surfaces of the rods and the interlocking of the rods. If one rod is on top of another (Fig. 3A) and it is not allowed to roll because of adjacent rods not shown in Fig. 3, the resistance to slippage depends on the area of contact, the effective normal stress, the cohesive bond and the contact friction. The situation can be modeled by a block on a surface, as shown in Fig. 3B. The horizontal force, $\underline{P}$, required to slide the block is equal to the cohesive force, $\underline{C}_f$, plus the frictional force, Q tan μ, so that

$$P = C_f + Q \tan \mu \tag{3}$$

If the normal force, $\underline{Q}$, is zero, the horizontal force merely must equal the cohesive force for sliding to occur. If, however, the rods are interlocked as shown in Fig. 3C, the resistence to sliding can be modelled as in Fig. 3D, where a block is to be pushed up an inclined plane by a horizontal force, $\underline{P}$. Summing forces and rearranging terms,

$$P = \{C_f/[\cos\beta(1 - \tan\beta\tan\mu)]\} + Q \tan (\mu + \beta) \tag{4}$$

An equivalent result has been derived by Rowe (1962, eq. 11). Comparison of eqs. (3) and (4) indicates that the angle of interlocking, $\underline{\beta}$, of the ideal rods is added to the angle of sliding friction, $\underline{\mu}$, to produce the effective friction angle of the ideal rods,

$$\phi_e = \beta + \mu \ . \tag{5}$$

In addition, however, eq. (4) indicates that the angle of interlocking affects the cohesion of the ideal rods so that the effective cohesion is

$$C_e = C_o/[\cos\beta(1 - \tan\beta\tan\mu)], \tag{6}$$

where C_o is the cohesive force per unit of area between rods.

Thus, if the volume percent of the granular phase in the ideal debris is small, the strength of the debris will be determined essentially by the cohesive strength of the fluid phase. If the volume percent is sufficiently large, the particles of the granular phase begin to touch and the strength will consist of the contact friction of the grains plus the cohesive strength of the fluid phase. Finally, if the volume percent of the granular phase is even larger, the grains will interlock and both the internal friction angle and the cohesion of the debris will increase.

Effective friction angle, eq. (5), and effective cohesion, eq. (6), were implicitly derived in terms of effective stress, σ_e,

$$\sigma_e = \sigma - u, \tag{7}$$

where, σ is total stress, and u is pore pressure (e.g., Lambe and Whitman, 1969). For soils with water occupying the voids between particles, pore pressure buoys the soil particles, reducing the strength of the soils. Similarly the boulders shown in Fig. 1 probably were supported during flow by the strength of the debris and by buoyancy. The buoyant force acting on a boulder is equal to the weight of the displaced volume of material, according to Archimedes' Principle. An approximate formula relating the weight of an ellipsoidal clast to the buoyant force plus the force due to the debris strength has been derived by Johnson (1970, p. 486):

$$(4/3)\pi(abh)\gamma_c = (4/3)\pi(abhn)\gamma_d + \pi(ab)C\ f(\phi), \tag{8}$$

where a, b, and h are one-half the width, breadth and height, respectively, γ_c is unit weight of the clast, γ_d is unit weight of the debris, $f(\phi)$ is a function of ϕ (Rodine and Johnson, Part II, in press, fig. 9) ranging from 6.1 for $\phi = 0$ to 62.0 for $\phi = 30°$, and n is the ratio of the volume of the submerged part of the clast to the total clast volume. Rearranging eq. (8) provides an expression for the maximum height of clast that can be supported.

$$h = (3/4)\ C\ f(\phi)/\ (\gamma_c - n\gamma_d) \tag{9}$$

If a clast is completely submerged, n in eq. (9) is unity in which case the gross unit weight of the debris, γ_d, is a critical parameter in determining the size of clast that can be transported. Now, if the clast is much larger than the particles of the remainder of the granular phase of the debris, as the blocks shown in Fig. 1, the unit weight of the debris displaced by the clast certainly is equal to the average unit weight of the granular and fluid phases of the debris, exclusive of the large clast. Suppose, however, that the debris is composed of a fluid phase plus sand plus many boulders, or that the debris is composed of a wide size range of particles. We suggest that the unit weight of debris relative to support of a clast is the unit weight the debris would have if all particles equal to and larger than that clast were removed from the debris. Thus, if the debris consists of a fluid phase plus sand and boulders, the unit weight of the debris relative to support of the sand is the unit weight of the fluid phase and the unit weight of the debris relative to support of the boulders is the unit weight of the mixture of the fluid phase and the sand.

We calculate unit weight of debris relative to transport of granular components as follows. Fig. 4A shows the size distribution for a sample of natural debris from Arroyo Ciervo, Fresno County, California (Bull, 1964) assuming a specific gravity of 2.65 for the particles. About 14.0 volume percent of water would transform the montmorillonite-rich clay fraction of the debris from a stiff to a fluid material, so we will assume that 14.0 percent of water is added to the debris (e.g., Hampton, 1970). Then, relative to silt, the density, ρ_d, of the debris would be,

$$\rho_d = (\rho_{clay}V_{clay} + \rho_{H_2O}V_{H_2O})/(V_{clay} + V_{H_2O}) = 1.59 \text{ gm/cc}$$

Similarly, relative to pebbles,

$$\rho_d = (\rho_{sand}V_{sand} + \rho_{silt}V_{silt} + \rho_{clay}V_{clay} + \rho_{H_2O}V_{H_2O})/$$
$$(V_{sand} + V_{silt} + V_{clay} + V_{H_2O}) = 2.28 \text{ gm/cc}$$

Unit weight is computed by multiplying the debris density by the acceleration of gravity.

Figure 4B, showing the density of the debris relative to the support of each size class, indicates that the density is increased more by addition of the finer size fractions than of the coarser. Apparently, only minor errors would be introduced in computing buoyancy of coarse clasts even if the effective density of the debris, including all particle sizes up to and including the coarse clast size, were used in the computations.

Now we can construct a theory of gross strength of debris. The gross strength of debris depends upon the packing and densities of

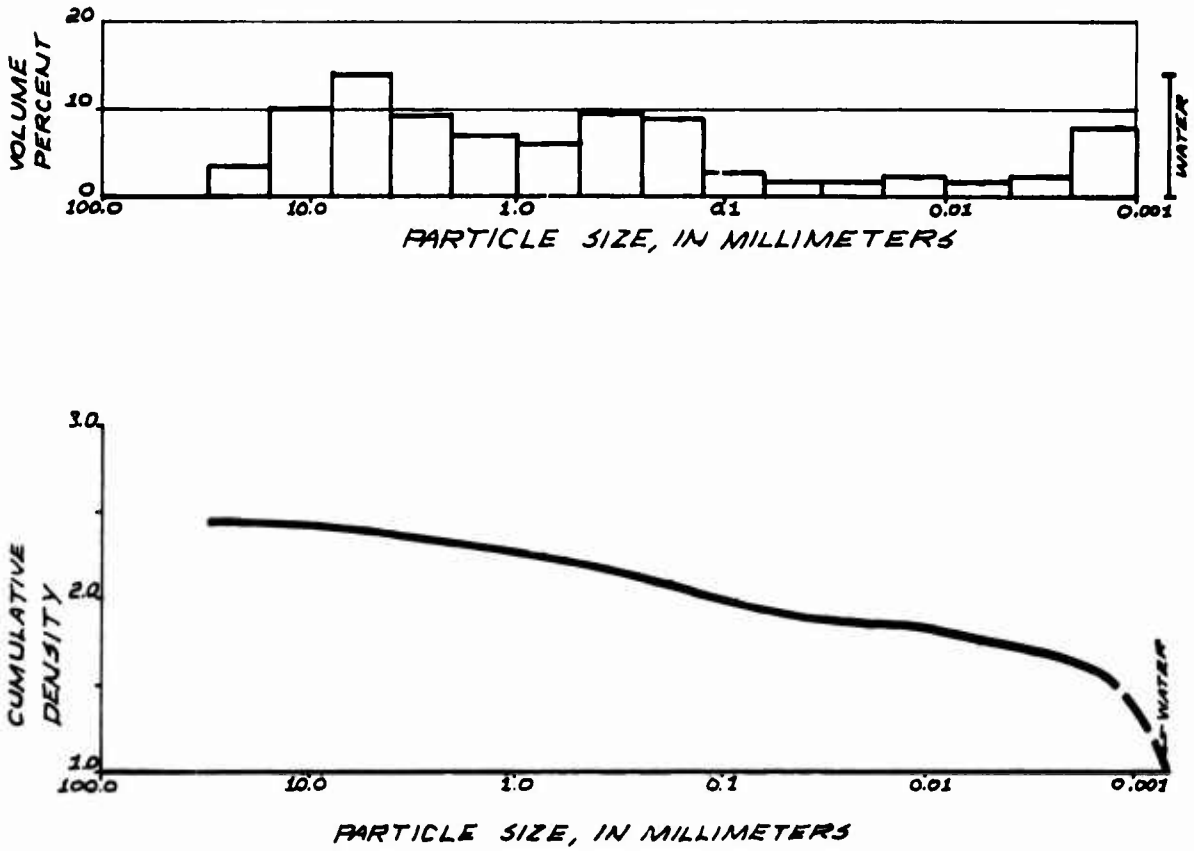

Figure 4. Sample of a debris-flow deposit at Arroyo Ciervo, Fresno County, California (Bull, 1964, Sample no. 18).

A. Size distribution of material coarser than 1 micron.

B. Cumulative density as a function of particle size.

the clasts and upon the cohesive strength and density of the fluid phase. We would attribute much of the cohesive strength of debris to the fluid phase and most of the frictional strength and part of the cohesive strength of debris to the granular phase but, there are interactions between the phases in at least two ways. One is interlocking, as already discussed (eq. (6)). The other is the removal of water from the fluid phase to wet the clasts added to the mixture. We have noted empirically that the wetting of clasts does not appreciably affect the gross strength of the debris, except for fine silt particles which have large surface areas per unit of volume. If there is sufficient fluid phase so that the clasts of the granular phase are not touching one another, normal stresses should have no effect on the strength of the debris and the strength of the mixture should be nearly the same as the cohesive strength of the fluid phase. If the clasts in the granular phase touch, but do not interlock, the gross strength of the mixture will depend on effective normal stresses, the angles of contact friction and cohesion between clasts as well as the cohesion of the fluid phase. The effective normal stresses would be different for different size classes in the granular phase because the debris has different effective densities for the various classes, as explained above, so that they would be difficult to calculate. Finally, if the clasts interlock, the gross strength of the debris depends on the angles of interlocking as well as the parameters stated above. This would be by far the most difficult situation to analyze quantitatively.

EFFECTS OF CONCENTRATION OF THE GRANULAR PHASE ON THE STRENGTH OF DEBRIS

Our theory of debris strength is difficult to check experimentally because it is largely qualitative. However, one aspect of the theory can be evaluated. The theory predicts that the strength of debris should be essentially the strength of the fluid phase if the clasts of the granular phase are disperse, whereas the strength of the debris should be much higher if the clasts interlock. The strength thus is influenced by the packing of the granular phase. In following pages we will test the theory with samples of artificial debris and then apply packing theory to extend the experimental results and provide an explanation for the ability of natural debris to flow on very gentle slopes, yet transport large clasts.

Debris Containing Mono-sized Spheres

We have conducted a series of experiments using kaolinite clay and glass beads, plastic beads and quartz sand to determine effects of concentration of spherical particles on strength of debris (Fig. 5). The grain size of the kaolinite clay is minus 2 microns (supplied courtesy of Dr. Murray, Georgia Kaolinite Co.), as shown in Fig. 6. The glass beads are used for sandblasting and are closely sized (Fig. 6). The samples of artificial debris were mixed thoroughly by hand for about 10 to 15 minutes before first testing. The strength testing requires several individual measurements, involving about 15 minutes (Rodine and Johnson, Part II, in press) so the samples were restirred between measurements in order to maintain homogeneity. Volume percentages of the components of the debris reported in the

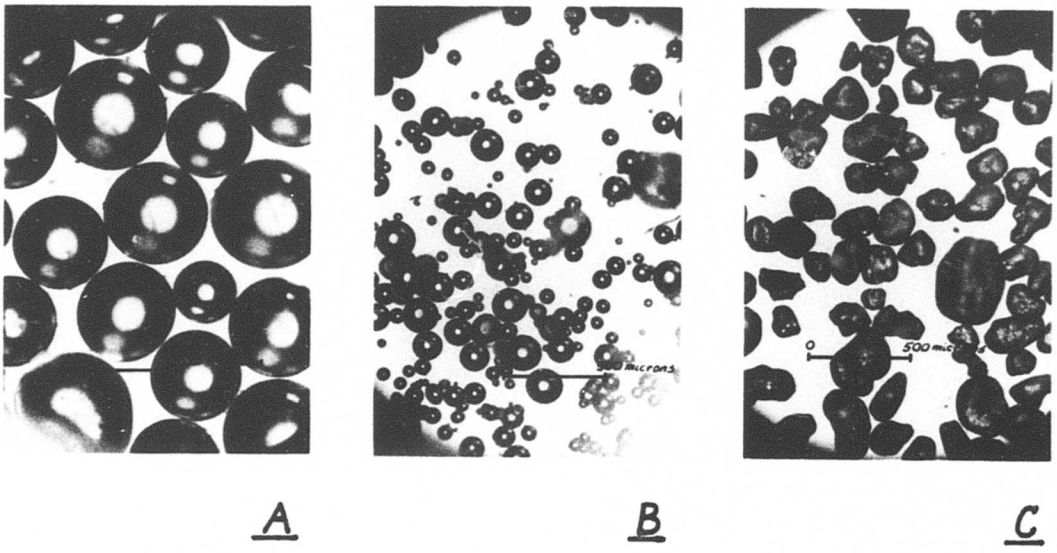

Figure 5. Spherical and subrounded experimental materials.

A. Sand-sized glass beads.

B. Sand-sized plastic beads.

C. Quartz sand.

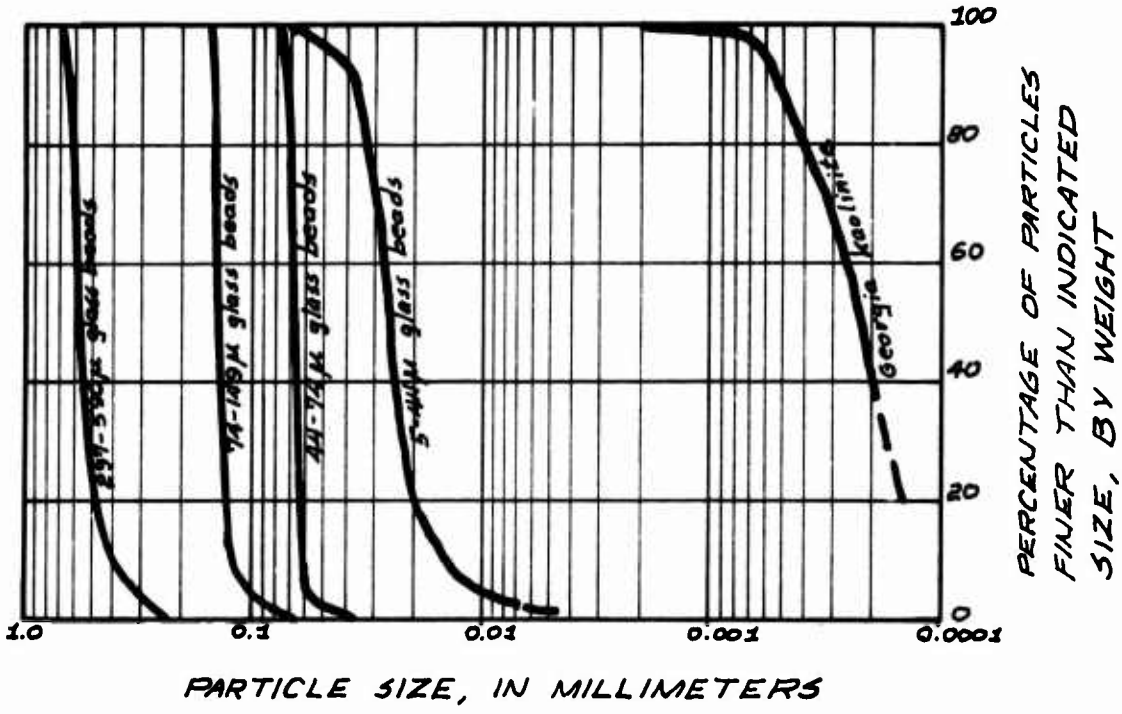

Figure 6. Size distributions of the glass beads and kaolinite clay used in the experiments.

following pages were calculated from measurements of weight percentages, assuming specific gravity of 2.65 for clay and quartz sand and measured values of 1.55 for the glass beads and 1.54 for the plastic beads. Computed values of volume percent should be quite accurate except in samples with high concentrations of granular solids, which contain appreciable air due to the dilation of the sample.

The fluid phase for all experiments was composed of 52 volume percent (30 wt. %) of deionized water mixed with kaolinite clay plus 1% by weight of the clay of Calgon (hexametaphosphate) and apparent Coulomb properties of about $\phi \simeq 0°$ and $C \simeq 150$ dn/cm^2 and a specific gravity of 1.75 (unit wt. 1720 dn/cm^3). The slurry theoretically has enough strength to suspend spherical quartz grains 16 mm in diameter (Fig. 2).

Apparent strength properties of debris consisting of various proportions of the fluid phase and mixtures of mono-sized particles are shown in Fig. 7. Samples of debris with four different sizes of glass beads, one size of plastic bead, and one size of quartz sand were tested. Figure 7A shows apparent friction angle and Fig. 7B shows apparent cohesion of the debris as a function of volume percent of granular phase. In general, the curves indicate that the strength remains equal to that of the fluid phase if less than about 50% of the volume is occupied by granular particles. Apparent angles of internal friction of debris containing spherical beads larger than 44 microns all abruptly increase beginning at concentrations of about 55% beads and apparent cohesion abruptly increases starting at about 60% beads, except for debris containing glass beads of 44-74 microns in diameter,

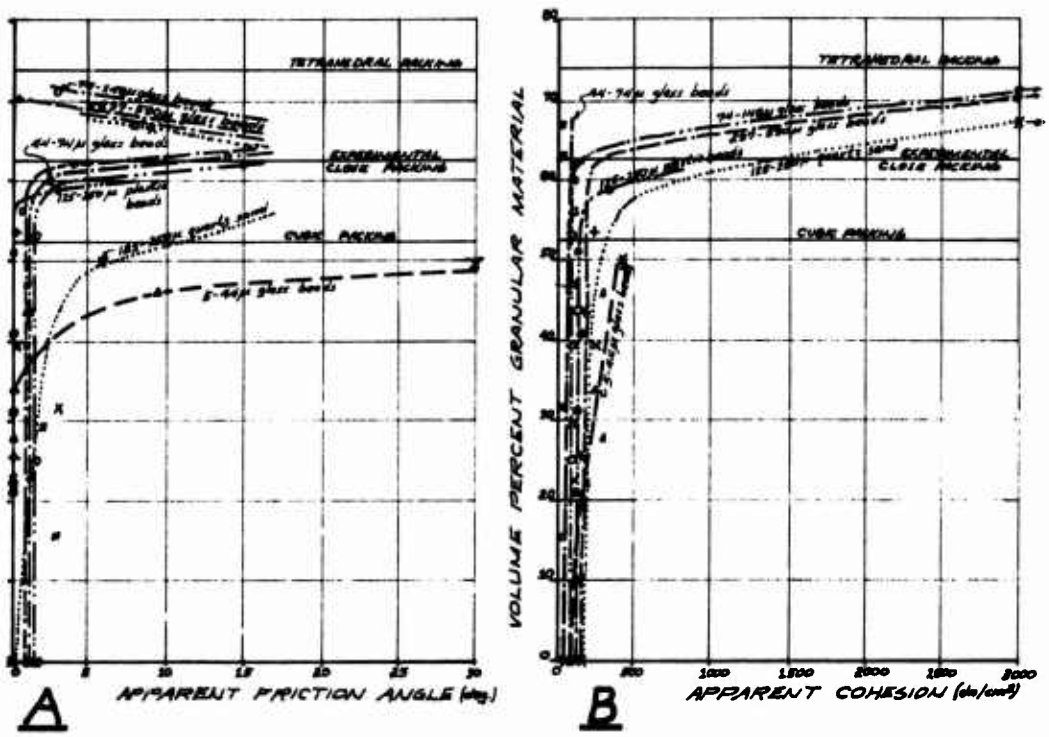

Figure 7. Experimental results of the strength of mono-sized spheres plus clay-water slurry as a function of the volume percent of the granular phase.

A. Apparent friction angle.

B. Apparent cohesion.

the apparent cohesion of which does not increase unless the beads comprise at least 67% of the mixture. The apparent friction angle of debris increases with increasing concentrations between approximately 55 and 64%, however, with further increases in concentrations the apparent friction angle decreases. The relations between concentration of solids and strength parameters for quartz sand are similar to those for spherical beads, except that the strength parameters start to increase at concentrations of about 10% lower than those for spherical beads.

Certainly the most striking differences in relations between strength parameters and concentration of granular solids were detected in samples containing silt-sized particles as the granular phase. The test with debris containing glass beads of 5 to 44 microns show a gradual increase in apparent cohesion for concentrations between 20 and 50 volume percent and an abrupt increase in apparent angle of internal friction at a concentration of about 40 percent.

The changes in apparent angle of friction for most samples, starting to increase at about 55 volume percent, reaching a maximum at about 64 volume percent, and decreasing for higher apparent concentrations, probably can be understood in terms of packing. Interlocking of particles probably starts at about 55 percent. Cubically packed spheres, which do not interlock at all, occupy 52.4% of the volume of the packed space (e.g., White and Walton, 1937). The tightest known theoretical packing of uniform spheres is tetahedral, where 74% of the packed space is occupied by spheres. However, experiments indicate that real spheres cannot be packed in dense, tetra-

hedral arrays, rather that the limit of packing density is about 62.5 volume percent (Mc Geary, 1961). We suggest that the decrease in angle of friction for apparent volume concentrations greater than about 64% reflects the experimental packing limit of 62.5%. Thus, if the concentration of spheres exceeds 62.5% of the total volume, the sample dilates, incorporates air, and particle interlocking is reduced. Further, the dilatancy, in turn, probably is resisted by adhesion of the fluid phase to the particles, increasing the apparent cohesion of the debris, as shown in Fig. 7B. In this respect the debris behaves much as wet beach sand which dilates under the action of pressure applied by one's foot (e.g., Mead, 1925).

The increase in apparent angle of friction for the samples of sand (Fig. 5C) at concentrations of about 45% rather than 55% probably is a result of grain roughness and departure from sphericity (Morris, 1960). The gradual increase in apparent cohesion of debris containing silt as the granular phase, even for low concentrations of silt (Fig. 7B), probably reflects an increase in strength of the fluid phase resulting from water leaving the fluid phase to wet surfaces of fine silt particles (e.g., Trask, 1959). The apparent cohesive strength of the fluid phase is quite sensitive to changes in water contents (Fig. 2). Perhaps the silt and coarse clay particles aggregate to produce the marked increase in friction at concentrations of 40%.

The experiments indicate that debris comprised of clay, water and mono-sized clasts could contain up to about 55% by volume of clasts and yet flow on extremely low slopes (eq. (2)) because the apparent

friction angle of the debris could be essentially zero (Fig. 7A). Further, the experiments indicate that if any one size class in a granular material occupies more than 55% of the total volume of material, the material would have high strength. Some results suggest that the limit may be at least as low as 45%, depending on the sphericity and roughness of the particles. It is for this reason, we suggest, that closely sized material containing minor amounts of clay, such as dune sand or beach sand, do not readily mobilize as debris flows.

Two Size Classes of Spherical Clasts

The more the number of size classes of clasts in debris, the more difficult is the problem of predicting conditions under which the clasts will interlock, increasing apparent cohesion and apparent friction angle of debris. Now, we will consider two size classes, using the information gained by studying strengths of debris containing one class. We will assume that the larger spheres are packed cubically in order to estimate conditions of interaction among clasts. Fig. 8A shows a plan view of large and small spheres packed cubically. The small spheres are the largest that can be placed in the space between eight large spheres such that diagonal planes of slip for the large spheres are the same as those for the small spheres. Fig. 8B is a cross section along A-A' in Figure 8A, showing the relative dispositions of the small and large spheres and the position of the trace of one of the planes of slip.

The volume percentages of the two granular phases and the fluid phase can be represented on the diagram shown in Fig. 9A, where the

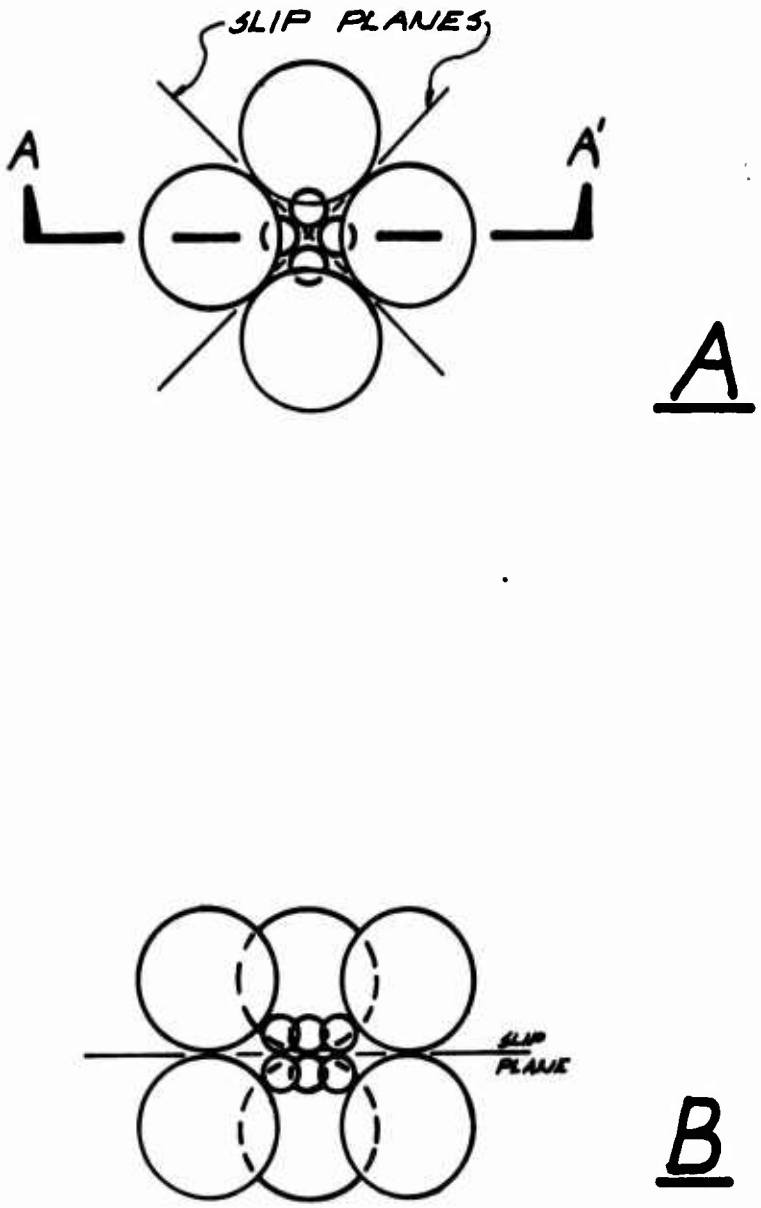

Figure 8. Cubic packing of spherical particles with the largest included particles that do not cause interlocking across the planes of slip.

A. Plan view with slip planes and location of section A-A'.

B. Cross-section A-A'.

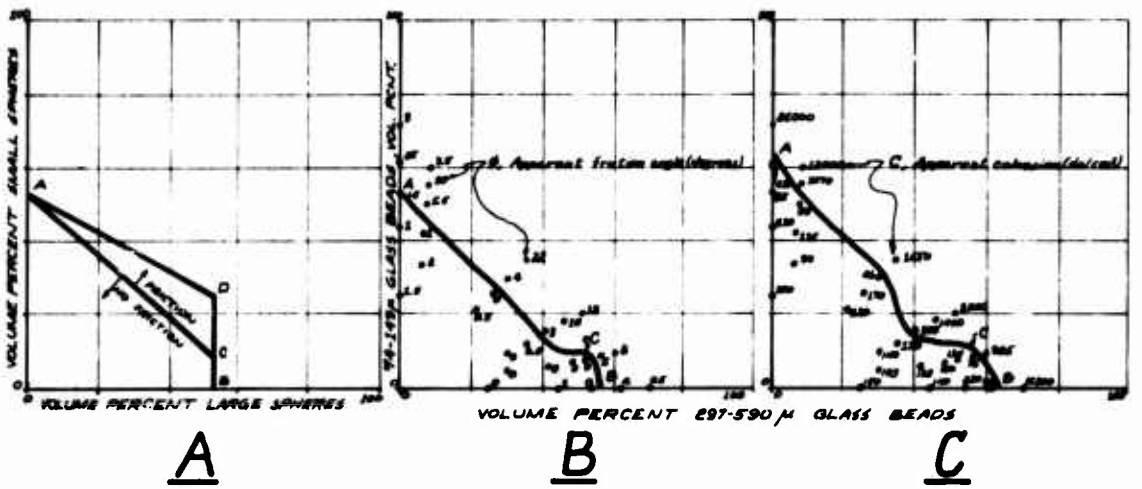

Figure 9. Volume percent of large spheres as a function of the volume percent of small spheres with clay-water slurry filling the voids.

A. Theoretical interlocking.

B. Experimental results for apparent friction angle.

C. Experimental results for apparent cohesion.

axes of the graph represent volume percentages of large and small spheres. The fluid phase fills the remaining volume of voids. For example, point A represents cubic packing of small spheres, alone, which theoretically occupy 52.4% of the total volume. The remaining 47.6% is occupied by the fluid phase. Point B is a similar point, for the large spheres, alone. The theoretical combination of large and small spheres shown in Fig. 9A allows 52.4% of large spheres, 8.0% of small spheres and 39.6% of fluid phase (point C, Fig. 9A).

Now, according to our hypothesis, line B C in Fig. 9A is an approximate boundary separating non-frictional mixtures toward the left and frictional mixtures toward the right. Similarly, point A should represent a limit between frictional concentrations above and non-frictional concentrations below. The boundary between frictional and non-frictional concentrations between A and C is unknown so we merely estimate the boundary by a straight line, A C (Fig. 9A).

If the smaller spheres were infinitesimally smaller than the larger spheres, the larger spheres theoretically would occupy 52.4 % of the total volume in cubic packing and the smaller spheres could occupy 52.4% of the remaining 47.6%, or 25.0% making a total of 77.4% solids and 22.6% fluid phase (point D, Fig. 9A). Thus, line A D B in Fig. 9A represents another approximate boundary between frictional and non-frictional mixtures of two sizes of spheres plus a fluid phase.

Results of strength tests with debris containing glass beads of 297-590 microns diameter mixed with various proportions of glass beads of 74-149 microns diameter in a fluid phase of kaolinite and water are shown in Fig. 9B. The solid line in Fig. 9B is an approxi-

mate boundary of tests where apparent friction angles were very low. Higher apparent friction values plotted above that line apparently reflect particle interlocking. The cusp near the lower, right-hand end of the line, near C, is an area of low apparent friction angle, where the total volume of solids is as high as 64%.

The apparent cohesive strengths for the same mixtures are shown in Fig. 9C. The boundary between low and high apparent cohesion values is roughly parallel to that between low and high friction values, shown in Fig. 9B, but it is displaced toward higher solid volume percentages.

The most important conclusion of the experiments is that debris can contain as much as 64 volume percent solids of two sizes of coarse clasts without affecting the strength of the debris.

Debris Containing Multi-sizes of Spherical Particles

Thus far we have shown that increase in apparent Coulomb properties of artificial debris can be correlated with ideal cubic and tetrahedral packing of spherical particles of either one size or two sizes. Cubic packing provides an estimate of the lower limit and tetrahedral packing an estimate of the upper limit of concentrations for interlocking of grains, as reflected in a marked increase of apparent internal friction angle of the debris. Further, the simple packing models and the experiments provide a first clue about the ability of debris flows to transport high concentrations of granular solids and yet have low apparent angles of internal friction. The grains apparently do not interlock if their concentrations are less

than or roughly equal to concentrations of particles in cubic packing. Typical debris-flow deposits, however, contain many sizes of particles so we need packing models for multi-sizes of spherical particles.

One method we have used to investigate theoretical packing of debris particles uses a large, three-dimensional mathematical array in a computer to determine possible size distributions of cubically packed spheres (Rodine, 1974, appendix). The array is partly filled with the largest sphere, part of which occupies one corner of the cubic array. The remaining space is then searched for the largest sphere that can fit into it and space for that sphere filled. Searching and filling of void spaces continues until the radius of the last sphere is equal to the distance between array points. The procedure is time consuming; an array 20 x 20 x 20 requires about 3.3 minutes of computer time to fill with theoretical spheres, using an IBM 360-67 computer. Two theoretical size distributions derived with the computer are shown in Fig. 10. The calculations require too much computer time to do a thorough analysis, but the results shown in Fig. 10 indicate that a wide size distibution markedly reduces the void spaces and increases the density, presumably without increasing the apparent strength of the mixture. Thus, whereas ideal debris containing a single size of spheres packed cubically has 47.6% void space and debris containing two sizes of spheres packed cubically has about 39.6% void space, debris with a wide range of sphere sizes can be packed cubically with voids of less than 17%. The remaining void spaces could presumably be filled with a mixture of water and clay, so that the resulting debris could have strength properties characteristic of the clay-water mixture.

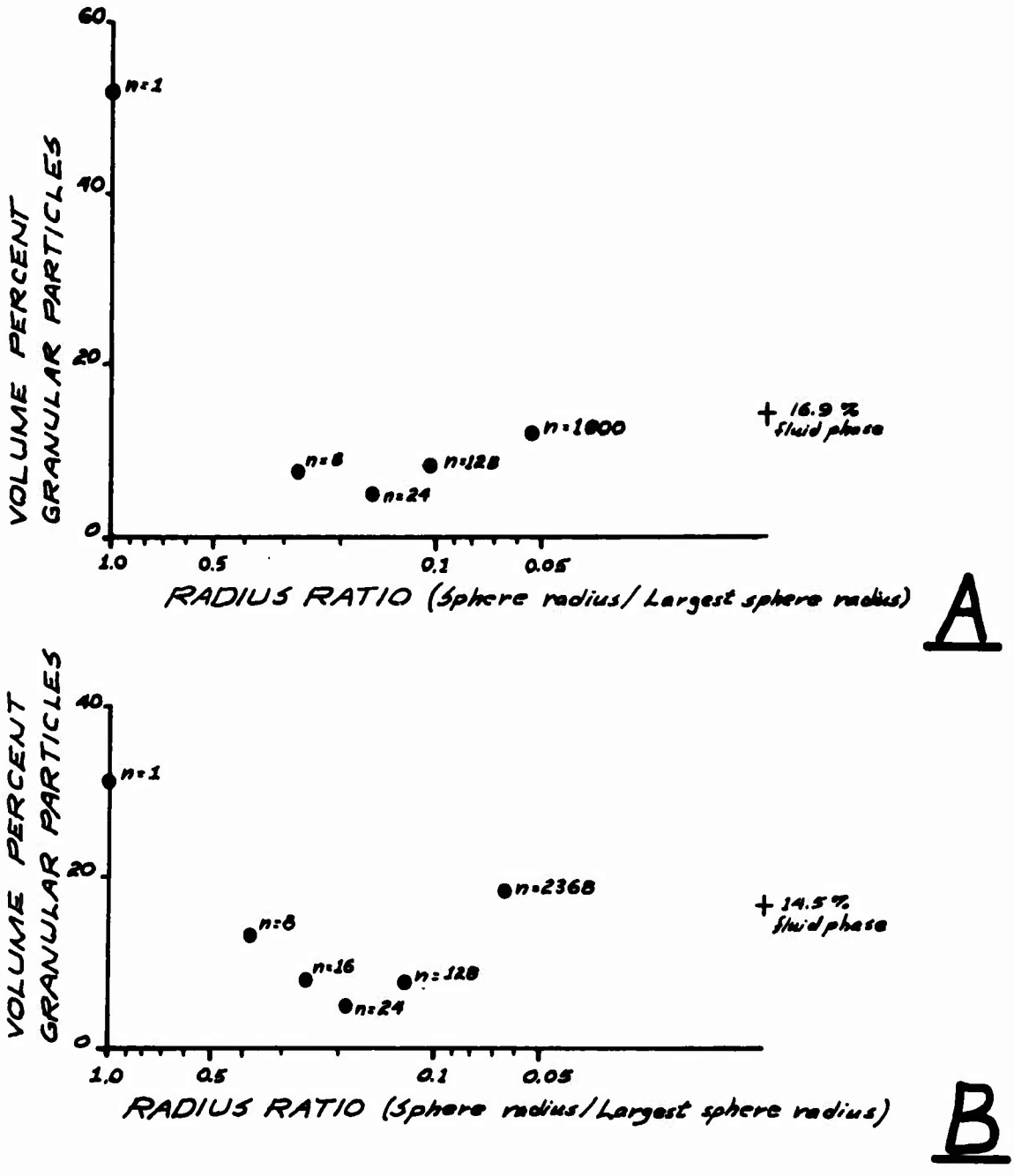

Figure 10. Size distribution of various spheres packed cubically such that no interlocking across slip planes can occur.

A. Large spheres packed cubically and filled between with smaller sized spheres.

B. Large spheres slightly dispersed from cubic packing and surrounded by smaller spheres.

The second method of theoretically packing spheres presumes that the spheres are packed in dense tetrahedrons. The theory behind the method was derived by Wise (1952). Essentially one assumes that all particles are tetrahedrally packed because such packing will accomodate combinations of spheres with most sizes. One selects any four spheres in a sample and computes the amount of volume of solids in the tetrahedron formed by connecting the centers of the spheres through the points where the four spheres touch. The selection and computation continue until all possible combinations of sphere sizes have been exhaused. Then, the percentage of solids in an aggregate of spheres packed tetrahedrally is some function of the percentage of solids in each of the possible tetrahedrons. A tedious part of the analysis is the selection of the functional relationship. Considering the large number of possible tetrahedrons in any assemblage of various sizes of spheres, the task of performing the calculations appears formidable. The process is considerably shortened, however, by using probability theory (Wise, 1952, p. 325):

> ". . . . in dense random packing, given the radius distribution, there must certainly be a non-zero probability distribution function--in four dimension--for the four radii. It must have a single weighing factor for the statistical distribution, and another one for size, since a large sphere must nearly always have more spheres round it and be part of more tetrahedra than a small one."

Once the tetrahedral probability distribution function is known, all possible combination, of tetrahedra formed by a given distribution of spheres can be calculated, and the solid and total volume, can be derived and multiplied by the tetrahedral probability distribution

function in order to compute the percentage of the total volume occupied by solid and by void. The answers can be evaluated by checking that all spheres in each size class are used in constructing tetrahedras.

We have selected the following tetrahedral probability function (W) for each set of spherical particles, with radii r_1, r_2, r_3, r_4:

$$W(r_1,r_2,r_3,r_4) = [P(r_1)\ P(r_2)\ P(r_3)\ P(r_4)]\ (r_1r_2r_3r_4)^{1.9} \qquad (10)$$

where P(r) is the frequency probability of spheres of radius $\underline{r}$. The product of the radii to the exponential 1.9 is an empirical factor which was selected by trial and error using simple size distributions where the expected results could be derived analytically. Solutions of eq. (10) for various size distributions require integration in four dimens --for which a computer program was written (Rodine, 1974, appendix).

Answers derived using eq. (10) agree quite well with analytical results for tetrahedral packing. For example, for three sphere sizes with $r_1 > > r_2 > > r_3$ one would expect sphere $\underline{r}_1$ to pack with a solid volume of 74.0%, sphere $\underline{r}_2$ to pack inside the voids formed by the $\underline{r}_1$ spheres or 74% (0.26) = 19% of the total volume, and sphere $\underline{r}_3$ to pack inside the voids formed by the $\underline{r}_2$ spheres or 74% (0.07) = 5% of the total volume. Thus, the total solid volume is the sum of the volumes occupied by the three sphere sizes or 74 + 19 + 5 = 98% total solid volume. Using eq. (10) the computer results predict a 98.9% total solid volume, for a difference of about one percent.

Dense packing of spherical clasts with a wide size range probably is intermediate between that of ideal cubic and of ideal tetra-

hedral. The cubic model for many sphere sizes described above is difficult to use because of the "brute force" computer approach required and the inability to handle a variety of size distributions. The tetrahedral model, however, executes within a few seconds time on the computer, can work with virtually any given size distribution, and the results are easily interpreted in terms of porosity.

The tetrahedral model can be used as follows. Determine the size distribution of the granular phase, that is, excluding clay-sized particles. Use the tetrahedral packing model to calculate pore volume of the debris and compare the calculated volume to the volume percentage of fluid phase in the natural debris. Now, if the volume percentage of the fluid phase is equal to or less than the theoretical value, the debris must be tightly interlocked and have high strength. But, if the volume percentage of the fluid phase exceeds the theoretical volume the packing can be less dense than tetrahedral and the gross strength of the debris can be essentially that of the fluid phase. Indeed, for three sphere sizes $r_1 > > r_2 > > r_3$ in cubic packing the porosity is 11% and in tetrahedral packing the porosity is 2%, so a porosity change of only 9% is required to reduce the theoretical strength from a maximum to zero. It, therefore, appears reasonable to presume that particle interlocking for many natural size distributions contributes nothing to the strength of debris if the volume percentage of the fluid phase exceeds by a small amount the percent porosity calculated using tetrahedral packing.

In order to avoid computer processing of size distribution data for every sample of interest to yield theoretical porosity, a graphical

method has been developed, incorporating statistical parameters explained by Kittleman (1964). Size distributions are plotted on Rosin probability paper, a line fit to the data, and the slope of the line calculated. Rosin probability paper is used because, according to Kittleman (1964), Rosin's distribution more closely approximates distributions of crushed particles and some sediments than the normal (Gaussian) distribution. The slope of the line on Rosin probability paper is used to determine the porosity through the use of Fig. 11. For example, Fig. 12 shows size distribution data plotted on Rosin probability paper for a braided river deposit (Doeglas, 1962). The slope of the line is -1.8. Use of Fig. 11 predicts porosity of 17%; the computer solution predicts a porosity of 19%. This material contains about 5% by volume of clay-sized particles, less than 6 microns. Thus, unless the clay-sized material were able to absorb at least three times its volume of water, maintaining sufficient strength to support sand particles, the fluid phase could not fill the voids. Only a few natural clays are capable of absorbing such high percentages of water while maintaining significant strength to support sand grains (e.g., Seed et al., 1964A; Trask, 1959). Thus, the relatively well sorted alluvium almost certainly will not form debris flows that could move on a low slope.

Another example, Fig. 4, shows size distribution data for a sample of a debris flow deposit (Bull, 1964). The slope of a line fit to the data shown in Fig. 4 when plotted on Rosin probability paper is -.41, and Fig. 11 predicts about 1% porosity whereas the computer program predicts 3% porosity. This sample contained about

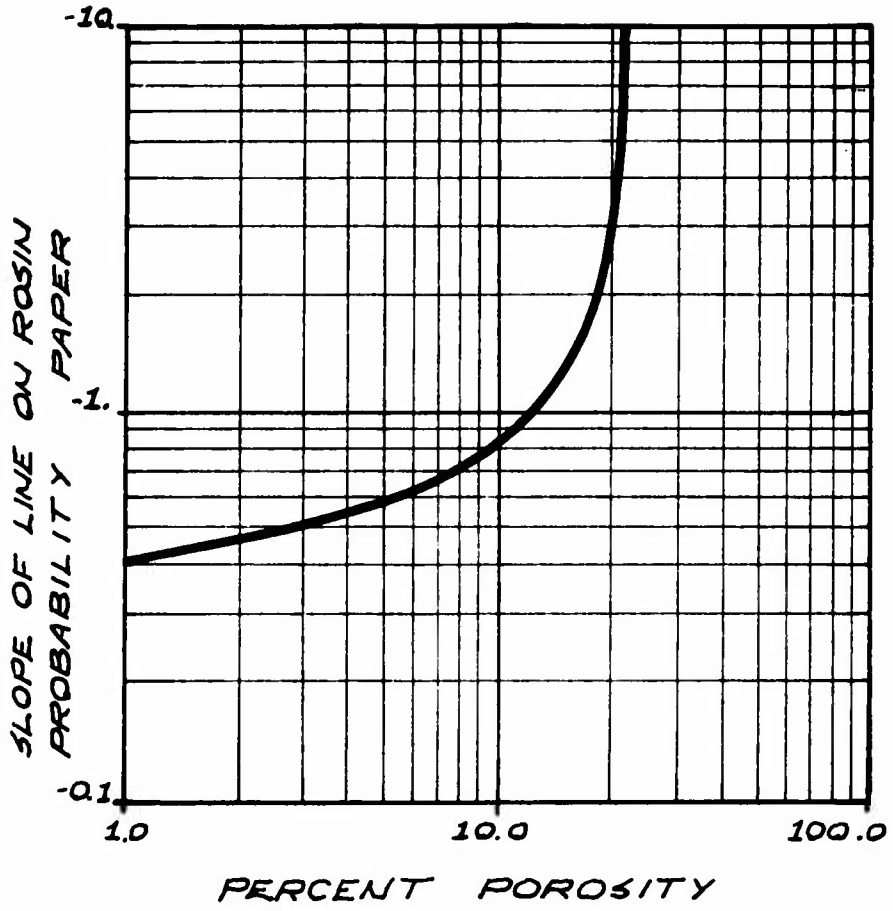

Figure 11. Theoretical relationship between percent porosity and slope of a straight line on Rosin probability paper.

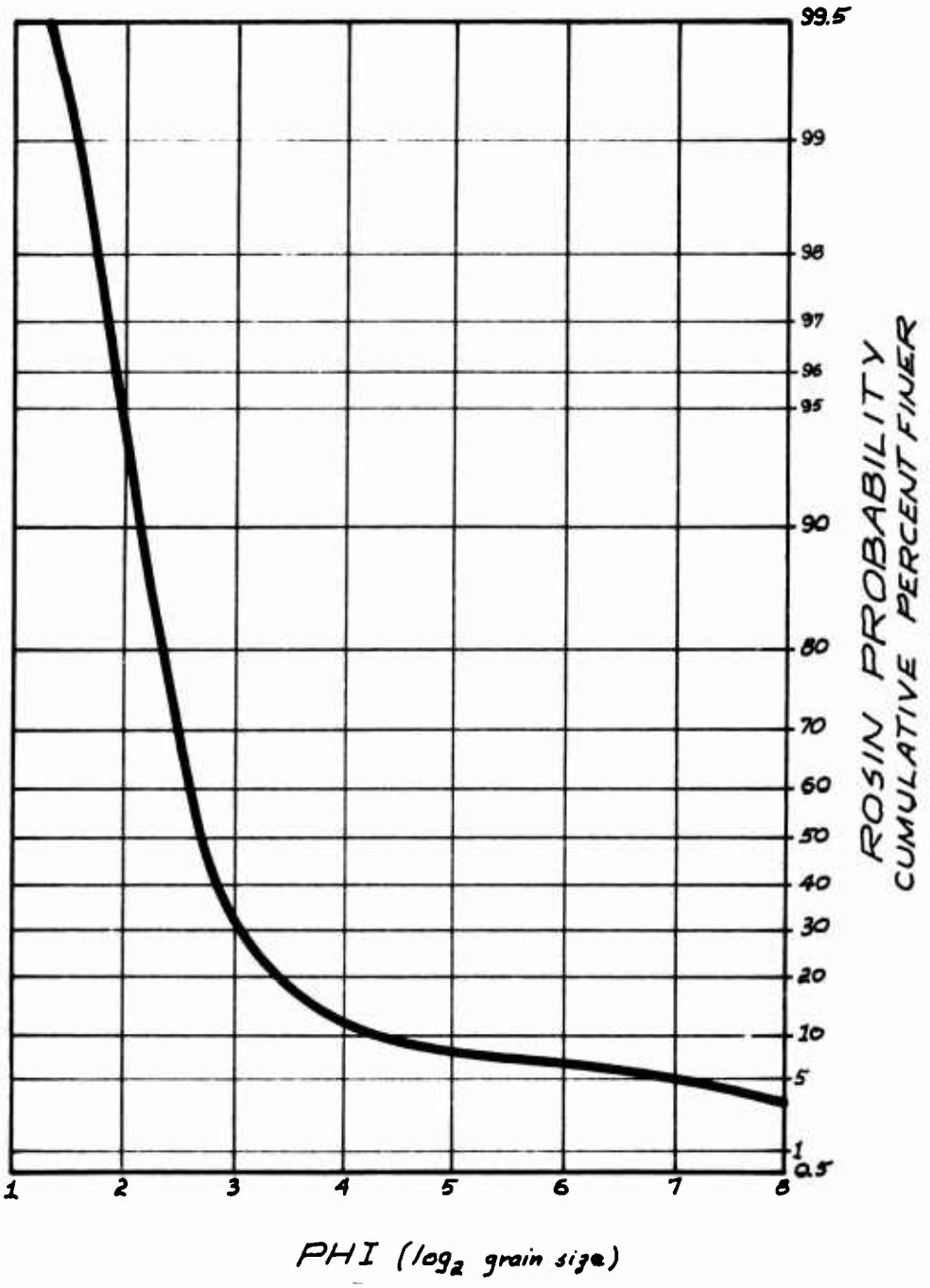

Figure 12. Size distribution of a braided river deposit (Doeglas, 1962) as a function of Rosin probability.

8% material finer than 2.0 microns, presumably clay. Thus, the incorporation of water theoretically would create a clay-water slurry that would bulk the sample, eliminate particle interlocking, and give the resulting debris the strength properties of the fluid phase.

Table 1 shows porosities calculated for several types of sediment. The values suggest that the granular phases of a wide range of materials could be packed so that the volume percentages of voids are quite small. Debris-flow materials apparently can generally pack more densely than the samples of dune sand, loess and alluvium, but there is overlap in the theoretical porosities. Fig. 11 shows that the theoretical porosity of ideal debris decreases with decreasing slopes of cumulative curves on Rosin's graph paper. The lower the slope the more poorly sorted the material; so the poor sorting of debris-flow materials, recognized by many investigators (e.g., Krumbein, 1940, 1942; Sharp and Nobles, 1953; Troxell and Peterson, 1937; Rodine, Part I, in press) is apparently a reason that debris flows can have very high densities, in some cases densities approaching that of solid rock, yet, can flow on very low slopes.

Poor sorting, alone, however, does not uniquely describe material that can be readily mobilized to form debris flows. According to our theory of debris strength, at least three factors are as important as sorting--the composition and amount of clay and the absolute sizes of the clasts. The absolute sizes of the clasts determine the strength required of the fluid phase in order for the clasts to be suspended by the debris. Thus, we imagine that the cohesive strength

TABLE 1

SAMPLE	POROSITY		VOLUME PERCENT	SLOPE
	COMPUTER ANALYSIS	FIGURE 11	CLAY	ANGLE (degrees)
Dune sand (1)	19	18	0	
Loess (1)	16	14	0	
River sand (1)	15	10	0	
Braided river (2)	19	17	4	
Water-laid deposit (3)	3	6	1	
Intermediate deposit (3)	3	4	9	
Debris-flow deposit (3)	3	1	10	
Alluvial fan (4)	4	6	2	
Volcanic lahar (5)	7	1	1	
Debris-flow source mat'l Arroyo Hondo (6)	15	6	20	30
Non-debris-flow mat'l Arroyo Hondo (6)	18	7	1	30
Debris-flow source mat'l Wrightwood (6)		2	1	35
Debris-flow source mat'l Thompson Cr. (6)		3	3	30
Debris-flow source mat'l Wrightwood quarry (6)		9	1	35
Debris-flow deposit Wrightwood quarry (6)		7	1	
Debris-flow source mat'l Big Sur (6)		9	2	30

(1) Krumbein and Sloss, 1963
(2) Doeglass, 1962
(3) Bull, 1964
(4) Leggett, et al, 1966
(5) Mullineaux and Crandell, 1962
(6) Rodine, Part I, 1974

and the density of the mixture of the finest clasts and the fluid phase support the next coarser clasts, and so forth until all sizes are suspended. The composition and amount of the clay fraction determines the amount of volume the fluid phase can occupy while maintaining sufficient strength and density to play its role in supporting all the clasts. Thus, 10 volume percent of kaolinite mixed with water may fill the same percentage of voids and have the same apparent cohesion as 2 volume percent of montmorillonite clay (e.g., Trask, 1959; Hampton, 1972). We would suggest that the relation between water content and strength of the clay fraction of samples be determined empirically, as in Fig. 2, in computations of the rheological properties of debris. Conical penetrometers could be used to make the measurements (Rodine and Johnson, Part III, in press).

SUMMARY

The ability of debris flows containing abundant coarse clasts to flow on low slopes can be understood in terms of the high density of the debris, the wide size distribution or poor sorting of the granular phase and the ability of the strength and density of the clay-water, fluid phase to suspend fine-grained particles. Experiments and theoretical analysis of debris containing mono-sized spherical clasts, which individually can be suspended by the fluid phase, indicate that the clasts can be so concentrated that they could be arranged as densely as in cubic packing, with a solid volume of 52.4%, yet the gross strength of the debris is essentially the strength of the fluid phase, alone. If the spheres are more concentrated, the gross strength of the debris is markedly increased. Experiments with debris containing two sizes of spherical clasts indicate that the clasts have no influence on the gross strength of the debris if they comprise at most 64% of the total volume of debris, depending on the relative sizes of the coarse and fine clasts. Theoretical analysis of ideal and natural size distributions of various sediments suggests that the clasts, if sufficiently poorly sorted, can comprise more than 95% of the volume of debris, yet have essentially no influence on the gross strength of the debris. Finally, experiments with completely remolded fluid phase composed of kaolinite and water suggest that the fluid phase has essentially zero apparent friction and that the apparent cohesion is determined by the water content of the fluid phase. In this way we can understand that low interlocking of clasts allows debris to flow as a virtually frictionless mass on low slopes.

The ability of debris flows to transport isolated large boulders and blocks can be understood in terms of high density and strength of the debris. The density of a flow in which clasts comprise on the order of 95% of the total volume of the flow is nearly equal to the average density of the solid clasts themselves. Thus, large blocks can be suspended by debris with low strength.

BIBLIOGRAPHY

Bonney, C.T., 1902, Moraines and mud-streams in the Alps: Geological Magazine, New Series, Decade 9, Volume 9, pp. 8-16.

Bull, W.B., 1964, Alluvial fans and near-surface subsidence in western Fresno County, California: United States Geological Survey Professional Paper 437-A, 70 p.

Curry, R.R., 1966, Observations of alpine mudflows in the Tenmile Range, central Colorado: Geological Society of America Bulletin, Volume 77, pp. 771-776.

Doeglas, D.J., 1962, The structure of sedimentary deposits of braided rivers: Sedimentology, Volume 1, pp. 167-190.

Fryxell, F.M., and Horberg, L., 1943, Alpine mudflows in Grand Teton National Park, Wyoming: Geological Society of America Bulletin, Volume 54, pp. 457-472.

Hampton, M.A., 1970, Subaqueous debris flow and generation of turbidity currents: Unpublished Ph.D. dissertation, Stanford University, Stanford, California.

_____, 1972, The role of subaqueous debris flow in generating turbidity currents: Journal of Sedimentary Petrology, Volume 42, Number 4, pp. 775-793.

Johnson, A.M., 1965, A model for debris flow: Unpublished Ph.D. dissertation, Pennsylvania State University, University Park, Pennsylvania.

_____, 1969, Properties of kaolite-sand-water slurries and of some natural debris: IN, Johnson, A.M. and Hampton, M.A.,

Subaerial and subaqueous flow of slurries, Chapter 3, Unpublished final report to United States Geological Survey, Branner Library, Stanford, California.

_____, 1970, Physical processes in geology: Freeman, Cooper and Company, 577 p.

_____, and Hampton, M.A., 1968, Subaerial and subaqueous flow of slurries: Unpublished annual report to United States Geological Survey, Branner Library, Stanford, California.

_____, _____, 1969, Subaerial and subaqueous flow of slurries: Unpublished final report to United States Geological Survey, Branner Library, Stanford, California.

Kittleman, L.R., 1964, Application of Rosin's distribution in size-frequency analysis of clastic rocks: Journal of Sedimentary Petrology, Volume 34, Number 3, pp. 483-502.

Krumbein, W.C., 1940, Flood gravel of San Gabriel Canyon, California: Geological Society of America Bulletin, Volume 51, pp. 639-676.

_____, 1942, Flood deposits of Arroyo Seco, Los Angeles County, California: Geological Society of America Bulletin, Volume 53, pp. 1355-1402.

_____, and Sloss, L.L., 1963, Stratigraphy and sedimentation: Freeman and Company, 660 p.

Lambe, T.W., and Whitman, R.V., 1969, Soil mechanics: John Wiley and Sons, New York, 553 p.

Legett, R.F., Brown, R.J., and Johnson, G.H., 1966, Alluvial fan formation near Aklavik, Northwest Territories, Canada:

Geological Society of America Bulletin, Volume 77, pp. 15-30.

Mc Geary, R.K., 1961, Mechanical packing of spherical particles: Journal of the American Ceramic Society, Volume 44, Number 10, pp. 513-522.

Mead, W.J., 1925, The geologic role of dilatancy: Journal of Geology, Volume 33, Number 7, pp. 685-698.

Morris, H.C., 1960, Effect of particle shape and texture on the strength of non-cohesive aggregates: American Society for Testing Materials, Special Technical Publication Number 254, pp. 350-363.

Mullineaux, D.R., and Crandell, D.R., 1962, Recent lahars from Mount St. Helens, Washington: Geological Society of America Bulletin, Volume 73, pp. 855-870.

Rodine, J.D., 1974, Analysis of mobilization of debris flows: Unpublished Ph.D. dissertation, Stanford University, Stanford, California.

_____, in press, Analysis of mobilization of debris flows: Part I. Processes of initiation of debris flows.

_____, and Johnson, A.M., in press, Analysis of mobilization of debris flows: Part II. A method of determining Coulomb strength properties of soft, remolded debris using paired conical penetrometers.

Rowe, P.W., 1962, The stress-dilatancy relation for static equilibrium of an assembly of particles in contact: Proceedings of the Royal Society of London, Series A., Volume 269, pp. 500-527.

Seed, H.B., Woodward, R.J., and Lundgren, R., 1964A, Clay mineralogical aspects of the Atterberg limits: American Society of Civil Engineers, Soil Mechanics and Foundation Division, Proceedings, Volume 90, SM 4, pp. 107-121.

_____, _____, _____, 1964B, Fundamental aspects of the Atterberg limits: American Society of Civil Engineers, Soil Mechanics and Foundation Division, Proceedings, Volume 90, SM 6, pp. 75-105.

Temple, P.H., and Rapp, A., 1972, Landslides in the Mgeta area, western Uluguru Mountains, Tanzania: Geografiska Annaler, pp. 157-193.

Trask, P.D., 1959, Effect of grain size on strength of mixtures of clay, sand and water: Geological Society of America Bulletin, Volume 70, pp. 569-580.

Troxell, H.C., and Peterson, J.Q., 1937, Flood in La Cañada Valley, California: United States Geological Survey Water Supply Paper 796-A, pp. 53-98.

White, H.E., and Walton, S.F., 1937, Particle packing and particle shape: Journal of the American Ceramic Society, Volume 20, pp. 155-166.

Wise, M.E., 1952, Dense random packing of unequal spheres: Phillips Research Reports, Volume 7, pp. 321-343.

ANALYSIS OF THE MOBILIZATION OF DEBRIS FLOWS

PART IV: MOBILITY INDEX -- A MEASURE OF THE POTENTIAL FOR DEBRIS FLOW

ABSTRACT

Prediction of the debris-flow potential of an area has previously been limited to projections of the historical record of debris-flow deposits. The purpose of this paper is to present a quantitative measure of the potential for debris flow - the mobility index.

The potential for debris flow is controlled by the balance and interaction of many factors. The availability of water is an essential factor. Vegetation only locally affects the potential for debris flow. Bedrock nature and hillside aspect primarily affect intrinsic properties of the derived soils. Coulomb strength and unit weight are considered the most important debris properties. The geometric elements of the source area considered critical are slope angle and size of the channel through which the debris moves.

Mobility index, $\underline{M}$, is defined as the ratio of the water content, $\underline{W}$, of the debris at mobilization to the field capacity, $\underline{W}_{fc}$, or $M = \underline{W}/\underline{W}_{fc}$. Water content of mobilized debris is determined by using an equation for the channel through which the debris flows and laboratory test data of the apparent cohesion, apparent friction angle and unit weight as a function of the water content.

Examination of mobility index calculations for debris-flow source areas at Thompson Creek, Utah, Arroyo Hondo, California, Los Altos Hills, California, Big Sur, California, and near Wrightwood, California, discloses that mobility index can closely approximate the potential for debris flow.

INTRODUCTION

The record of debris-flow deposits in alluvial fans in some areas of the southwestern United States allows geologists to predict confidently that sometime in the future the fans will again be visited by debris flows. For example, many alluvial fans in the Los Angeles, California, area contain debris-flow deposits, where, indeed, the prophecy of debris-flow activity was fulfilled in 1934, in 1938, and again in 1969 when massive flooding and debris flows caused millions of dollars worth of property damage and wreaked havoc on the lives of many people (e.g., Troxell and Peterson, 1937; Krumbein, 1940; 1942; Jahns, 1949). However, virtually no debris-flow deposits have been found in recent alluvium bordering the southwestern side of San Francisco Bay, California. Thus, when a resident of the town of Los Altos Hills, California, was forced to evacuate his home early in the morning of 28 February 1969 because a mass of flowing, clay-rich debris was crushing his corrugated plastic fence and engulfing the cars parked in his carport, both the resident and local geologists were taken by surprise (e.g., Hampton, 1970). Investigation of the unexpected debris flow disclosed that road fill 200 meters up a small ravine behind the carport had mobilized after several days of intense rainfall. Apparently, the historical approach to the prediction of debris-flow activity is not fail-safe, even in areas where no debris-flow deposits are recorded, because the areas can change, as by man's activities at Los Altos Hills.

The purpose of this paper is to establish a method of predicting the likelihood of debris-flow activity in a wide range of environments,

including those we have studied (Rodine, Part I, in press). The method we shall propose is based on field, laboratory, and theoretical analysis of selected factors that appear to determine the probability of debris flow, and on current understanding of the process of debris flow. It is partly an extension of earlier work: A Coulomb-viscous model for debris flow was proposed by Johnson (1965) based on field observations, experimentation, and theory, and some predictions of the model have been verified (Johnson, 1970; Johnson and Hampton, 1968, 1969; Johnson and Rahn, 1970; Hampton, 1970, 1972). Part of the necessary background of the research reported here was the development of a suitable method of determining Coulomb strength parameters of weak debris (Rodine and Johnson, Part II, in press), the field study of processes of initiation of debris flows (Rodine, Part I, in press), and the analysis of strength properties in terms of packing and density of debris charged with coarse particles (Rodine, Part III, in press).

The research was supported by the U.S. Army Research Office, Grant No. DA-ARO-D-31-124-71-G158, under the supervision of Finn Bronner. We wish to thank Dr. Bronner for helpful criticism, John Baltierra of Stanford University for laboratory assistance, and Dr. Robert Fleming, University of Cincinnati, Ohio, for criticizing the manuscript.

POTENTIAL FOR DEBRIS FLOW

The likelihood, or potential, for debris flow in some areas obviously is greater than that in others. For example, Heath Canyon at Wrightwood, California is visited periodically by hundreds of debris flows that occur during a period of several days when a spring warm spell thaws an unusually heavy snowpack in the San Gabriel Mountains (Sharp and Nobles, 1953). On the other hand, debris flow is virtually restricted to tiny rivulets of mud on the faces of road-cuts in terrain covered by clay-rich soils in foothills along the southwestern side of San Francisco Bay, California.

The potential for debris flow seems to be controlled by the balance and interaction of many factors, most of which have been recognized for decades (e.g., Rickmers, 1913, p. 195; Blackwelder, 1928; Sharpe, 1938, p. 56). The availability of water, for example has long been recognized as a necessary condition for debris flow. Water sufficient for mobilization of debris has been furnished by internal pore fluids (Terzaghi, 1950, p. 112), by volcanic eruptions (Scrivenor, 1929; Mullineaux and Crandell, 1962), by springs discharging from within the debris (Johnson and Rahn, 1970; Denness, 1973; Rodine, Part I, in press), by melting of snow (Sharp and Nobles, 1953; Conway 1907), by concentration of water in the thawed surface zone of frozen soil (Johnson and Rahn, 1970), by concentration of water in soil above a non-wettable zone developed by the intense heat of brush fires (Cleveland, 1973), and by intense rainstorms (Bonney, 1902; Singewald, 1928; Matthes, 1930, p. 109; Fryxell and Horberg, 1943; Swanston, 1970; Wentworth, 1943; Croft, 1962; Rapp, 1963; Curry,

1966; Temple and Rapp, 1972; Rodine, Part I, in press). Thus there are many ways in which water can be provided for the mobilization of debris flows.

The close correlation between lack or type of vegetation with debris-flow activity, reported by some investigators, indicates that vegetation can also affect the potential for debris flow. The destruction or lack of native vegetation was cited as a primary cause of debris flows, in Alaska (Swanston, 1970), in Utah (Bailey et al., 1934; Croft, 1962), in California (Cleveland, 1973; Bailey and Rice, 1969), and in Tanzania (Temple and Rapp, 1972). Flowage of debris occurred in 22 out of 25 landslides under forest cover and in 16 out of 25 landslides under grass cover in an area of New Zealand studied by Pain (1971). Debris flows mobilized in tropical rainforests in Hawaii (Wentworth, 1943) and in forested areas in Wyoming (Fryxell and Horberg, 1943), Norway (Rapp, 1963) and Virginia (Williams and Guy, 1971). However, the initiation of debris flows in forested, grass-covered and barren areas, even where the areas are contiguous, suggests that lack or type of vegetation is a necessary condition for the mobilization of debris flows only locally.

The effect of the nature of the bedrock on the availability of materials for debris flow was considered to be minimal by Williams and Guy (1971) in Virginia and by Bailey and Rice (1969) in southern California. On the other hand, Sharp and Nobles suggested that (1953, p. 559): ". . . a badly sheared and shattered bedrock which yields much fine and poorly sorted micaceous debris upon weathering. . ." was an essential condition to the development of debris flows at Wrightwood, California and study of debris-flow source areas along

Arroyo Hondo, California (Rodine, Part I, in press), disclosed that debris there preferentially became mobilized from a clay-rich soil horizon sandwiched between sand-rich soil horizons, presumably because of differences in the internal properties of the soils weathered from different parent bedrocks. Compositional and structural properties of bedrock probably affect the potential for debris flow primarily by controlling properties of the debris weathered from it.

The preferential development of debris flows on hillsides with a northeasterly aspect, noted in a study of debris flows in Nelson County, Virginia, resulting from Hurricane Camille, 1969, was attributed to high, pre-storm, moisture contents of the debris, direction of sunshine, and direction of storm movement (Williams and Guy, 1971). The source area in Heath Canyon at Wrightwood, California, faces northward and Sharp and Nobles (1953) reasoned that the northerly aspect was critical for collection of snowpacks that linger into late spring, where they melt during unseasonably warm weather and trigger debris flows. Debris-flow initiation was related to aspect of hillsides and occurrence of brush in southern California, however, where grass cover was homogeneous on all hillsides, debris flows developed on slopes at random, independent of orientation (Bailey and Rice, 1969). Hillside aspect probably most strongly influences the in-situ properties of debris.

Another factor is acceleration of debris particles in source areas by vibration of the debris by torrential stream waters, by thunder or by earthquakes. More than 1000 landslides occurred in response to ground accelerations during the San Fernando, California,

earthquake of 1971 (e.g., Morton, 1971; Greensfelder, 1971) and debris-flow activity was noted in response to the San Francisco, California earthquake of 1906 (Lawson, 1908, p. 392-398). No known debris flows have mobilized in response to vibrations produced by storm waters or by thunder (Williams and Guy, 1973).

Many internal properties of debris affect the potential for debris flow, including degree of consolidation, size distributions and shapes of granular materials, texture, porosity, hydraulic conductivity, pore pressure, strength, density, and percentage and composition of the clay fraction. Size distributions of debris-flow materials typically are multimodal, with an even, wide spread of size classes (e.g., Sharp and Nobles, 1953; Rapp, 1963; Wentworth, 1943; Troxell and Peterson, 1956; Rodine, Part III, in press). Analysis of soil texture, at the surface and above and below the slip planes of slides in source areas of debris flows, failed to show significant differences in a study in southern California (Bailey and Rice, 1969). The porosity of debris collected from several different debris-flow source areas theoretically can be as low as one percent (Rodine, Part III, in press). Hydraulic conductivity of soil cores, taken from below a slip plane of a landslide in a debris-flow source area in southern California, typically were lower than those of cores taken at similar depths in adjacent control sites (Bailey and Rice, 1969). Hydraulic conductivity, keyed to increase of pore pressure and reduction of shear strength is considered to be a critical factor in debris-flow initiation in Tanzania (Temple and Rapp, 1972) and at Big Sur, California (Cleveland, 1973). The reduction of debris strength due to an

increase in pore pressure is cited as a cause of debris mobility on Oahu, Hawaii (Wentworth, 1943). The strength of debris depends on the grain-size distribution of debris-flow material (Rodine, Part III, in press). Rapp concluded that : ". . . the 'mud' fraction is probably essential not only in flows of purely fine-grained earth but also in flows of bouldery material. . ." (1963, p. 197); indeed, a small amount of clay probably is essential for mobility (Rodine, Part III, in press).

Other factors affecting the potential for debris flow are the geometric elements of the source areas including steepness of slope, existence of depressions or troughs in the hillside, and depth of the debris. Debris flows have mobilized from slopes greater than 39 degrees in southern California (Bailey and Rice, 1969), from slopes inclined between 15 and 30 degrees in Norway (Rapp, 1963), from slopes steeper than a minimum of 17 degrees in Virginia (Williams and Guy, 1973), between 42 and 48 degrees for 80 percent of the debris flows recorded during a study on Oahu, Hawaii (Wentworth, 1943), and from slopes generally in excess of 30 degrees in the western United States (Rodine, Part I, in press). The length of the hillslope was found to have little effect on the potential for debris flow in Virginia (Williams and Guy, 1973). Debris flows typically initiate in pre-existing swales and hillside troughs (Williams and Guy, 1973; Rapp, 1963; Wentworth, 1943). The debris in source areas usually is shallow, with thicknesses of one meter in Virginia (Williams and Guy, 1973), about 2/3 meter in California (Bailey and Rice, 1969), about 1/3 to 2/3 meter on Oahu (Wentworth, 1943), and 0.4 meter average in Norway (Rapp, 1963).

The last factor is existence of a channel through which the debris flow moves. Selection of this factor is motivated by both observational and theoretical considerations. If a debris flow moves over a flat tilted plane it thins by spreading laterally and distally with an elongated lobate shape and stops when the thickness reaches a critical value (Johnson, 1965). However, if the debris flow is channelized it may move many miles on gentle slopes, as at Wrightwood, California (Sharp and Nobles, 1953). Even a slight depression can serve to channelize the debris because of the ability of debris flows to construct lateral ridges or levees which tend to contain the flow (Sharp, 1942; Johnson, 1965; 1970, p. 515, 568). Indeed, observation of many debris flows, debris-flow deposits, and debris-flow source areas suggests that debris flows have, in general, three phases: 1, initiation via landsliding and mobilization via dilation and incorporation of water; 2, flow through U-shaped channels bounded by levees; and 3, deposition in lobate masses (Rodine, Part I, in press). Therefore a channel through which debris may flow is almost always a critical factor, especially if the debris moves away from the immediate source area.

Each of these factors and probably others has been important to the development of debris flows in different areas. The large number and diversity of the factors is somewhat discouraging to those who would predict the occurrence of debris flows. There is hope of prediction though if we select only a few key factors.

SELECTION OF FACTORS FOR ANALYSIS

Of the factors that determine the potential for debris flow, discussed in earlier pages, some are essential in order for mobilization to occur and others have a more limited effect on the potential of debris to become mobile. We know of no way to evaluate effectively all the factors, so we will select those essential factors that can be quantified. Water is universally required in order to mobilize debris, therefore, for our analysis we can assume that sufficient water will at some time become available for debris mobilization. The factors that we will consider in the following analysis are: The field capacity of in-situ soil, the Coulomb strength and unit weight of the mobile debris, and the source area geometry as measured by the slope angle and radius of the channel through which the debris flows.

Analysis of the potential for debris flow could include an evaluation of the in-situ properties of the soil. As explained earlier (Rodine, Part I, in press) most debris flows initiate by landsliding at various scales, and then mobilize by dilating and incorporating water. Thus an evaluation of the in-situ properties would have to include development of methods of prediction of landsliding--a most difficult task as evidenced by the scores of years of research by soils engineers on this subject (e.g.; Lambe and Whitman, 1969; Terzaghi, 1950; Skempton, 1964). Accordingly, we will attempt to circumvent the problem of predicting individual landslide failures that become debris flows and consider that strength and unit weight of in-situ soils are functions of water content (e.g., Lambe and Whitman, 1969; Schofield and Wroth, 1968). In fact, we will presume that

the in-situ soil properties are adequately represented by one measurement--that of the water content of saturated, in-situ soil or field capacity of the soil.

The properties that most strongly affect debris mobility are the Coulomb strength parameters, apparent cohesion and apparent friction angle, and the unit weight (e.g., Rodine, Part III, in press). Values for each of these three variables can be determined as functions of the water content of the debris (Rodine and Johnson, Part II, in press).

The slope and shape of channels through which the debris must flow are two other factors we will select. For example, flow on an infinite slope theoretically is possible if the thickness equals or exceeds the critical thickness,

$$H_c = C/[\gamma \cos \delta \ (\tan \delta - \tan \phi)] \qquad (1)$$

where C is apparent cohesion, γ is unit weight, δ is slope angle, and ϕ is apparent friction angle (Johnson, 1965). If flow takes place in a semi-circular channel a similar equation can be derived by assuming that the normal stress exerted by the debris on the bed of the channel is hydrostatic, equal to the pressure developed by the column of debris above. For the semi-circular channel, the critical radius for flow is:

$$R_c = 2C/[\gamma \cos \delta \ (\tan \delta - (4/\pi) \tan \phi)] \qquad (2)$$

Thus, the critical radius for flow of Coulomb material in a semi-circular channel is roughly equal to twice the critical thickness of an infinite flow, as noted for a simple plastic material (Johnson, 1970, p. 501).

Several different channel cross-sections are shown in Fig. 1 along with appropriate formulae for the critical dimensions derived largely from theoretical and experimental analysis of debris flow in channels (Johnson, 1965; 1970, Ch. 15). Where flow width is four or more times as large as the depth (Fig. 1a), eq. (1) describes the critical thickness of flow. If flow width is much less than the depth (Fig. 1b), eq. (1) describes one half the critical width of flow. For flow in a semi-circular channel (Fig. 1c), eq. (2) describes the critical radius of flow. Where flow is in a rectangular channel with a width approximately equal to twice the depth (Fig. 1d), eq. (2) describes the critical thickness of flow. Finally, for flow in a right triangular channel (Fig. 1e), the critical depth of flow is roughly 1.4 times the radius of a semi-circular channel, because of immobile masses of debris that cling to the edges and bottom of the channel (Johnson, 1965; 1970, p. 562).

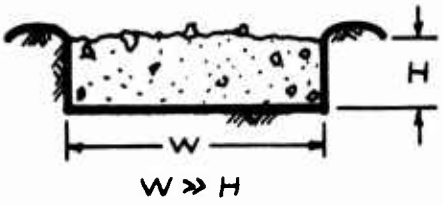

$$H = C/\{\gamma \cos\delta [\tan\delta - \tan\phi]\}$$

A

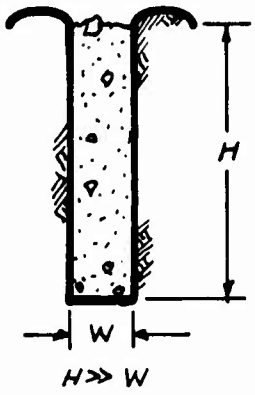

$$W/2 = C/\{\gamma \cos\delta [\tan\delta - \tan\phi]\}$$

B

$$R = 2C/\{\gamma \cos\delta [\tan\delta - (4/\pi)\tan\phi]\}$$

C

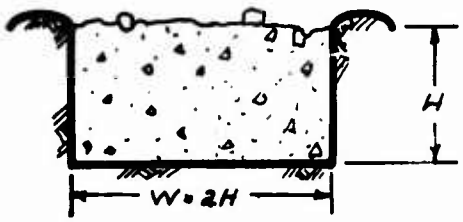

$$H = 2C/\{\gamma \cos\delta [\tan\delta - (4/\pi)\tan\phi]\}$$

D

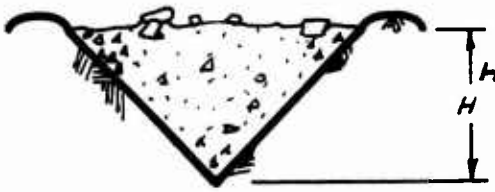

$$H = 2.8C/\{\gamma \cos\delta [\tan\delta - (4/\pi)\tan\phi]\}$$

E

Figure 1. Channel cross-sections and formulas for critical dimensions.

A. Rectangular channel, width much greater than depth.

B. Rectangular channel, depth much greater than width.

C. Semi-circular channel.

D. Rectangular channel, width equal to twice the depth.

E. Right triangular channel.

COMPARISON OF WATER CONTENTS OF FLOWING DEBRIS AND IN-SITU SOIL—MOBILITY INDEX

Now that we have selected a few factors that affect the potential for debris flow, we will examine various measures of the potential. One possible measure of the potential for debris flow could be determined from strength data derived from testing of remolded debris. Figure 2 shows test results of a sample collected from Thompson Creek, Utah (e.g., Rodine, Part I, in press), where apparent friction angle, apparent cohesion and unit weight are plotted as functions of water content, expressed as weight percent of the total solids plus water. Let us consider the curve relating water content and apparent friction angle. The curve shows that above a certain water content (a, Fig. 2) the apparent friction angle is low and relatively independent of water content, whereas below that water content the apparent friction angle increases markedly. Now, apparent friction angle is a critical parameter in determining whether debris will flow in channels (eqs. (1) and (2)) and point a represents the water content for which friction is low, so we could select that water content as an index of the mobility of the debris. The index would be analogous to the Atterberg limits of soil mechanics (e.g., Lambe and Whitman, 1969), and it could be compared with similarly determined index values from other source areas, providing a measure of the relative mobility of the debris in the source areas. If we compare the water content for point a (Fig. 2) with the field capacity of the soil, we could compute an index that would be sensitive to the properties of the in-situ material. However, the indices considered thus far

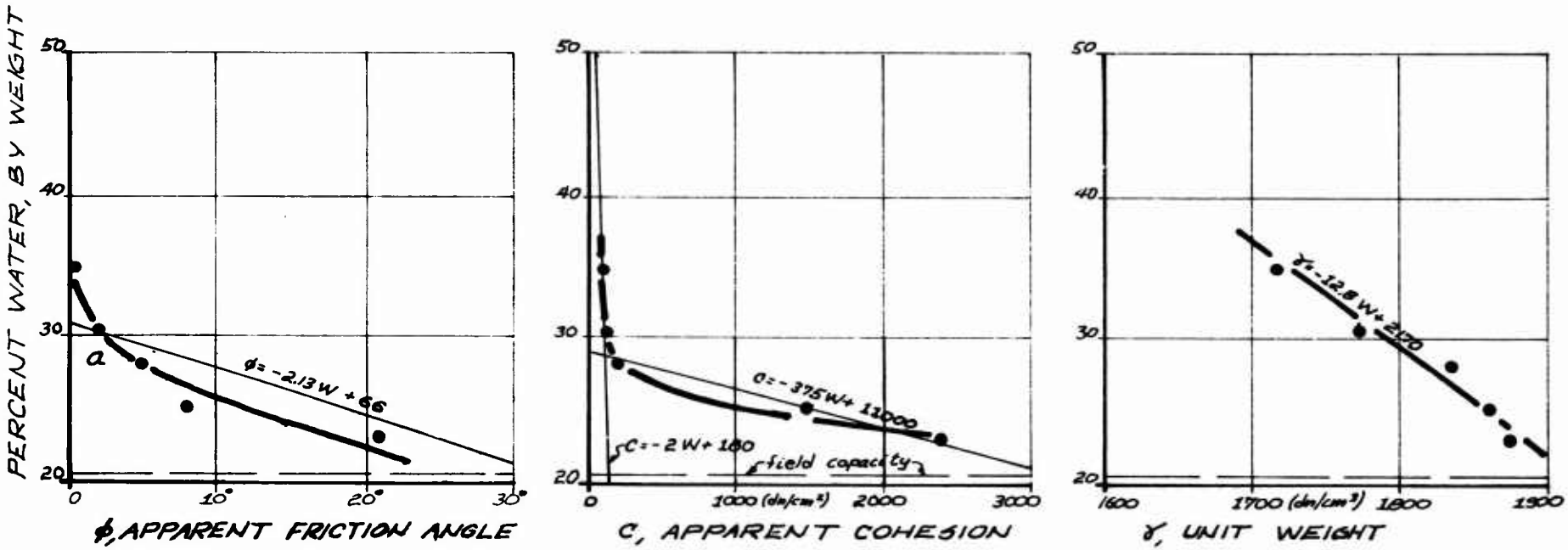

Figure 2. Apparent friction angle, ϕ, apparent cohesion, C, and unit weight γ, as functions of water content, W, for a sample of debris-flow material from Thompson Creek, Utah.

ignore the geometry of the initiation sites and the cohesive and unit weight properties of the debris. Thus, we define the mobility index, M, as the ratio of the water content at mobilization, W, to the field capacity, W_{fc},

$$M = W/W_{fc} \tag{3}$$

where W is the water content of debris that will just barely flow through the channel in the source area.

We will illustrate the computation of the mobility index by considering a specific source area, JR116 at Thompson Creek, Utah (Rodine, Part I, in press). First, samples are collected from the sides or head of the source area scar. We have taken samples for field capacity by saturating a small area of in-situ soil with water and placing about 300 cc of the saturated soil in a leak-tight container. For the strength testing we collect about 7 to 8 liters of material. Second, measure the slope angle in the source area, which is 30 degrees, and the channel critical dimension, which is a one meter radius at Thompson Creek. The samples are tested in the laboratory for field capacity, apparent cohesion, apparent friction angle and unit weight. We determine field capacity by measuring the total weight of the sample saturated in the field, oven drying the sample at 105°C, weighing the dried sample, and calculating the field capacity by subtracting the dry weight from the wet weight, dividing by the total weight of the sample plus water and multiplying the result by 100. We measure apparent friction angle, ϕ, apparent cohesion, C, and unit weight γ, of the sample at various water contents using a method described earlier (Rodine and Johnson, Part II, in press).

Mobility index calculations begin by plotting $\underline{\phi}$, $\underline{C}$ and $\underline{\gamma}$ as a function of the water content, and fitting straight line segments to the data (e.g., see Fig. 2). The fitted lines are expressed in terms of their slope, $\underline{S}$, coordinate intercept, $\underline{K}$, and water content, $\underline{W}$,

$$\left.\begin{aligned} \phi &= S_1(W_{fc}/M) + K_1 \ , \\ C &= S_2(W_{fc}/M) + K_2 \ , \\ \gamma &= S_3(W_{fc}/M) + K_3 \ , \end{aligned}\right\} \qquad (4)$$

where $W_{fc}/M \equiv W$.

Insertion of eqs. (4) into eq. (2) leads to,

$$H_c=R_c=2[S_2(W_{fc}/M)+K_2]/\{[S_3(W_{fc}/M)+K_3]\cos\delta[\tan\delta-(4/\pi)\tan(S_1(W_{fc}/M)+K_1)]\}. \qquad (5)$$

For the Thompson Creek example,

$$\left.\begin{aligned} \phi &= -2.13\ (20.4/M) + 66 \ , \\ C &= -375\ \ (20.4/M) + 11000 \ , \\ \gamma &= -12.8\ (20.4/M) + 2170 \ , \end{aligned}\right\} \qquad (6a)$$

and,

$$H_c=2[(-7650\ /M)+11000\ ]/\{[(26.1/M)+2170\ ]\cos\delta[\tan\delta-1.27\tan((43.5/M)+66\ )]\} \qquad (6b)$$

for $W \leq 29.0$ or $M \leq 1.42$. Solutions of eq. (6b) for various mobility index values are shown in Fig. 3, where the coordinates δ = 30 deg. and $\underline{H_c}$ = 1 meter gives a mobility index of about .99. Thus it appears that the debris flows at Thompson Creek mobilized from soil approximately saturated to field capacity, and that little water needed to be in-

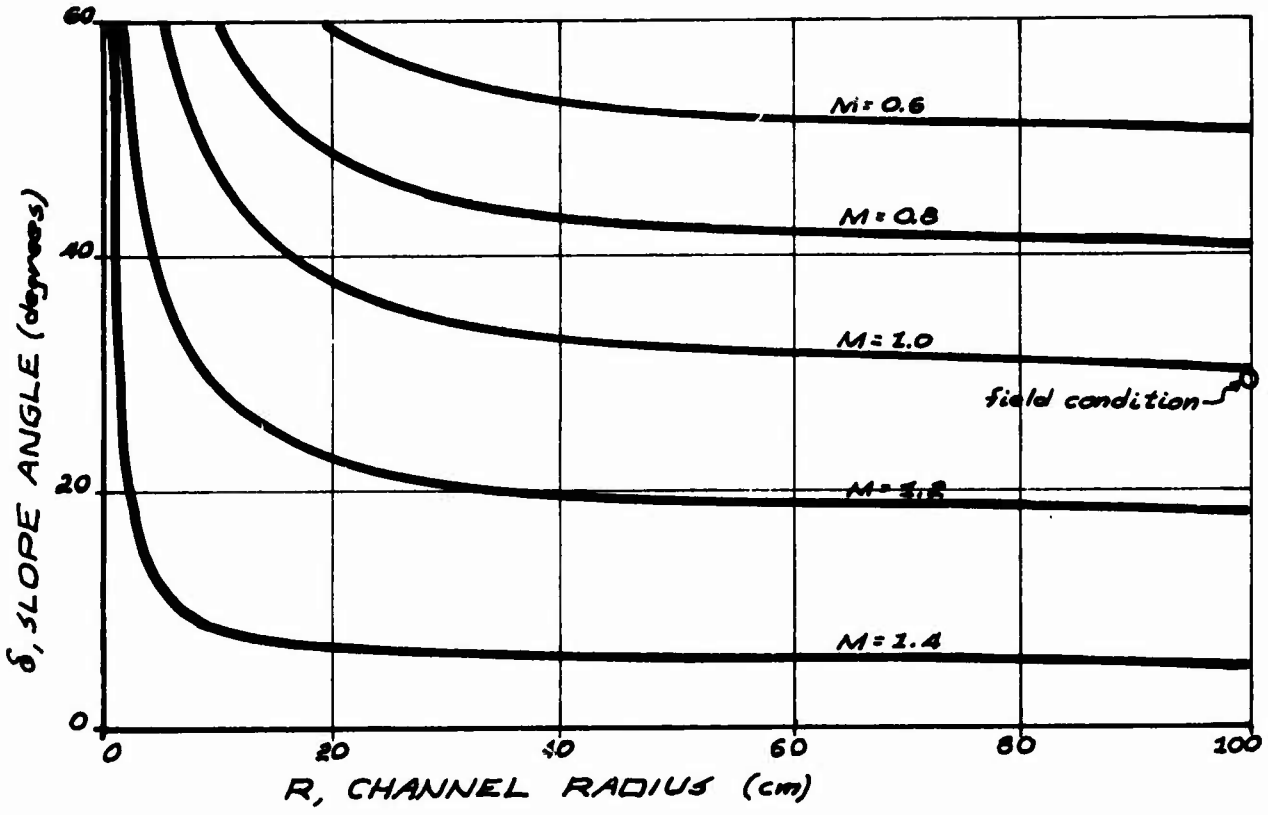

Figure 3. Critical thickness, H_c, as a function of critical slope angle, δ_c, for various mobility indices, M, for debris-flow source materials from Thompson Creek, Utah.

corporated by the debris during the transition from sliding to flow. If the estimate of thickness were in error by a factor of two, the mobility index would have been 1.04 for H_c = 0.5 m and about 0.98 for H_c = 2 m. Thus the mobility index for this site is not highly dependent upon an accurate measurement of the thickness of the debris flow immediately after mobilization.

However, recognition of the channel is probably the most difficult problem for computations of mobility indices. The channel must be the path down which the debris will flow just after initiation--not a main channel that serves as the flow path after many debris flows have been contributed from side drainages. If a debris-flow deposit can be walked uphill to its source, and the source scar shows that the debris mobilized from a thin flat sheet of soil, eq. (1) is appropriate and the slope angle and thickness of the sheet are the critical measurements (e.g., see San Rafael, California, in Rodine, Part I, in press). Or, if the source area is a series of semi-circular rills, eq. (2) is appropriate and the slope angle and rill radius are the critical measurements (e.g., see Big Sur, California, in Rodine, Part I, in press). Careful study of landslide scars may indicate that the soil did not fail as a unit but as slices thinner than the depth of the scar, thus the slice thickness and not the scar depth and the slope angle would be the critical measurements (e.g., see Roofing Granule Quarry, California, in Rodine, Part I, in press). In areas where no evidence of debris-flow activity is found, selection of the geometry of the channel can be most difficult. The soil thickness might indicate the maximum critical dimension but

then judgement is required to select an appropriate shape of channel (Fig. 1). Further, the total thickness of soil can be the wrong measurement of the critical dimension in places where the field capacity rapidly changes with depth, as we show in following pages. In areas where this change is suspected we suggest that field capacity be determined as a function of depth of the soil and that the mobility index be determined as a function of the soil thickness.

MOBILITY INDICES FOR SELECTED DEBRIS-FLOW SOURCE AREAS

Mobility indices have been determined for soils from selected debris-flow source areas ranging in climate from semi-arid at Arroyo Hondo, California, to mediterranean at Big Sur, California, and in composition from silty-clay debris at Los Altos Hills, California, to coarse-grained granular debris containing boulders up to 1.3 meters in maximum diameter at Richfield, Utah (Rodine, Part I, in press).

Arroyo Hondo, Fresno County, California

Debris was selectively mobilized from a clay-rich soil derived from a claystone unit of 30 to 50 meters thickness at Arroyo Hondo, California (Rodine, Part I, in press). The claystone is underlain by medium-grained sandstone that weathers to a sandy to silty soil. Soil derived from both units is exposed on the same slope in one area so that only first-order factors should control differences in debris-flow potential according to our understanding of mobility and potential. The ground slopes at an average of 30 degrees in both units. The sandy soil is thin, averaging about 2 cm, and has a field capacity of 22.5 weight percent water. The sandy soil did not mobilize as debris flows so there are no debris-flow channels nearby. However, the radius of the channel could not be greater than the soil thickness of 2 cm. The clay-rich soil is 10 to 20 cm thick and contains crudely semi-circular channels with radii averaging 10 cm, and it has a field capacity of 37.0 percent. Laboratory measurements of the strength parameters and the unit weight as a function of the

water content indicate that, for similar values the clay-rich material requires more water than the sandy soil (Fig. 4a, 4b). However, the sandy soil has a mobility index of about 1.15 (Fig. 4c) and the clay-rich soil has a mobility index of about 1.01 (Fig. 4d), which suggests that the sandy debris has a lower potential for debris flow than the clay-rich debris, in accordance with the field observations.

Los Altos Hills, California

Small debris flows, derived from a black, silty-clay soil at the top of a road cut, periodically flow down into the street gutter along La Mesa Drive, Los Altos Hills, about 55 km south of San Francisco, California (see, Rodine, Part I, fig. 1, in press). The soil apparently is derived from underlying claystone of the Miocene Monterey Formation. It has a homogeneous composition in this area (Fleming, 1971). The debris probably mobilizes in response to heavy winter rains and horticultural watering. Large debris flows are unknown in the black, silty clay. Small flows occur in some cut banks. The mobility index should help explain the low debris-flow potential of the black, silty clay soil.

The source area at La Mesa Drive contained small arcuate scars marking the initiation sites that averaged 5 to 10 cm in depth and 47 degrees in slope. Field capacities decreased with depth from 32.2 percent within 5 cm of the ground surface, to 25.0 percent at 15 to 18 cm below the surface, and to 18.7 percent at 30 to 33 cm below the surface. Strength tests and unit weight of the source material are shown in Fig. 5a. Mobility indices increased with depth, from

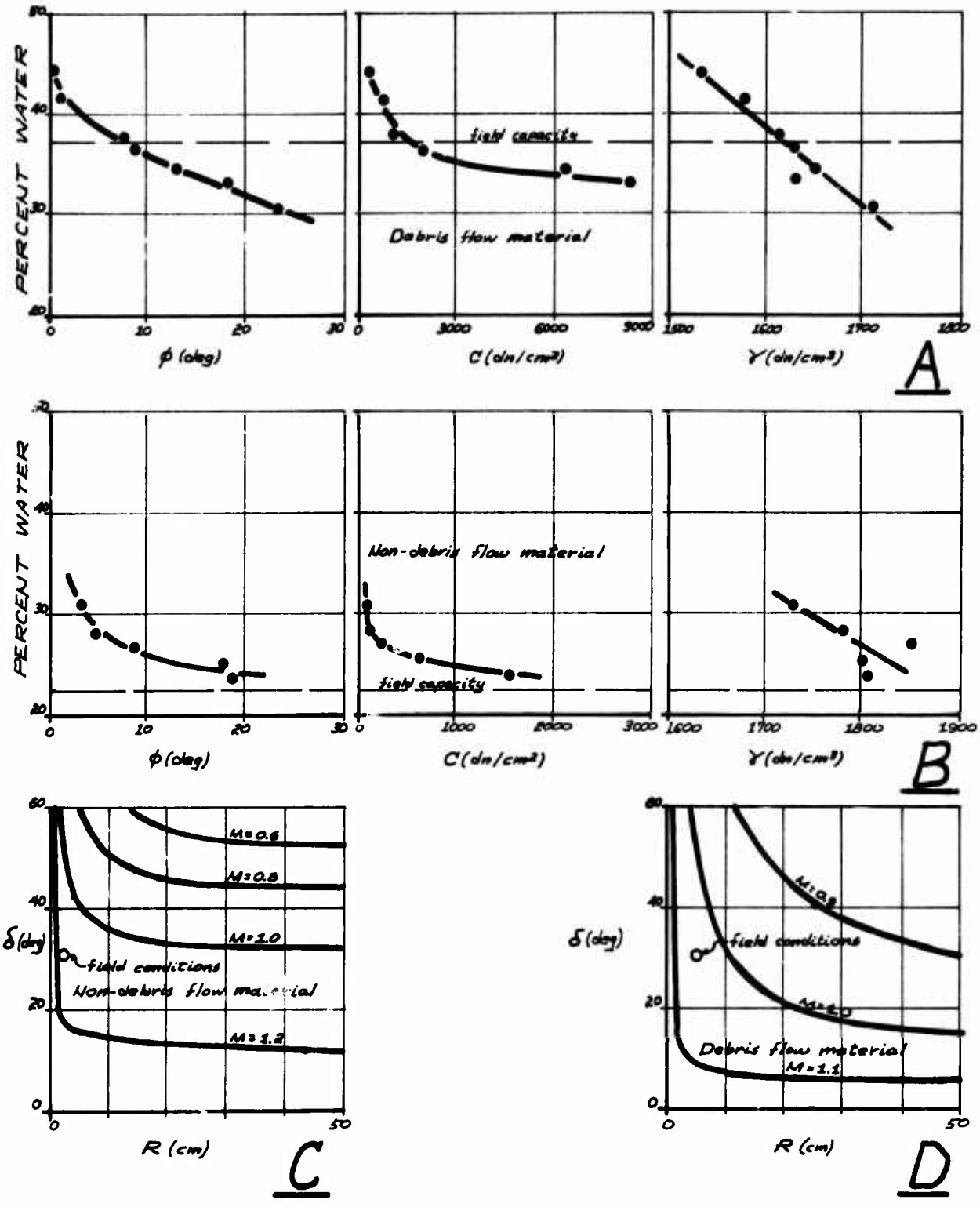

Figure 4. Properties and mobility indices of source materials from Arroyo Hondo, Fresno County, California.

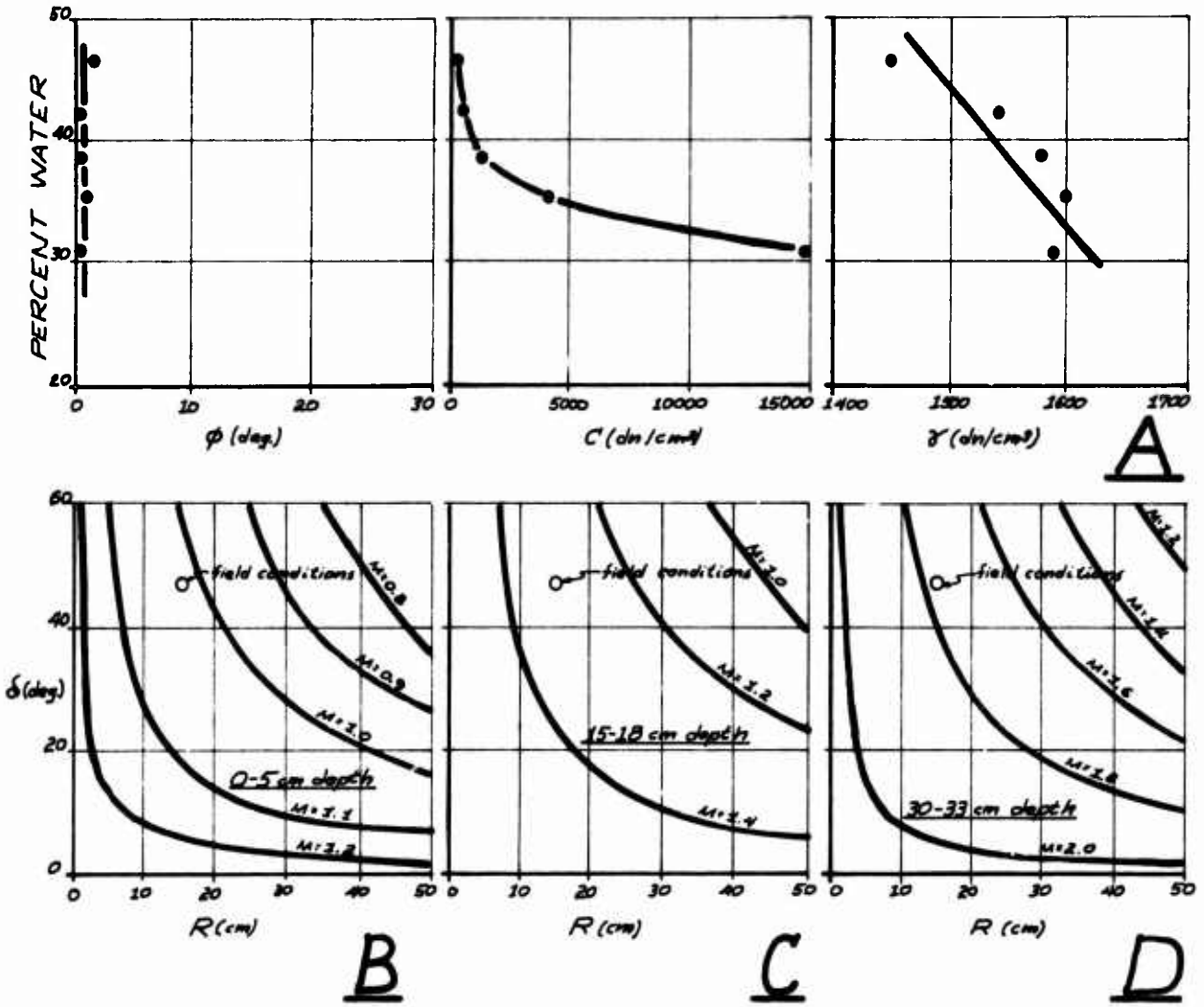

Figure 5. Properties and mobility indices of source materials from Los Altos Hills, Santa Clara County, California.

a value of 1.02 near the surface, to 1.32 at 15 to 18 cm below the surface, to 1.77 at 30 to 33 cm depth (Fig. 5b, 5c, 5d).

The decrease of field capacity and the increase of mobility index with depth suggest that mobility of the debris can be correlated with degree of compaction. The rapid increase of the mobility index with depth explains why the debris flows are small. Large amounts of mixing, churning, and water incorporation would be required to mobilize even 30 cm of soil. The most important conclusion is that the potential for debris flow can change markedly with depth even in a soil that is homogeneous compositionally.

Big Sur, California

Four samples were collected and tested from debris-flow source areas above the village of Big Sur, California (e.g., Rodine, Part I, in press). Samples JR153 and JR154 were collected from the sides of small arcuate scars about 15 cm deep, and samples JR155 and JR156 were taken from the sides of rills 10 and 12 cm deep, respectively. The slope angle was 45 degrees at JR153, 30 degrees at JR154, 32 degrees at JR155 and 40 degrees at JR156. The strength and mobility index data are shown in Figs. 6a to 6b. Three of the four areas sampled have mobility indices of approximately one, JR154-1.02, JR155-1.00, and JR156-.98. The area sampled by JR153 has a low mobility index, 0.4, perhaps a result of an error in the field determination of the channel radius. If the debris mobilized from a series of landslide masses of 2 cm thickness, the mobility index would be approximately equal to one.

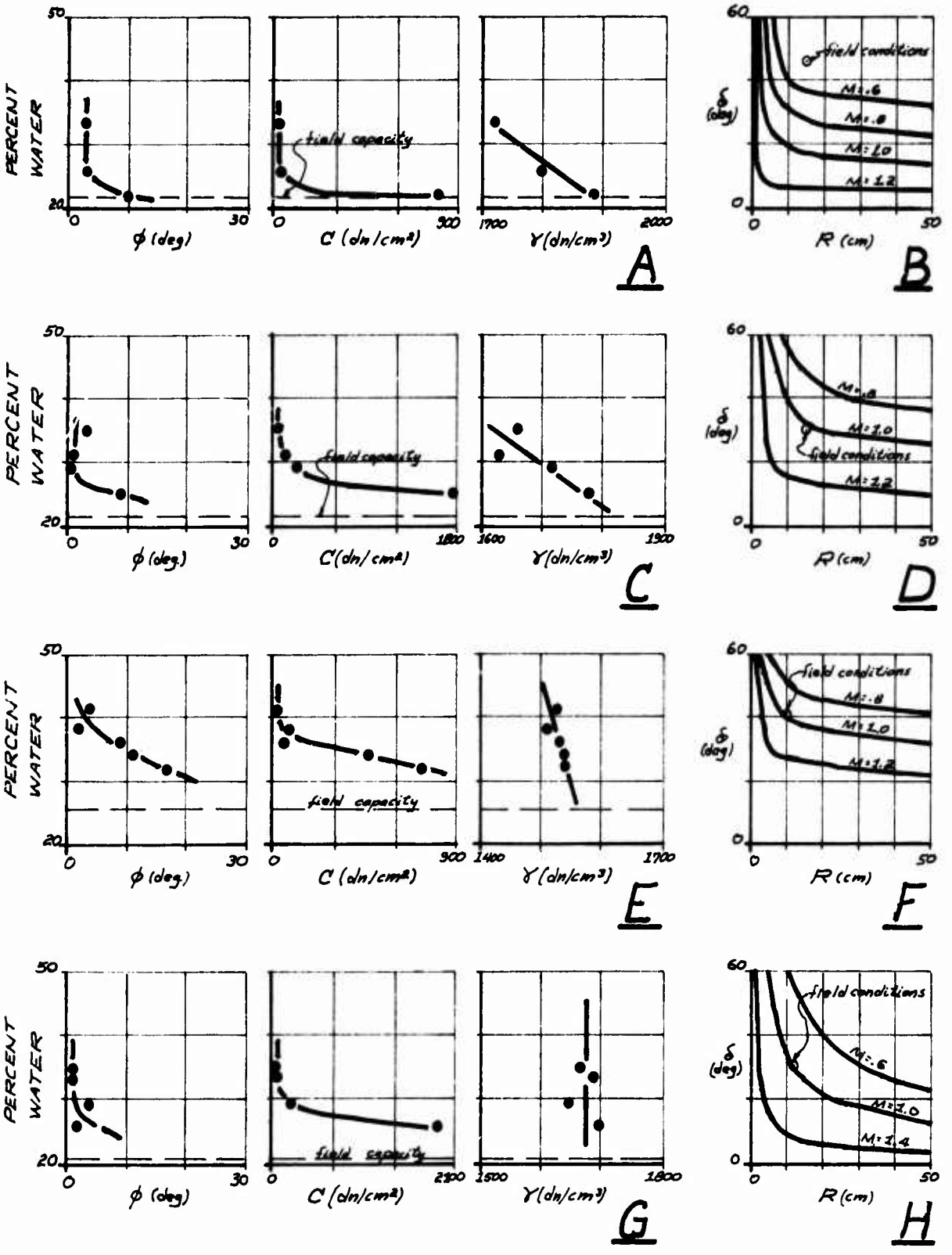

Figure 6. Properties and mobility indices of source materials from Big Sur, Monterey County, California.

Marble Quarry, Wrightwood, California

Study of rills in a debris-flow source area at a marble quarry near Wrightwood, California, suggested that the rills were sites of debris-flow mobilization and that the initiation mechanism was landsliding (Rodine, Part I, in press). The source area slopes at 35 degrees. Strength curves of the source material are shown on Fig. 7a. Using Fig. 7b and a measured rill radius of 12 cm leads to a very low mobility index. However, if the small arcuate scars of one cm height found inside the rills are used as the channel radius the mobility index is 1.0. The hypothesis based on field observations that the rills were formed by the mobilization of many small landslide blocks appears to be well supported by the calculations of mobility index.

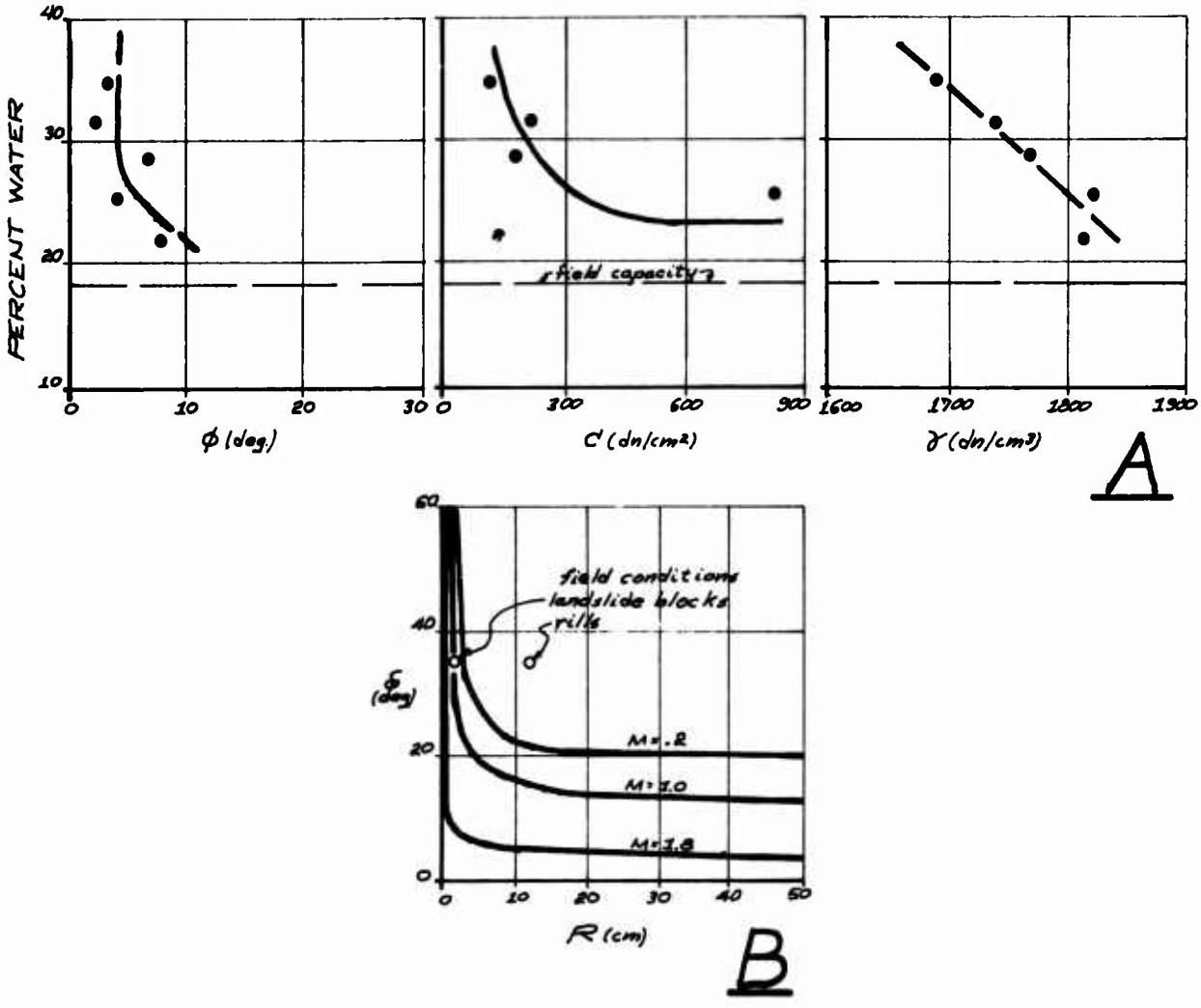

Figure 7. Properties and mobility indices of source materials from Marble Quarry near Wrightwood, San Bernardino County, California.

BIBLIOGRAPHY

Bailey, R. G., and Rice, R. M., 1969, Soil slippage: An indicator of slope instability on chapparal watersheds of southern California: Professional Geographer, Volume 21, Number 3, pp. 172-177.

Bailey, R. W., Forsling, C. L., Becraft, R. J., 1934, Floods and accelerated erosion in northern Utah: United States Department of Agriculture, Miscellaneous Publication Number 196, 21 p.

Blackwelder, E., 1928, Mudflow as a geologic agent in semiarid mountains: Geological Society of America Bulletin, Volume 39, pp. 465-484.

Bonney, C. T., 1902, Moraines and mud-streams in the Alps: Geological Magazine, Decade 4, Volume 9, pp. 8-16.

Cleveland, G. B., 1973, Fire + rain = mudflows, Big Sur, 1972: California Division of Mines and Geology, California Geology, pp. 8-16.

Conway, M., 1907, The fan mountains in the Duab of Turkestan--discussion: The Geographical Journal, Volume 30, pp. 501-502.

Croft, A. R., 1962, Some sedimentation phenomena along the Wasatch Mountain Front: Journal Geophysical Research, Volume 67, Number 4, pp. 1511-1524.

Curry, R. R., 1966, Observations of alpine mudflows in the Tenmile Range, Central Colorado: Geological Society of America Bulletin, Volume 77, pp. 771-776.

Denness, B., 1973, The mudflows at Mutiscua Departmento De Norte De Santander, Colombia (abs): Engineering Group of the Geological Society, Symposium on Mudflows, Lecture 6.

Fleming, R. W., 1971, Soil creep in the vicinity of Stanford University: Unpublished Ph.D. dissertation, Stanford University, Stanford, California.

Fryxell, F. M., and Horberg, L., 1943, Alpine mudflows in Grand Teton National Park, Wyoming: Geological Society of America Bulletin, Volume 54, pp. 457-472.

Greensfelder, R., 1971, Seismological and crustal movement investigations of the San Fernando Earthquake: California Division of Mines and Geology, California Geology, Volume 24, Number 4-5, pp. 62-66.

Hampton, M. A., 1970, Subaqueous debris flow and generation of turbidity currents: Unpublished Ph.D. dissertation, Stanford University, Stanford, California.

_____, 1972, The role of subaqueous debris flow in generating turbidity currents: Journal of Sedimentary Petrology, Volume 42, pp. 775-793.

Jahns, R. H., 1949, Desert floods: Engineering Science Monthly, California Institute of Technology, Contribution Number 499, pp. 10-15.

Johnson, A. M., 1965, A model for debris flow: Unpublished Ph.D. dissertation Pennsylvania State University, University Park, Pennsylvania.

_____, 1970, Physical processes in geology: Freeman, Cooper and Company, 577 p.

_____, and Hampton, M. A., 1968, Subaerial and subaqueous flow of slurries: Annual progress report to United States Geological Survey, Branner Library, Stanford University, Stanford, California.

Johnson, A. M., and Hampton, M. A., 1969, Subaerial and subaqueous flow of slurries: Final progress report to United States Geological Survey, Branner Library, Stanford University, Stanford, California.

_____, and Rahn, P. H., 1970, Mobilization of debris flows: Zeitscrift für Geomorphologie, Supplementband 9, pp. 168-186.

Krumbein, W. C., 1940, Flood gravel of San Gabriel Canyon, California: Geological Society of America Bulletin, Volume 51, pp. 639-676.

_____, 1942, Flood deposits of Arroyo Seco, Los Angeles County, California: Geological Society of America Bulletin, Volume 53, pp. 1355-1402.

Lambe, T. W., and Whitman, R. V., 1969, Soil Mechanics: John Wiley and Sons, 553 p.

Lawson, A. C. (editor), 1908, The California earthquake of April 18, 1906--Report of the State Earthquake Investigation Commission: Carnegie Institution of Washington, Volume 1, 451 p.

Matthes, F. E., 1930, Geologic history of the Yosemite Valley: United States Geological Survey Professional Paper 160.

Morton, D. M., 1971, Seismically triggered landslides above San Fernando Valley: California Division of Mines and Geology, California Geology, Volume 24, Number 4-5, pp. 81-82.

Mullineaux, D. R., and Crandell, D. R., 1962, Recent lahars from Mount St. Helens, Washington: Geological Society of America Bulletin, Volume 73, pp. 855-870.

Pain, C. F., 1971, Rapid mass movement under forest and grass in the Hunua Ranges, New Zealand: Australian Geographical Studies, Volume 9, pp. 77-84.

Rapp, A., 1963, The debris slides at Ulvådal, Western Norway, An example of catastrophic slope processes in Scandinavia: Nachrichten Der Akademie Der Wissenschaften In Göttingen II. Mathematisch Physikalische Klasse, Number 13, pp. 195-210.

Rickmers, W. R., 1913, The Duab of Turkestan: Cambridge University Press, 563 p.

Rodine, J. D., in press, Analysis of mobilization of debris flows: Part I, Processes of initiation of debris flows.

_____, in press, Analysis of mobilization of debris flows: Part III, the ability of debris heavily freighted with coarse clastic materials to flow on gentle slopes.

_____, and Johnson, A. M., in press, Analysis of mobilization of debris flows: Part II, A method of determining Coulomb strength properties of soft, remolded debris using paired conical penetrometers.

Scrivenor, J. B., 1929, The mudstreams ("Lahars") of Gunong Keloet in Java: Geological Magazine, Volume 66, Number 10, pp. 433-434.

Sharp, R. P., 1942, Mudflow levees: Journal of Geomorphology, Volume 5, pp. 222-227.

_____, and Nobles, L. H., 1953, Mudflow of 1941 at Wrightwood, Southern California: Geological Society of America Bulletin, Volume 64, pp. 547-560.

Sharpe, C.F.S., 1938, Landslides and related phenomena: Colombia University Press, 137 p.

Singewald, J. T., 1928, Mudflow as a geologic agent in semiarid mountains--discussion: Geological Society of America Bulletin, Volume 39, pp. 480-483.

Skempton, A. W., 1964, Long-term stability of clay slopes: Geotechnique, Volume 14, pp. 75-102.

Swanston, D. M., 1970, Mechanics of debris avalanching in shallow till soils of southeast Alaska: United States Department of Agriculture Forest Service Research Paper PNW-103.

Temple, P. H., and Rapp, A., 1972, Landslides in the Mgeta Area, western Uluguru Mountains, Tanzania: Geografiska Annaler, Volume 54A, pp. 157-193.

Terzaghi, K., 1950, Mechanism of landslides: IN, Application of geology to engineering practice, Berkey Volume, Geological Society of America, pp. 83-123.

Troxell, H. C., and Peterson, J. Q., 1937, Flood in La Cañada Valley, California, January 1, 1934: United States Geological Survey Water Supply Paper 796-C, pp. 53-98.

Wentworth, C. K., 1943, Soil avalanches on Oahu, Hawaii: Geological Society of America Bulletin, Volume 54, pp. 53-64.

Williams, G. P., and Guy, H. P., 1971, Debris avalanches--a geomorphic hazard: IN, Environmental Geomorphology, State University New York, Binghampton, pp. 25-46.

_____, _____, 1973, Erosional and depositional aspects of Hurricane Camille in Virginia, 1969: United States Geological Survey Professional Paper 804, 80 p.

APPENDIX

COMPUTER PROGRAM TO PACK SPHERES IN A CUBIC ARRAY

```
      $WATFIV                                                                4.
      C----- PROGRAM TO FIT SPHERES INTO AN ORTHOGONAL CELL IN EITHER THE      5.
      C----- TIGHTEST POSSIBLE PACKING OR USING A SPECIFIED SIZE DISTRIBUTION. 6.
      C----- JIM RODINE, STANFORD UNIVERSITY, JUNE 1971. REVISED:7-'71        7.
    1       REAL ARRAY(12,12,12), SPH(10), RAD(8), MAXRAD                     8.
    2       INTEGER OPTION, COUNT                                             9.
      C----- READ INITIAL DATA PARAMETERS.                                    10.
      C----- I IS THE ROW COORDINATE OF THE MATRIX UNIT CELL.                 11.
      C----- J IS THE COLUMN COORDINATE OF THE MATRIX UNIT CELL.              12.
      C----- K IS THE SLICE COORDINATE OF THE MATRIX UNIT CELL.              13.
      C----- RAD(1) IS THE RADIUS OF THE LARGEST SPHERE TO BE PLACED IN THE  14.
      C----- UNIT CELL. IT IS PLACED WITH ITS CENTER AT I=1, J=1, K=1.        15.
      C----- NUBALL IS THE NUMBER OF SPHERES TO BE PLACED.                    16.
      C----- OPTION IS THE PACKING CHOICE.                                    17.
      C-----    OPTION = 0 FOR THE TIGHTEST POSSIBLE PACKING.                 18.
      C-----    OPTION = 1 FOR PACKING TO A GIVEN DISTRIBUTION OF SIZES.      19.
      C----- IFPLOT IS THE PLOTTING OPTION ROUTINE.                           20.
      C          IFPLOT = 1 FOR THE GRAPHICAL DISPLAY.                       21.
      C          IFPLOT = 0 FOR NO GRAPHICAL DISPLAY.                        22.
    3       READ(5,1) I, J, K, RAD(1), NUBALL, OPTION, IFPLOT                 23.
    4     1 FORMAT (3I5, 1F10.2, 3I5)                                         24.
      C----- WRITE INITIAL DATA PARAMETERS.                                   25.
    5       WRITE (6,2) I, J, K, RAD(1), NUBALL, OPTION, IFPLOT               26.
    6     2 FORMAT (1H ,20X,'ORIGINAL DATA PARAMETERS READ INTO PROGRAM',/,5X, 27.
           C'NUMBER OF ROWS =',I5,5X,'NUMBER OF COLUMNS =',I5,5X,'NUMBER OF SL 28.
           CICES =',I5,/,5X,'RADIUS OF LARGEST GIVEN SPHERE =',F10.2,5X,'NUMBE 29.
           CR OF DIFFERENT SIZED BALLS =',I5,/,5X,'PACKING OPTION =',I5,       30.
           C ' (0 = TIGHTEST POSSIBLE PACKING, 1 = PACKING TO THE GIVEN DISTRI 31.
           CBUTION)',/,5X,'GRAPHICAL DISPLAY OPTION =',I5,' (0 = NO PLOT, 1 = 32.
           CPLOT RESULTS)')                                                    33.
      C----- FOR A GIVEN DISTRIBUTION OF SPHERES READ THE RADII.              34.
    7       READ (5,5) (RAD(II), II=2,NUBALL)                                 35.
    8     5 FORMAT (8F9.2)                                                    36.
      C----- IF THE LARGEST POSSIBLE SPHERES ARE TO BE FITTED, DIVERT TO      37.
      C       CARD NUMBER 98.                                                 38.
    9       IF (OPTION.EQ.0) GO TO 98                                         39.
      C----- WRITE THE GIVEN RADII.                                           40.
   10       WRITE (6,6) (RAD(II), II=2,NUBALL)                                41.
   11     6 FORMAT (1H0,20X,'THE PROGRAM WILL ATTEMPT TO FIT THE FOLLOWING SPH 42.
           CERE SIZES',/,10X,'SPHERE-2 RADIUS =',F6.2,5X,'SPHERE-3 RADIUS =', 43.
           C F6.2,5X,'SPHERE-4 RADIUS =',F6.2,5X,'SPHERE-5 RADIUS =',F6.2,/,  44.
           C 10X,'SPHERE-6 RADIUS =',F6.2,5X,'SPHERE-7 RADIUS =',F6.2,5X,     45.
           C 'SPHERE-8 RADIUS =',F6.2)                                        46.
      C----- CALL SUBROUTINE FILL1 TO FILL IN THE FIRST SPHERE.               47.
   12    98 CALL FILL1(ARRAY,SPH,RAD(1),I,J,K,TOTAL)                         48.
   13       IF (NUBALL.EQ.1) GO TO 1000                                       49.
   14       INDEX = 1                                                         50.
   15       IMIN1 = I - 1                                                     51.
   16       JMIN1 = J - 1                                                     52.
   17       KMIN1 = K - 1                                                     53.
      C------------------------------------------------------------------------ 54.
      C----- ENTER MASTER DO LOOP                                             55.
   18       DO 200 N=2,NUBALL                                                 56.
   19       IF (N.EQ.2) GO TO 49                                              57.
   20       IF ((MAXRAD.LT.RAD(N)).AND.(OPTION.EQ.1)) GO TO 51                58.
   21    49 MAXRAD = 1.                                                       59.
   22       COUNT = 0                                                         60.
   23       TEMPR = 1.                                                        61.
   24       INDEX1 = 0                                                        62.
      C----- USE SPECIFIED SPHERE SIZE IF DESIRED.                            63.
```

```
25          IF (OPTION.EQ.1) TEMPR = RAD(N)                                  64.
      C---- COMPUTE LARGEST RADIUS SPHERE SIZE THAT WILL FIT INTO EACH AVAIL-  65.
      C     ABLE COORDINATE POSITION.                                        66.
26          DO 106 II = 2,IMIN1                                              67.
27          DO 107 JJ = 2,JMIN1                                              68.
28          DO 108 KK = 2,KMIN1                                              69.
      C---- EXCLUDE ARRAY LOCATIONS FILLED WITH OTHER SPHERES                 70.
29          IF (ARRAY(II,JJ,KK).LT.0.0) GO TO 108                            71.
30          CALL ENLARG(ARRAY, I, J, K, II, JJ, KK)                          72.
      C----- IF THE RADIUS IS NOT SPECIFIED DIVERT TO CARD 50.                73.
31       54 IF (OPTION.EQ.0) GO TO 50                                        74.
      C----- USE MAXRAD TO KEEP TRACK OF THE MAXIMUM POSSIBLE SPHERE         75.
      C      RADIUS LOCATIONS AVAILABLE.                                     76.
32          IF (MAXRAD.LT.ARRAY(II,JJ,KK)) MAXRAD = ARRAY(II,JJ,KK)          77.
33          IF (MAXRAD.GT.RAD(N)) MAXRAD = RAD(N)                            78.
      C----- IF THE ARRAY LOCATION WILL NOT FIT THE CHOSEN SPHERE PASS TO     79.
      C      STATEMENT NUMBER 108.                                           80.
34          IF (ARRAY(II,JJ,KK).LT.RAD(N)) GO TO 108                         81.
35          COUNT = COUNT + 1                                                82.
36          CALL SETARY(ARRAY,I,J,K,II,JJ,KK,RAD(N),1,SPH(N),&108)           83.
37          GO TO 108                                                        84.
38       50 IF (ARRAY(II,JJ,KK).LT.TEMPR) GO TO 108                          85.
39          IF (ARRAY(II,JJ,KK).EQ.TEMPR) GO TO 112                          86.
40          IF (ARRAY(II,JJ,KK).GT.TEMPR) GO TO 113                          87.
41      112 INDEX1 = INDEX1 + 1                                              88.
42          GO TO 108                                                        89.
43      113 INDEX1 = 1                                                       90.
44          TEMPR = ARRAY(II,JJ,KK)                                          91.
45          ID = II                                                          92.
46          JD = JJ                                                          93.
47          KD = KK                                                          94.
48      108 CONTINUE                                                         95.
49      107 CONTINUE                                                         96.
50      106 CONTINUE                                                         97.
      C----- IF NO SITE IS AVAILABLE FOR THE SPHERE DIVERT TO CARD 51.       98.
51       53 IF ((COUNT.EQ.0).AND.(OPTION.EQ.1)) GO TO 51                     99.
      C----- IF ONLY ONE SPHERE LOCATION IS TO BE FILLED                     100.
      C      GO DIRECTLY TO THE SUBROUTINE CALL - CARD 121.                  101.
52          IF (INDEX1.EQ.1) GO TO 121                                       102.
      C      GO TO STATEMENT NUMBER 502 IF NO ADDITIONAL SPHERES CAN BE FITTED 103.
53          IF (INDEX1.EQ.0.AND.COUNT.EQ.0) GO TO 502                        104.
      C----- IF OPTION IS DISTRIBUTED PACKING DIVERT TO CARD 122.             105.
54          IF (OPTION.EQ.1) GO TO 122                                       106.
      C----- USE ELIMINATION PROCEDURE TO FILL THE AVAILABLE SPHERE SITES.    107.
55          INDEX = 0                                                        108.
      C----- CALL SUBROUTINE DOIT TO FILL THE SPHERE SITES AND TO BLANK OUT   109.
      C      THE REMAINING VOID AREA IF NECESSARY.                           110.
56          CALL DOIT(ARRAY,IMIN1,JMIN1,KMIN1,INDEX,INDEX1,SPH(N),TEMPR,1)   111.
57          COUNT = INDEX                                                    112.
58          GO TO 122                                                        113.
59      121 CALL SETARY(ARRAY,I,J,K,ID,JD,KD,TEMPR,INDEX1,SPH(N), &122)      114.
60          CALL DOIT(ARRAY,IMIN1,JMIN1,KMIN1,INDEX,INDEX1,SPH(N),TEMPR,0)   115.
      C----- COMPUTE NEW VOLUME PARAMETERS                                    116.
61          GO TO 123                                                        117.
62      122 INDEX1 = COUNT                                                   118.
63      123 CALL VOLUME(N,RAD(1),TEMPR,INDEX1,TOTAL)                         119.
64          GO TO 200                                                        120.
      C----- WRITE 51 WHEN NO SPHERE RADIUS EXISTS.                           121.
65       51 WRITE (6,7) N, RAD(N), MAXRAD                                    122.
66        7 FORMAT (1HO,'THERE IS NO LOCATION AVAILABLE FOR SPHERE NUMBER',  123.
```

```
      C  I3,', WITH A RADIUS =',F7.2,', THE LARGEST AVAILABLE SITE RADIUS 124.
      C =',F7.2)                                                         125.
     C----- END OF MASTER DO LOOP                                        126.
67     200 CONTINUE                                                      127.
     C------------------------------------------------------------------ 128.
68     502 WRITE (6,503)                                                 129.
     C----- IF NO PLOT IS DESIRED DIVERT TO CARD 1000                   130.
69         IF (IFPLOT.EQ.0) GO TO 1000                                   131.
     C----- CALL THE PLOTTING SUBROUTINE                                132.
70         CALL PLOT(ARRAY,I,J,K)                                        133.
71         GO TO 1000                                                    134.
     C----- PROGRAM COMPLETION RETURN WRITE STATEMENT.                   135.
72     503 FORMAT (1H ,10X,'****PROGRAM INTERVAL RETURN - THE ARRAY HAS NO LO 136.
       CCATION FOR ANOTHER SPHERE****')                                  137.
73    1000 RETURN                                                        138.
74         END                                                           139.
```

```
75          SUBROUTINE ENLARG(A,I,J,K,II,JJ,KK)                              140.
      C---- SUBROUTINE TO FIT THE LARGEST SIZE SPHERE INTO A COORDINATE        141.
      C     LOCATION.                                                         142.
      C----- DIMENSION ARRAY                                                  143.
76          REAL A(12,12,12)                                                  144.
      C----- CREATE STATEMENT FUNCTION FOR SQUARE ROOT.                       145.
77          RSQRT(IA,IB,IC) = SQRT(FLOAT((IA*IA) + (IB*IB) + (IC*IC)))       146.
      C---- SET SPHERE SEARCH COORDINATES.                                    147.
78          IMIN = II - 1                                                     148.
79          IMAX = II + 1                                                     149.
80          JMIN = JJ - 1                                                     150.
81          JMAX = JJ + 1                                                     151.
82          KMIN = KK - 1                                                     152.
83          KMAX = KK + 1                                                     153.
      C----- ASSIGN INITIAL RADIUS VALUE.                                     154.
84          TEMPR = 1.                                                        155.
      C----- CHECK TO SEE IF ANY LOCATION IS ALREADY FILLED.                  156.
85          IF ((A(IMIN,JJ,KK).EQ.(-1.)).OR.(A(IMIN,JJ,KK).EQ.(-2.)).OR.     157.
           C (A(IMIN,JJ,KK).EQ.(-3.)).OR.(A(IMIN,JJ,KK).EQ.(-4.)).OR.       158.
           C (A(IMIN,JJ,KK).EQ.(-5.)).OR.(A(IMIN,JJ,KK).EQ.(-6.)).OR.       159.
           C (A(IMIN,JJ,KK).EQ.(-7.)).OR.(A(IMIN,JJ,KK).EQ.(-8.)).OR.       160.
           C (A(IMIN,JJ,KK).EQ.(-9.))) GO TO 1000                           161.
86          IF ((A(IMAX,JJ,KK).EQ.(-1.)).OR.(A(IMAX,JJ,KK).EQ.(-2.)).OR.     162.
           C (A(IMAX,JJ,KK).EQ.(-3.)).OR.(A(IMAX,JJ,KK).EQ.(-4.)).OR.       163.
           C (A(IMAX,JJ,KK).EQ.(-5.)).OR.(A(IMAX,JJ,KK).EQ.(-6.)).OR.       164.
           C (A(IMAX,JJ,KK).EQ.(-7.)).OR.(A(IMAX,JJ,KK).EQ.(-8.)).OR.       165.
           C (A(IMAX,JJ,KK).EQ.(-9.))) GO TO 1000                           166.
87          IF ((A(II,JMIN,KK).EQ.(-1.)).OR.(A(II,JMIN,KK).EQ.(-2.)).OR.     167.
           C (A(II,JMIN,KK).EQ.(-3.)).OR.(A(II,JMIN,KK).EQ.(-4.)).OR.       168.
           C (A(II,JMIN,KK).EQ.(-5.)).OR.(A(II,JMIN,KK).EQ.(-6.)).OR.       169.
           C (A(II,JMIN,KK).EQ.(-7.)).OR.(A(II,JMIN,KK).EQ.(-8.)).OR.       170.
           C (A(II,JMIN,KK).EQ.(-9.))) GO TO 1000                           171.
88          IF ((A(II,JMAX,KK).EQ.(-1.)).OR.(A(II,JMAX,KK).EQ.(-2.)).OR.     172.
           C (A(II,JMAX,KK).EQ.(-3.)).OR.(A(II,JMAX,KK).EQ.(-4.)).OR.       173.
           C (A(II,JMAX,KK).EQ.(-5.)).OR.(A(II,JMAX,KK).EQ.(-6.)).OR.       174.
           C (A(II,JMAX,KK).EQ.(-7.)).OR.(A(II,JMAX,KK).EQ.(-8.)).OR.       175.
           C (A(II,JMAX,KK).EQ.(-9.))) GO TO 1000                           176.
89          IF ((A(II,JJ,KMIN).EQ.(-1.)).OR.(A(II,JJ,KMIN).EQ.(-2.)).OR.     177.
           C (A(II,JJ,KMIN).EQ.(-3.)).OR.(A(II,JJ,KMIN).EQ.(-4.)).OR.       178.
           C (A(II,JJ,KMIN).EQ.(-5.)).OR.(A(II,JJ,KMIN).EQ.(-6.)).OR.       179.
           C (A(II,JJ,KMIN).EQ.(-7.)).OR.(A(II,JJ,KMIN).EQ.(-8.)).OR.       180.
           C (A(II,JJ,KMIN).EQ.(-9.))) GO TO 1000                           181.
90          IF ((A(II,JJ,KMAX).EQ.(-1.)).OR.(A(II,JJ,KMAX).EQ.(-2.)).OR.     182.
           C (A(II,JJ,KMAX).EQ.(-3.)).OR.(A(II,JJ,KMAX).EQ.(-4.)).OR.       183.
           C (A(II,JJ,KMAX).EQ.(-5.)).OR.(A(II,JJ,KMAX).EQ.(-6.)).OR.       184.
           C (A(II,JJ,KMAX).EQ.(-7.)).OR.(A(II,JJ,KMAX).EQ.(-8.)).OR.       185.
           C (A(II,JJ,KMAX).EQ.(-9.))) GO TO 1000                           186.
      C---- ENTER LOOP TO EXPAND SPHERE TO ITS LARGEST POSSIBLE SIZE.        187.
91          DO 1 N = 1,I                                                     188.
      C----- ASSIGN RADIUS VALUE TO ARRAY.                                   189.
92          A(II,JJ,KK) = TEMPR                                              190.
      C----- ADD 1. TO RADIUS VALUES.                                        191.
93          TEMPR = TEMPR + 1.                                               192.
      C----- SET SPHERE SEARCH COORDINATES.                                   193.
94          IMIN = IMIN - 1                                                  194.
95          IMAX = IMAX + 1                                                  195.
96          JMIN = JMIN - 1                                                  196.
97          JMAX = JMAX + 1                                                  197.
98          KMIN = KMIN - 1                                                  198.
99          KMAX = KMAX + 1                                                  199.
```

```
      C----- CHECK TO SEE IF THE NEW VALUES ARE OUTSIDE THE COORDINATE BOUNDS  200.
100         IF ((IMIN.LT.1).OR.(IMAX.GT.I).OR.(JMIN.LT.1).OR.(JMAX.GT.J).OR.   201.
           C (KMIN.LT.1).OR.(KMAX.GT.K)) GO TO 1000                            202.
      C----- ENTER LOOP TO CHECK ALL VALUES INSIDE THE SPHERE BEING TESTED.     203.
101         DO 2 III = IMIN,IMAX                                                204.
102         IRI = II - III                                                      205.
103         DO 3 JJJ = JMIN,JMAX                                                206.
104         IRJ = JJ - JJJ                                                      207.
105         DO 4 KKK = KMIN,KMAX                                                208.
106         IRK = KK - KKK                                                      209.
107         RADIUS = PSQRT(IRI,IRJ,IRK)                                         210.
      C----- EXCLUDE POINTS LYING OUTSIDE OR ON THE SPHERE.                      211.
108         IF (RADIUS.GE.TEMPR) GO TO 4                                        212.
      C----- ABORT SEARCH IF ANOTHER SPHERE IS LOCATED IN PLACE WITHIN THE       213.
      C       BOUNDS OF THE SPHERE TESTED FOR.                                  214.
109         IF ((A(III,JJJ,KKK).EQ.(-1.)).OR.(A(III,JJJ,KKK).EQ.(-2.)).OR.     215.
           C (A(III,JJJ,KKK).EQ.(-3.)).OR.(A(III,JJJ,KKK).EQ.(-4.)).OR.        216.
           C (A(III,JJJ,KKK).EQ.(-5.)).OR.(A(III,JJJ,KKK).EQ.(-6.)).OR.        217.
           C (A(III,JJJ,KKK).EQ.(-7.)).OR.(A(III,JJJ,KKK).EQ.(-8.)).OR.        218.
           C  (A(III,JJJ,KKK).EQ.(-9.))) GO TO 1000                            219.
110        4 CONTINUE                                                          220.
111        3 CONTINUE                                                          221.
112        2 CONTINUE                                                          222.
113        1 CONTINUE                                                          223.
      C----- RETURN TO THE MAIN PROGRAM.                                       224.
114     1000 RETURN                                                            225.
115         END                                                                 226.
```

```
116         SUBROUTINE FILL1(ARRAY,SPH,RAD,I,J,K,TOTAL)                       227.
117         REAL ARRAY(12,12,12), SPH(10)                                     228.
      C----- COMPUTE TOTAL VOLUME OF THE UNIT CELL.                           229.
118         TOTAL = (I - 1)*(J - 1)*(K - 1)                                   230.
      C----- FILL SPHERE IDENTIFICATION ARRAY (SPH)                          231.
119         DO 99 II = 1,10                                                   232.
      C----- NOTE: SPHERES ARE LABELED WITH A MINUS SIGN.                    233.
120      99 SPH(II) = -II                                                     234.
      C---- FILL IN ARRAY AREAS OCCUPIED BY SPHERE-1                         235.
121         DO 103 II = 1,I                                                   236.
122         IRI = II - 1                                                      237.
123         DO 104 JJ = 1,J                                                   238.
124         IRJ = JJ - 1                                                      239.
125         DO 105 KK = 1,K                                                   240.
126         IRK = KK - 1                                                      241.
      C----- COMPUTE RADIUS TO ARRAY POINT.                                  242.
127         TEMPR = SQRT(FLOAT((IRI*IRI) + (IRK*IRK) + (IRJ*IRJ)))           243.
      C----- IF THE COMPUTED RADIUS EXCEEDS THE SPHERE-1 RADIUS - DIVERT POINT 244.
128         IF (TEMPR.GT.RAD) GO TO 100                                       245.
      C----- ASSIGN SPHERE-1 IDENTIFIER TO ARRAY.                            246.
129         ARRAY(II,JJ,KK) = SPH(1)                                          247.
130         GO TO 105                                                         248.
      C----- PLACE A ZERO IN ALL UNFILLED SPACES.                            249.
131      100 ARRAY(II,JJ,KK) = 0.0                                            250.
132      105 CONTINUE                                                         251.
133      104 CONTINUE                                                         252.
134      103 CONTINUE                                                         253.
      C---- CALCULATE VOLUMES OF SOLID AND VOID SPACE                        254.
135         CALL VOLUME(1,RAD,RAD,1,TOTAL)                                    255.
      C----- RETURN TO THE MAIN PROGRAM                                      256.
136         RETURN                                                            257.
137         END                                                               258.
```

```
138           SUBROUTINE DOIT(ARRAY,IMIN1,JMIN1,KMIN1,INDEX,INDEX1,SPH1,TEMPR,  259.
             C NOYES)                                                           260.
139           REAL ARRAY(12,12,12)                                               261.
140           IF (NOYES.EQ.0) GO TO 52                                           262.
141           DO 115 II = 2,IMIN1                                                263.
142           DO 116 JJ = 2,JMIN1                                                264.
143           DO 117 KK = 2,KMIN1                                                265.
144           IF (ARRAY(II,JJ,KK).NE.TEMPR) GO TO 117                            266.
145           CALL SETARY (ARRAY,I,J,K,II,JJ,KK,TEMPR,INDEX1,SPH1, &117)         267.
146           INDEX = INDEX + 1                                                  268.
147       117 CONTINUE                                                           269.
148       116 CONTINUE                                                           270.
149       115 CONTINUE                                                           271.
          C----- BLANK OUT RADIUS VALUES IN THE ARRAY.                          272.
150        52 DO 118 II = 2,IMIN1                                                273.
151           DO 119 JJ = 2,JMIN1                                                274.
152           DO 120 KK = 2,KMIN1                                                275.
153           IF (ARRAY(II,JJ,KK).GT.0.0) ARRAY(II,JJ,KK) = 0.0                  276.
154       120 CONTINUE                                                           277.
155       119 CONTINUE                                                           278.
156       118 CONTINUE                                                           279.
          C----- RETURN TO THE MAIN PROGRAM.                                    280.
157           RETURN                                                             281.
158           END                                                                282.
```

```
159         SUBROUTINE SETARY(A,I,J,K,II,JJ,KK,RAD,IND,SPHERE, *)                283.
      C----- SUBROUTINE TO PLACE SPHERE SYMBOL INTO PROPER ARRAY POSITION.       284.
      C       DIMENSION ARRAY                                                    285.
160         REAL A(12,12,12)                                                     286.
      C----- SET UP STATEMENT FUNCTION FOR SQUARE ROOT.                          287.
161         RSQRT(IA,IB,IC) = SQRT(FLOAT((IA*IA) + (IB*IB) + (IC*IC)))           288.
162         IRAD = RAD                                                           289.
      C---- SET BOUNDS ON THE SPHERE TO BE PLACED.                              290.
163         IMIN = II - IRAD                                                     291.
164         IMAX = II + IRAD                                                     292.
165         JMIN = JJ - IRAD                                                     293.
166         JMAX = JJ + IRAD                                                     294.
167         KMIN = KK - IRAD                                                     295.
168         KMAX = KK + IRAD                                                     296.
      C----- DIVERT SINGULAR SPHERE LOCATION TO PLACEMENT LOOPS.                 297.
169         IF (IND.EQ.1) GO TO 4                                                298.
      C----- ENTER CHECKING DO LOOPS.                                            299.
170         DO 1 I3 = IMIN,IMAX                                                  300.
171         IRI = II - I3                                                        301.
172         DO 2 J3 = JMIN,JMAX                                                  302.
173         IRJ = JJ - J3                                                        303.
174         DO 3 K3 = KMIN,KMAX                                                  304.
175         IRK = KK - K3                                                        305.
      C----- COMPUTE DISTANCE TO ARRAY LOCATION FROM THE CENTER OF THE SPHERE.  306.
176         TEMPR = RSQRT(IRI,IRJ,IRK)                                           307.
177         TEMPR = TEMPR + .2                                                   308.
      C----- CHECK TO SEE IF ARRAY LOCATION IS WITHIN THE SPHERE.                309.
178         IF (TEMPR.GE.RAD) GO TO 3                                            310.
      C----- IF ANOTHER SPHERE IS LOCATED THE PROCESS IS ABORTED.                311.
179         IF (A(I3,J3,K3).EQ.SPHERE) RETURN 1                                  312.
180       3 CONTINUE                                                             313.
181       2 CONTINUE                                                             314.
182       1 CONTINUE                                                             315.
      C----- ENTER PLACEMENT DO LOOPS.                                          316.
183       4 DO 5 I3 = IMIN,IMAX                                                  317.
184         IRI = II - I3                                                        318.
185         DO 6 J3 = JMIN,JMAX                                                  319.
186         IRJ = JJ - J3                                                        320.
187         DO 7 K3 = KMIN,KMAX                                                  321.
188         IRK = KK - K3                                                        322.
      C----- COMPUTE DISTANCE TO ARRAY LOCATION FROM CENTER OF SPHERE.          323.
189         TEMPR = RSQRT(IRI,IRJ,IRK)                                           324.
      C----- CHECK TO SEE IF ARRAY LOCATION IS WITHIN THE SPHERE.                325.
190         IF (TEMPR.GT.RAD) GO TO 7                                            326.
      C----- ASSIGN SPHERE SYMBOL TO ARRAY LOCATION.                             327.
191         IF (A(I3,J3,K3).LT.(0.01)) GO TO 8                                   328.
192         A(I3,J3,K3) = SPHERE                                                 329.
193         GO TO 7                                                              330.
194       8 A(I3,J3,K3) = (-9.)                                                  331.
195       7 CONTINUE                                                             332.
196       6 CONTINUE                                                             333.
197       5 CONTINUE                                                             334.
      C----- END OF SUBROUTINE SETARY                                           335.
198    1000 RETURN                                                             336.
199         END                                                                  337.
```

```
200         SUBROUTINE VOLUME(N,R,RT,NS,T)                                    338.
      C---- N = ITERATION NUMBER                                              339.
      C     R = RADIUS OF THE LARGEST SPHERE.                                 340.
      C     RT = RADIUS OF THE SPHERE BEING PLACED.                           341.
      C     NS = NUMBER OF SPHERES BEING PLACED.                              342.
      C     T = TOTAL VOLUME OF THE UNIT CELL.                                343.
201         IF (N.EQ.1) SOLID = 0.                                            344.
202         RNS = NS                                                          345.
203         VOLSOL = 4.1888*RT*RT*RT*RNS                                      346.
204         IF (N.EQ.1) VOLSOL = VOLSOL/8.                                    347.
205         SOLID = SOLID + VOLSOL                                            348.
206         PSOLID = (SOLID/T)*100.                                           349.
207         VOLVD = T - SOLID                                                 350.
208         PVOLVD = (VOLVD/T)*100.                                           351.
209         RATIO = RT/R                                                      352.
210         SPHVOL = (VOLSOL/T)*100.                                          353.
211         WRITE (6,1) N,RT,NS,VOLSOL,SPHVOL,SOLID,PSOLID,VOLVD,PVOLVD,RATIO 354.
212       1 FORMAT (1HO,9X,'VOLUME PARAMETERS AFTER INSERTION OF SPHERE NUMBER 355.
           C',I3,', WITH A RADIUS =',F4.1,/,5X,'TOTAL NUMBER OF SPHERES PLACED 356.
           C =',I5,5X,'VOLUME OCCUPIED BY THE NEW SPHERES =',F10.3,', OR',    357.
           C F7.3,' PERCENT',/,5X,'TOTAL VOLUME OF ALL PLACED SPHERES =',     358.
           C F10.3,', OR',F7.3,' PERCENT. TOTAL VOID VOLUME REMAINING =',     359.
           C F10.3,', OR',F7.3,' PERCENT',/,5X,'RATIO OF THE PLACED SPHERE TO 360.
           CTHE FIRST SPHERE =',F7.4)                                         361.
      C---- RETURN TO THE MAIN PROGRAM                                        362.
213         RETURN                                                            363.
214         END                                                               364.
```

```
215           SUBROUTINE PLOT(A,I,J,K)                                          365.
      C-----  SUBROUTINE TO PLOT RESULTS.                                       366.
      C        DIMENSION THE ARRAY.                                             367.
216           REAL A(12,12,12)                                                  368.
      C-----  WRITE THE TITLE ACROSS THE TOP OF THE DISPLAY.                    369.
217           WRITE (6,15)                                                      370.
218        15 FORMAT (1H ,////,30X,'CROSS-SECTION DISPLAYS OF THE SOLUTION',/,  371.
          C 10X,'NUMBERS INDICATE THE ORDER OF SPHERE EMPLACEMENT - 9 INDICAT 372.
          CES A COMMON POINT')                                                 373.
      C-----  MULTIPLY ARRAY BY -1. TO YIELD POSITIVE NUMBERS FOR PLOTTING.     374.
219           DO 123 II = 1,I                                                   375.
220           DO 124 JJ = 1,J                                                   376.
221           DO 125 KK = 1,K                                                   377.
222        125 A(II,JJ,KK) = A(II,JJ,KK)*(-1.)                                  378.
223        124 CONTINUE                                                         379.
224        123 CONTINUE                                                         380.
      C----- ENTER THE PRIMARY DO LOOP.                                        381.
      C-----  DIVERT ARRAYS WITH A WIDTH GREATER THAN 10 TO CARD 20.            382.
225           IF (J.GT.10) GO TO 20                                             383.
      C-----  ENTER PLOTTING LOOP.                                             384.
226           DO 1 KK = 1,K                                                     385.
      C-----  SELECT PROPER WRITE STATEMENTS.                                  386.
227           IF ((KK.EQ.2).OR.(KK.EQ.4).OR.(KK.EQ.6).OR.(KK.EQ.8).OR.         387.
          C (KK.EQ.10)) WRITE (6,10) KK                                        388.
228           IF ((KK.EQ.1).OR.(KK.EQ.3).OR.(KK.EQ.5).OR.(KK.EQ.7).OR.         389.
          C (KK.EQ.9)) WRITE (6,11) KK                                         390.
      C-----  PRINT ARRAY                                                      391.
229           DO 2 II = 1,I                                                     392.
230        2 WRITE (6,12) (A(II,JJ,KK), JJ=1,J)                                 393.
231        1 CONTINUE                                                           394.
232           GO TO 1000                                                        395.
      C-----  DIVERT ARRAYS WITH A WIDTH GREATER THAN 25 TO CARD 30.            396.
233        20 IF (J.GT.25) GO TO 30                                             397.
      C-----  ENTER PLOTTING LOOP.                                             398.
234           DO 3 KK = 1,K                                                     399.
      C-----  WRITE TITLE.                                                     400.
235           WRITE (6,11) KK                                                   401.
      C-----  PRINT ARRAY                                                      402.
236           DO 4 II = 1,I                                                     403.
237        4 WRITE (6,13) (A(II,JJ,KK), JJ = 1,J)                               404.
238        3 CONTINUE                                                           405.
239           GO TO 1000                                                        406.
      C-----  ROUTINE FOR ARRAYS WITH A WIDTH GREATER THAN 25.                  407.
240        30 DO 5 KK = 1,K                                                     408.
      C-----  WRITE TITLE                                                      409.
241           WRITE (6,11) KK                                                   410.
      C-----  PRINT ARRAY                                                      411.
242           DO 6 II = 1,I                                                     412.
243        6 WRITE (6,14) (A(II,JJ,KK), JJ = 1,J)                               413.
244        5 CONTINUE                                                           414.
245       10 FORMAT (1HO,/,10X,'GRAPHICAL PLOT OF SLICE NUMBER',I3,//)          415.
246       11 FORMAT (1H1,/,10X,'GRAPHICAL PLOT OF SLICE NUMBER',I3,//)          416.
247       12 FORMAT (1HO,10F5.0)                                                417.
248       13 FORMAT (1HO,25F5.0)                                                418.
249       14 FORMAT (1H ,38F3.0)                                                419.
      C-----  RETURN TO THE MAIN PROGRAM                                       420.
250     1000 RETURN                                                            421.
251           END                                                               422.
```

COMPUTER PROGRAM TO PACK SPHERES IN A TETRAHEDRAL ARRAY

```
      $WATFIV                                                                  4.
      C       PURPOSE: STARTING WITH A GIVEN SIZE DISTRIBUTION OF PARTICLES:   5.
      C           1. COMPUTE THE ROSIN PROBABILITY OF THE DISTRIBUTION.        6.
      C           2. FIT A STRAIGHT LINE TO THE DATA USING A LEAST SQUARES FIT. 7.
      C           3. TEST FOR THE GOODNESS OF FIT USING REDUCED CHI-SQUARE.    8.
      C           4. PLOT THE DATA AND THE ANALYTICAL FUNCTION.                9.
      C           5. COMPUTE THE SOLID VOLUME USING A TETRAHEDRAL PACKING MODEL 10.
      C              A. FOR THE DATA.                                          11.
      C              B. FOR THE FITTED LINE.                                   12.
      C           7. JIM RODINE, STANFORD UNIVERSITY, JUNE 1973.               13.
    1       IMPLICIT REAL*8(A-H,O-Z)                                           14.
    2       REAL*8 R(20), P(20), PA(20),VR(20), HEAD(8), X(20), YFIT(20),      15.
           C YFITR(20), Y(20),DIFF(20),SIGMAY(20)                              16.
    3       REAL*4 PLOT(132,55)                                                17.
    4       MODE = 1                                                           18.
      C       NUM = NUMBER OF SAMPLE ANALYSIS.                                 19.
    5       READ (5,5) NUM                                                     20.
    6     5 FORMAT(I15)                                                        21.
    7       DO 300 J=1,NUM                                                     22.
      C       NPTS IS THE TOTAL OF THE DATA SETS TO BE INPUT.                  23.
      C       FILM IS THE THICKNESS OF A LAYER AROUND EACH SPHERE.             24.
      C       HEAD IS THE LITERAL HEADING FOR THE DATA SET.                    25.
    8       READ (5,1) NPTS, FILM, (HEAD(I), I=1,7)                            26.
    9     1 FORMAT(I15,F10.5,7A8)                                              27.
   10       NFREE = NPTS - 2                                                   28.
      C       READ DATA AT THE CENTER OF A PHI DISTRIBUTION CLASS.             29.
      C       R(I) IS THE SPHERE RADIUS.                                       30.
      C       P(I) IS THE PROBABILITY AT THE GIVEN SPHERE RADIUS.              31.
   11       DO 20 I=1,NPTS                                                     32.
   12    20 READ(5,2) R(I),P(I)                                                33.
   13     2 FORMAT(2F10.4)                                                     34.
   14       CALL FREQ(NPTS,R,P,PA,VR)                                          35.
   15       CALL ROSIN(R,P,X,Y,NPTS)                                           36.
   16       DO 50 I=1,NPTS                                                     37.
   17       TEMP = DABS(100./Y(I))                                             38.
   18       SIGMAY(I) = (1./TEMP)/DLOG(TEMP)                                   39.
   19    50 CONTINUE                                                           40.
   20       CALL LINFIT(X,Y,SIGMAY,NPTS,MODE,A,SIGMAA,B,SIGMAB,RLIN)           41.
   21       CALL FITY(X,A,B,YFIT,YFITR,NPTS)                                   42.
   22       CALL CHISQ(Y,SIGMAY,NPTS,NFREE,MODE,YFIT,CHI)                      43.
   23       CALL PLOTER(X,Y,HEAD,NPTS,YFIT)                                    44.
   24       CALL DIST(NPTS,R,PA,P,VR,DIFF,FILM,SOLID,TOTSUM)                   45.
      C       WRITE RESULTS                                                    46.
   25       WRITE(6,3) (HEAD(I), I=1,7), NPTS, FILM                            47.
   26     3 FORMAT(1H1,7A8,/,' THE TOTAL NUMBER OF DATA SETS =',I5,            48.
           C '  FILM THICKNESS (MILLIMETERS) =',F10.5)                        49.
   27       WRITE(6,10)                                                        50.
   28    10 FORMAT(1H0,3X,'I',5X,'RADIUS',6X,'WEIGHT',6X,'NUMBER',6X,'SIGMAY', 51.
           C 6X,'RADIUS',6X,'ROSIN',7X,'FITTED',6X,'FITTED',5X,'COMPUTED',    52.
           C 4X,'WT PROB -',/,10X,'(MM)',5X,'PROBABILITY PROBABILITY WT STD DE 53.
           CV',4X,'LOG(R)',4X,'PROBABILITY LOG LOG(P)  ROSIN PROB',4X,        54.
           C 'WT PROB',3X,'COMP WT PROB')                                     55.
   29       DO 11 I=1,NPTS                                                     56.
   30    11 WRITE(6,12) I,R(I),P(I),PA(I),SIGMAY(I),X(I),Y(I),YFIT(I),        57.
           C YFITR(I),VR(I),DIFF(I)                                           58.
   31    12 FORMAT(1H ,2X,I2,2X,10E12.5)                                       59.
   32       WRITE(6,13)                                                        60.
   33    13 FORMAT(1H0,'  FITTED LINE',4X,'INTERCEPT',4X,'FITTED LINE',4X,     61.
           C 'SLOPE STD',4X,'LINEAR CORR',5X,'REDUCED',5X,'TETRAHEDRAL',6X,   62.
           C 'SOLID',9X,'VOID',/,3X,'INTERCEPT',6X,'STD DEV',8X,'SLOPE',8X,   63.
```

```
     C '%VIATION',4X,'COEFFICIENT',4X,'CHI-SQUARE',3X,'FUNCTION SUM',     64.
     C 5X,'RATIO',9X,'RATIO')                                             65.
34       VOID = 1. - SOLID                                                66.
35       WRITE(6,15) A,SIGMAA,B,SIGMAB,RLIN,CHI,TOTSUM,SOLID,VOID         67.
36    15 FORMAT(1H ,9F14.5)                                               68.
37   300 CONTINUE                                                         69.
38       RETURN                                                           70.
39       END                                                              71.
```

```
      SUBROUTINE FREQ(NPTS,R,P,PA,VR)                                   72.
      IMPLICIT REAL*8(A-H, O-Z)                                         73.
      REAL R*8(20), P*8(20), PA*8(20),VR*8(20)                          74.
C      PURPOSE: TO COMPUTE AND NORMALIZE NUMBER FREQUENCY DATA GIVEN     75.
C               WEIGHT FREQUENCY DATA - ASSUMING SPHERICAL SHAPE.        76.
C         R = SPHERE RADIUS ARRAY                                        77.
C         P = WEIGHT PROBABILITY ARRAY.                                  78.
C         PA = NUMBER PROBABILITY ARRAY.                                 79.
C         VR = BLANK ARRAY FOR LATER USE IN STORING RECOMPUTED           80.
C              WEIGHT FREQUENCIES                                        81.
      PIE = 3.141592653589793                                           82.
      RNT = 0.0                                                         83.
      DO 100 I=1,NPTS                                                   84.
      PA(I) = (P(I)*3.)/(4.*PIE*R(I)*R(I)*R(I))                         85.
      RNT = RNT + PA(I)                                                 86.
  100 CONTINUE                                                          87.
C      REDEFINE PA(I) IN TERMS OF SIZE FREQUENCY PROBABILITY.           88.
C      ZERO VR(I) ARRAY.                                                89.
      DO 101 I=1,NPTS                                                   90.
      VR(I) = 0.0                                                       91.
  101 PA(I) = PA(I)/RNT                                                 92.
      RETURN                                                            93.
      END                                                               94.
```

```
54          SUBROUTINE ROSIN(R,P,X,Y,NPTS)                                    95.
      C      PURPOSE: TO COMPUTE THE DATA VALUES AS A FUNCTION OF THE          96.
      C               ROSIN PROBABILITY DISTRIBUTION                           97.
      C         R = INDEPENDENT VARIABLE ARRAY(RADIUS)                         98.
      C         P = DEPENDENT VARIABLE ARRAY(WEIGHT PROBABILITY)               99.
      C         X = INDEPENDENT VARIABLE EXPRESSED AS PHI-CLASS UNITS(LOG(R))  100.
      C         Y = DEPENDENT VARIABLE EXPRESSED AS ROSIN'S CUMULATIVE         101.
      C             PROBABILITY(LOG(LOG(100/P))                                102.
      C         NPTS = NUMBER OF PAIRS OF DATA SETS                            103.
55          IMPLICIT REAL*8(A-H, O-Z)                                         104.
56          REAL R*8(20),P*8(20),X*8(20),Y*8(20)                              105.
57          E = .6931471805000000                                             106.
58          PROB = 100.                                                       107.
59          DO 10 I=1,NPTS                                                    108.
60          PROB = PROB - P(I)*100.                                           109.
61          X(I) = - (DLOG(R(I)))/E                                           110.
62          IF(PROB.GE.99.) GO TO 8                                           111.
63          IF(PROB.LE.1.) GO TO 9                                            112.
64          TEMP = 100./PROB                                                  113.
65          TEMP = (DLOG(TEMP))/E                                             114.
66          Y(I) = (DLOG(TEMP))/E                                             115.
67          GO TO 10                                                          116.
68        8 Y(I) = -6.107846127                                               117.
69          GO TO 10                                                          118.
70        9 Y(I) = 2.732020845                                                119.
71       10 CONTINUE                                                          120.
72          RETURN                                                            121.
73          END                                                               122.
```

```
      SUBROUTINE LINFIT(X,Y,SIGMAY,NPTS,MODE,A,SIGMAA,B,SIGMAB,RLIN)
C      PURPOSE: MAKE A LEAST SQUARES FIT TO DATA WITH A STRAIGHT LINE
C      PROGRAM DERIVED AFTER BEVINGTON, PP.104-105.
C        X = ARRAY OF DATA POINTS FOR INDEPENDENT VARIABLE
C        Y = ARRAY OF DATA POINTS FOR DEPENDENT VARIABLE
C        SIGMAY = ARRAY OF STANDARD DEVIATIONS FOR DEPENDENT VARIABLE
C        NPTS = NUMBER OF PAIRS OF DATA POINTS
C        MODE = METHOD OF WEIGHTING LEAST SQUARES FIT
C             = +1 (INSTRUMENTAL) WEIGHT(I) = 1./SIGMAY(I)**2
C             = 0  (NO WEIGHTING) WEIGHT(I) = 1.
C             = -1 (STATISTICAL)  WEIGHT(I) = 1./Y(I)
C        A = INTERCEPT OF FITTED STRAIGHT LINE
C        SIGMAA = STANDARD DEVIATION OF A
C        B = SLOPE OF FITTED STRAIGHT LINE
C        SIGMAB = STANDARD DEVIATION OF B
C        RLIN = LINEAR CORRELATION COEFFICIENT
      IMPLICIT REAL*8(A-H, O-Z)
      REAL*8 X(20), Y(20), SIGMAY(20)
C      ACCUMULATE WEIGHTED SUMS
   11 SUM = 0.
      SUMX = 0.
      SUMY = 0.
      SUMX2 = 0.
      SUMXY = 0.
      SUMY2 = 0.
   21 DO 50 I=1,NPTS
      XI = X(I)
      YI = Y(I)
      IF(MODE) 31,36,38
   31 IF(YI) 34,36,32
   32 WEIGHT = 1./YI
      GO TO 41
   34 WEIGHT = 1./(-YI)
      GO TO 41
   36 WEIGHT = 1.
      GO TO 41
   38 WEIGHT = 1./SIGMAY(I)**2
   41 SUM = SUM + WEIGHT
      SUMX = SUMX + WEIGHT*XI
      SUMY = SUMY + WEIGHT*YI
      SUMX2 = SUMX2 + WEIGHT*XI*XI
      SUMXY = SUMXY + WEIGHT*XI*YI
      SUMY2 = SUMY2 + WEIGHT*YI*YI
   50 CONTINUE
C      CALCULATE COEFFICIENTS AND STANDARD DEVIATIONS
   51 DELTA = SUM*SUMX2 - SUMX*SUMX
      A = (SUMX2*SUMY - SUMX*SUMXY)/DELTA
   53 B = (SUMXY*SUM - SUMX*SUMY)/DELTA
   61 IF(MODE) 62,64,62
   62 VARNCE = 1.
      GO TO 67
   64 C = NPTS - 2
      VARNCE = (SUMY2 + A*A*SUM + B*B*SUMX2 - 2.*(A*SUMY + B*SUMXY -
     C A*B*SUMX))/C
   67 SIGMAA = DSQRT(VARNCE*SUMX2/DELTA)
   68 SIGMAB = DSQRT(VARNCE*SUM/DELTA)
   71 RLIN = (SUM*SUMXY - SUMX*SUMY)/
     C DSQRT(DELTA*(SUM*SUMY2 - SUMY*SUMY))
      RETURN
      END
```

```
115           SUBROUTINE FITY(X,A,B,YFIT,YFITR,NPTS)                          183.
      C        PURPOSE: CALCULATE FITTED ORDINATE (Y) VALUES FOR THE GIVEN    184.
      C                 ABCISSA VALUES (X).                                   185.
      C           X = DATA ARRAY VALUES FOR RADIUS EXPRESSED AS PHI UNITS(-LOGR) 186.
      C           A = INTERCEPT OF THE FITTED LINE.                          187.
      C           B = SLOPE OF THE FITTED LINE.                              188.
      C           YFIT = ORDINATE VALUES FOR FITTED LINE (ROSIN'S LOG LOG)    189.
      C           YFITR = ORDINATE VALUES FOR FITTED LINE (CUMULATIVE PROB.)  190.
      C           NPTS = NUMBER OF DATA POINTS                               191.
116           IMPLICIT REAL*8(A-H, O-Z)                                       192.
117           REAL*8 X(20), YFIT(20), YFITR(20)                               193.
118           E = .6931471805                                                 194.
119           DO 10 I=1,NPTS                                                  195.
120           YFIT(I) = A + B*X(I)                                            196.
121           TEMP1 = DEXP(YFIT(I)*E)                                         197.
122           TEMP = DEXP(TEMP1*E)                                            198.
123        10 YFITR(I) = 100./TEMP                                            199.
124           RETURN                                                          200.
125           END                                                             201.
```

```
126           SUBROUTINE CHISQ(Y,SIGMAY,NPTS,NFREE,MODE,YFIT,CHI)                202.
      C        PURPOSE: TO EVALUATE THE REDUCED CHI SQUARE FIT TO DATA          203.
      C        PROGRAM DERIVED AFTER BEVINGTON, P. 194                          204.
      C          Y = ARRAY OF DEPENDENT VARIABLE DATA POINTS                    205.
      C          SIGMAY = ARRAY OF STANDARD DEVIATIONS FOR DATA POINTS          206.
      C          NPTS = NUMBER OF DATA POINTS                                   207.
      C          NFREE = NUMBER OF DEGREES OF FREEDOM                           208.
      C          MODE = METHOD OF WEIGHTING LEAST SQUARES FIT                   209.
      C               = +1 (INSTRUMENTAL) WEIGHT(I) = 1./SIGMAY(I)**2           210.
      C               = 0  (NO WEIGHTING) WEIGHT(I) = 1.                        211.
      C               = -1 (STATISTICAL)  WEIGHT(I) = 1./Y(I)                   212.
      C          YFIT = ARRAY OF CALCULATED VALUES OF Y                         213.
      C          CHI = VALUE OF CHI SQUARE RETURNED TO MAIN PROGRAM             214.
127           IMPLICIT REAL*8(A-H, O-Z)                                         215.
128           REAL*8 Y(20),SIGMAY(20), YFIT(20)                                 216.
129        11 CHI = 0.                                                          217.
130        12 IF(NFREE) 13,13,20                                                218.
131        13 CHI = 0.                                                          219.
132           GO TO 40                                                          220.
      C        ACCUMULATE CHI SQUARE                                           221.
133        20 DO 30 I=1,NPTS                                                    222.
134        21 IF(MODE)22,27,29                                                  223.
135        22 IF(Y(I)) 25,27,23                                                 224.
136        23 WEIGHT = 1./Y(I)                                                  225.
137           GO TO 30                                                          226.
138        25 WEIGHT = 1./(-Y(I))                                               227.
139           GO TO 30                                                          228.
140        27 WEIGHT = 1.                                                       229.
141           GO TO 30                                                          230.
142        29 WEIGHT = 1./SIGMAY(I)**2                                          231.
143        30 CHI = CHI + WEIGHT*(Y(I) - YFIT(I))**2                            232.
      C        DIVIDE BY THE NUMBER OF DEGREES OF FREEDOM                      233.
144        31 FREE = NFREE                                                      234.
145        32 CHI = CHI/FREE                                                    235.
146        40 RETURN                                                            236.
147           END                                                               237.
```

```
148         SUBROUTINE PLOTER(R,P,T,NPTS,YFIT)                                238.
      C      PURPOSE: TO PRODUCE AND WRITE DATA AND FITTED LINE DISTRIBUTION  239.
      C               VALUES ON THE LINE PRINTER                              240.
      C          R = INDEPENDENT VARIABLE (RADIUS AFTER ROSIN TRANSFORMATION) 241.
      C          P = DEPENDENT DATA VARIABLE (PROBABILITY AFTER ROSIN)        242.
      C          A = INTERCEPT OF FITTED LINE                                243.
      C          B = SLOPE OF FITTED LINE                                    244.
      C          T = TITLE ARRAY                                             245.
      C          NPTS = NUMBER OF PAIRS OF DATA POINTS                       246.
      C          YFIT = DEPENDENT VARIABLE FOR FITTED LINE (ROSIN'S LOGLOGP) 247.
149         IMPLICIT REAL*8(A-H, O-Z)                                         248.
150         REAL*8 R(20), P(20), YFIT(20), T(8)                               249.
151         REAL*4 PLOT(132,55)                                               250.
152         DATA DASH,VERT,AST,PLUS,EXX,BLANK/'-','|','*','+','X',' '/       251.
      C      ZERO THE PLOTTING ARRAY                                         252.
153         DO 10 I=2,131                                                     253.
154         DO 11 J=2,54                                                      254.
155      11 PLOT(I,J) = BLANK                                                 255.
156      10 CONTINUE                                                          256.
      C      FILL IN THE BORDERS                                             257.
157         DO 12 I=1,132                                                     258.
158         DO 13 J=1,55,54                                                   259.
159         PLOT(I,J) = DASH                                                  260.
160      13 IF(MOD(I,10).EQ.2) PLOT(I,J) = VERT                               261.
161      12 CONTINUE                                                          262.
162         DO 14 I=1,132,131                                                 263.
163         DO 15 J=2,54                                                      264.
164         PLOT(I,J) = VERT                                                  265.
165      15 IF(MOD(J,6).EQ.3) PLOT(I,J) = DASH                                266.
166      14 CONTINUE                                                          267.
      C      FILL IN THE DATA POINTS                                         268.
167         DO 16 I=1,NPTS                                                    269.
168         RD = R(I)*10. + 42.                                               270.
169         IRD = RD                                                          271.
170         RP = P(I)*6. + 38.65                                              272.
171         JRP = RP                                                          273.
172         IF(IRD.GT.132) IRD = 132                                          274.
173         IF(IRD.LT.1) IRD = 1                                              275.
174         IF(JRP.GT.55) JRP = 55                                            276.
175         IF(JRP.LT.1) JRP = 1                                              277.
176         PLOT(IRD,JRP) = AST                                               278.
177         RPF = YFIT(I)*6. + 38.65                                          279.
178         JRPF = RPF                                                        280.
179         IF(JRPF.GT.55) JRPF = 55                                          281.
180         IF(JRPF.LT.1) JRPF = 1                                            282.
181         PLOT(IRD,JRPF) = PLUS                                             283.
182      16 IF(JRP.EQ.JRPF) PLOT(IRD,JRP) = EXX                               284.
      C      WRITE RESULTS                                                   285.
183         WRITE(6,1) (T(I), I=1,7)                                          286.
184       1 FORMAT(1H1,7A8,/)                                                 287.
185         WRITE(6,2) ((PLOT(I,J), I=1,132), J=1,55)                         288.
186       2 FORMAT(1H ,132A1)                                                 289.
187         WRITE(6,3)                                                        290.
188       3 FORMAT(1HO,'HORIZONTAL SCALE: 1 INCH = 1 PHI UNIT',               291.
          C '  VERTICAL SCALE: 1 INCH = LOG(LOG(100/P))',/,                   292.
          C ' * = DATA POINT, + = FITTED LINE POINT, X = COMMON POINT')      293.
189         IF (NPTS.GT.13) WRITE(6,4)                                        294.
190       4 FORMAT(1H ,'***NOTICE THE PLOT HAS TRUNCATED THE DATA ABOVE THE 13 295.
          CTH CLASS INTERVAL***')                                            296.
191         RETURN                                                            297.
```

```
192          END                                                    298.
```

```
193         SUBROUTINE DIST(NPTS,R,PA,P,VR,DIFF,FILM,SOLID,TOTSUM)                299.
      C----- SOLID VOLUME OF A DENSE RANDOM DISTRIBUTION OF SPHERES ASSUMING      300.
      C      TETRAHEDRAL PACKING WITH A KNOWN VOLUME DISTRIBUTION OF             301.
      C      PARTICLES. JIM RODINE, STANFORD UNIVERSITY, 3/'73.                  302.
      C      NPTS = NUMBER OF PAIRS OF DATA POINTS.                              303.
      C      R = ARRAY OF INDEPENDENT VARIABLE (RADIUS).                         304.
      C      PA = ARRAY OF DEPENDENT VARIABLE (NUMBER PROBABILITY BY CLASS).     305.
      C      P = ARRAY OF DEPENDENT VARIABLE (WEIGHT PROBABILITY BY CLASS).      306.
      C      VR = ARRAY TO CONTAIN THE RECOMPUTED WEIGHT PROBABILITIES.          307.
      C      DIFF = ARRAY TO CONTAIN THE DIFFERENCE BETWEEN P AND VR.            308.
      C      FILM = THICKNESS OF LAYER AROUND EACH SPHERE (MM).                  309.
      C      SOLID = RATIO OF SOLID TO TOTAL VOLUMES.                            310.
      C      TOTSUM = SUM OF THE TETRAHEDRAL PROBABILITY FUNCTION.               311.
194         IMPLICIT REAL*8(A-H,O-Z)                                            312.
195         REAL R*8(20), P*8(20), PA*8(20),  VR*8(20), DIFF*8(20)              313.
196         PIE = 3.141592653589793                                             314.
197         SVTOT = 0.0                                                         315.
198         TVTOT = 0.0                                                         316.
199         TOTSUM = 0.0                                                        317.
200         COEF = 0.0                                                          318.
201         DO 203 I1 = 1,NPTS                                                  319.
      C           ASSIGN AVERAGE SPHERE RADII.                                  320.
202           DO 202 I2 = I1,NPTS                                               321.
203             DO 201 I3 = I2,NPTS                                             322.
204               DO 200 I4 = I3,NPTS                                           323.
205               R1 = R(I1) + FILM                                             324.
206               R2 = R(I2) + FILM                                             325.
207               R3 = R(I3) + FILM                                             326.
208               R4 = R(I4) + FILM                                             327.
209               CALL ASSIGN(R1,R2,R3,R4,COEF)                                 328.
      C           COMPUTE TETRAHEDRAL ANGLES AT SPHERE CENTER.                  329.
210               C412=DARCOS((R4*(R4 + R1 + R2)-R1*R2)/((R4 + R1)*(R4 + R2)))  330.
211               C413=DARCOS((R4*(R4 + R1 + R3)-R1*R3)/((R4 + R1)*(R4 + R3)))  331.
212               C423=DARCOS((R4*(R4 + R2 + R3)-R2*R3)/((R4 + R2)*(R4 + R3)))  332.
213               C312=DARCOS((R3*(R3 + R1 + R2)-R1*R2)/((R3 + R1)*(R3 + R2)))  333.
214               C314=DARCOS((R3*(R3 + R1 + R4)-R1*R4)/((R3 + R1)*(R3 + R4)))  334.
215               C324=DARCOS((R3*(R3 + R2 + R4)-R2*R4)/((R3 + R2)*(R3 + R4)))  335.
216               C213=DARCOS((R2*(R2 + R1 + R3)-R1*R3)/((R2 + R1)*(R2 + R3)))  336.
217               C214=DARCOS((R2*(R2 + R1 + R4)-R1*R4)/((R2 + R1)*(R2 + R4)))  337.
218               C234=DARCOS((R2*(R2 + R3 + R4)-R3*R4)/((R2 + R3)*(R2 + R4)))  338.
219               C123=DARCOS((R1*(R1 + R2 + R3)-R2*R3)/((R1 + R2)*(R1 + R3)))  339.
220               C124=DARCOS((R1*(R1 + R2 + R4)-R2*R4)/((R1 + R2)*(R1 + R4)))  340.
221               C134=DARCOS((R1*(R1 + R3 + R4) R3*R4)/((R1 + R3)*(R1 + R4)))  341.
      C           COMPUTE ANGLES OF SPHERICAL TRIANGLES.                        342.
222               S4 = (C412 + C413 + C423)/2.                                  343.
223               TEMP1 = DSIN(S4 - C413)                                       344.
224               TEMP2 = DSIN(S4 - C423)                                       345.
225               TEMP3 = DSIN(S4 - C412)                                       346.
226               DSINS4 = DSIN(S4)                                             347.
227               B412 = ((TEMP1*TEMP2)/(DSINS4*TEMP3))                         348.
228               IF(B412.LT.0.0) GO TO 200                                     349.
229               B412 = 2.*DATAN(DSQRT(B412))                                  350.
230               B413 = ((TEMP3*TEMP2)/(DSINS4*TEMP1))                         351.
231               IF(B413.LT.0.0) GO TO 200                                     352.
232               B413 = 2.*DATAN(DSQRT(B413))                                  353.
233               B423 = ((TEMP3*TEMP1)/(DSINS4*TEMP2))                         354.
234               IF(B423.LT.0.0) GO TO 200                                     355.
235               B423 = 2.*DATAN(DSQRT(B423))                                  356.
236               S4 = (C312 + C314 + C324)/2.                                  357.
237               TEMP1 = DSIN(S4 - C314)                                       358.
```

```
238                TEMP2 = DSIN(S4 - C324)                                  359.
239                TEMP3 = DSIN(S4 - C312)                                  360.
240                DSINS4 = DSIN(S4)                                        361.
241                B312 = (TEMP1*TEMP2)/(DSINS4*TEMP3)                      362.
242                IF(B312.LT.0.0) GO TO 200                                363.
243                B312 = 2.*DATAN(DSQRT(B312))                             364.
244                B314 = (TEMP3*TEMP2)/(DSINS4*TEMP1)                      365.
245                IF(B314.LT.0.0) GO TO 200                                366.
246                B314 = 2.*DATAN(DSQRT(B314))                             367.
247                B324 = (TEMP3*TEMP1)/(DSINS4*TEMP2)                      368.
248                IF(B324.LT.0.0) GO TO 200                                369.
249                B324 = 2.*DATAN(DSQRT(B324))                             370.
250                S4 = (C213 + C214 + C234)/2.                             371.
251                TEMP1 = DSIN(S4 - C214)                                  372.
252                TEMP2 = DSIN(S4 - C234)                                  373.
253                TEMP3 = DSIN(S4 - C213)                                  374.
254                DSINS4 = DSIN(S4)                                        375.
255                B213 = (TEMP1*TEMP2)/(DSINS4*TEMP3)                      376.
256                IF(B213.LT.0.0) GO TO 200                                377.
257                B213 = 2.*DATAN(DSQRT(B213))                             378.
258                B214 = (TEMP3*TEMP2)/(DSINS4*TEMP1)                      379.
259                IF(B214.LT.0.0) GO TO 200                                380.
260                B214 = 2.*DATAN(DSQRT(B214))                             381.
261                B234 = (TEMP3*TEMP1)/(DSINS4*TEMP2)                      382.
262                IF(B234.LT.0.0) GO TO 200                                383.
263                B234 = 2.*DATAN(DSQRT(B234))                             384.
264                S4 = (C123 + C124 + C134)/2.                             385.
265                TEMP1 = DSIN(S4 - C124)                                  386.
266                TEMP2 = DSIN(S4 - C134)                                  387.
267                TEMP3 = DSIN(S4 - C123)                                  388.
268                DSINS4 = DSIN(S4)                                        389.
269                B123 = (TEMP1*TEMP2)/(DSINS4*TEMP3)                      390.
270                IF(B123.LT.0.0) GO TO 200                                391.
271                B123 = 2.*DATAN(DSQRT(B123))                             392.
272                B124 = (TEMP3*TEMP2)/(DSINS4*TEMP1)                      393.
273                IF(B124.LT.0.0) GO TO 200                                394.
274                B124 = 2.*DATAN(DSQRT(B124))                             395.
275                B134 = (TEMP3*TEMP1)/(DSINS4*TEMP2)                      396.
276                IF(B134.LT.0.0) GO TO 200                                397.
277                B134 = 2.*DATAN(DSQRT(B134))                             398.
       C           COMPUTE AREA OF EACH SPHERICAL TRIANGLE.                 399.
278                A14 = (B412 + B413 + B423 - PIE)*((R4 - FILM)**2)        400.
279                A13 = (B312 + B314 + B324 - PIE)*((R3 - FILM)**2)        401.
280                A12 = (B213 + B214 + B234 - PIE)*((R2 - FILM)**2)        402.
281                A11 = (B123 + B124 + B134 - PIE)*((R1 - FILM)**2)        403.
282                TEMP = R1*R2*R3*R4                                       404.
       C           COMPUTE VOLUME OF TETRAHEDRON.                           405.
283                VOLTET = DSQRT(((TEMP*2.*(R1*R2                          406.
           C       + R1*R3 + R1*R4 + R2*R3 + R2*R4 + R3*R4)) - (TEMP*TEMP*  407.
           C       (1./(R1*R1) + 1./(R2*R2) + 1./(R3*R3) + 1./(R4*R4)))))/9.)  408.
       C           COMPUTE VOLUME OF SPHERES OCCUPYING TETRAHEDRON.         409.
284                VR1 = A11*(R1 - FILM)/3.                                 410.
285                VR2 = A12*(R2 - FILM)/3.                                 411.
286                VR3 = A13*(R3 - FILM)/3.                                 412.
287                VR4 = A14*(R4 - FILM)/3.                                 413.
288                VOLSPH = VR1 + VR2 + VR3 + VR4                           414.
289                VOLRAT = VOLSPH/VOLTET                                   415.
       C           COMPUTE INCREMENT OF SYMMETRY FUNCTION.                  416.
290                SUM = PA(I1)*PA(I2)*PA(I3)*PA(I4)*((R1*R2*R3*R4)**1.9)*COEF  417.
291                TOTSUM = SUM + TOTSUM                                    418.
```

```
292                 TEMP1 = VOLSPH*SUM                                      419.
293                 TEMP2 = VOLTET*SUM                                      420.
294                 SVTOT = TEMP1 + SVTOT                                   421.
295                 TVTOT = TEMP2 + TVTOT                                   422.
296                 VR1 = VR1*SUM                                           423.
297                 VR2 = VR2*SUM                                           424.
298                 VR3 = VR3*SUM                                           425.
299                 VR4 = VR4*SUM                                           426.
300                 VR(I1) = VR(I1) + VR1                                   427.
301                 VR(I2) = VR(I2) + VR2                                   428.
302                 VR(I3) = VR(I3) + VR3                                   429.
303                 VR(I4) = VR(I4) + VR4                                   430.
304     200         CONTINUE                                                431.
305     201       CONTINUE                                                  432.
306     202     CONTINUE                                                    433.
307     203 CONTINUE                                                        434.
      C       COMPUTE THE SOLID VOLUME/TOTAL VOLUME RATIO.                  435.
308           SOLID = SVTOT/TVTOT                                           436.
309           SUM = 0.0                                                     437.
      C        NORMALIZE THE RECOMPUTED WEIGHT PROBABILITIES.               438.
310           DO 500 I=1,NPTS                                               439.
311       500 SUM = VR(I) + SUM                                             440.
312           DO 501 I=1,NPTS                                               441.
313           VR(I) = VR(I)/SUM                                             442.
314       501 DIFF(I) = P(I) - VR(I)                                        443.
315           RETURN                                                        444.
316           END                                                           445.
```

```
      SUBROUTINE ASSIGN(A,B,C,D,Q)                                      446.
      IMPLICIT REAL*8(A,B,C,D,Q)                                        447.
      IF(A.EQ.B.AND.A.EQ.C.AND.A.EQ.D) GO TO 100                        448.
      IF(A.EQ.B) GO TO 10                                               449.
      IF(A.EQ.C) GO TO 11                                               450.
      IF(A.EQ.D) GO TO 12                                               451.
      IF(C.EQ.D) GO TO 13                                               452.
      IF(B.EQ.D) GO TO 14                                               453.
      IF(B.EQ.C) GO TO 300                                              454.
      GO TO 500                                                         455.
   10 IF(C.EQ.D) GO TO 200                                              456.
      IF(A.EQ.C.OR.A.EQ.D) GO TO 400                                    457.
      GO TO 300                                                         458.
   11 IF(B.EQ.D) GO TO 200                                              459.
      IF(A.EQ.B.OR.A.EQ.D) GO TO 400                                    460.
      GO TO 300                                                         461.
   12 IF(B.EQ.C) GO TO 200                                              462.
      IF(A.EQ.B.OR.A.EQ.C) GO TO 400                                    463.
      GO TO 300                                                         464.
   13 IF(C.EQ.A.OR.C.EQ.B) GO TO 400                                    465.
      GO TO 300                                                         466.
   14 IF(B.EQ.A.OR.B.EQ.C) GO TO 400                                    467.
      GO TO 300                                                         468.
  100 Q = 1.                                                            469.
      GO TO 1000                                                        470.
  200 Q = 6.                                                            471.
      GO TO 1000                                                        472.
  300 Q = 12.                                                           473.
      GO TO 1000                                                        474.
  400 Q = 4.                                                            475.
      GO TO 1000                                                        476.
  500 Q = 24.                                                           477.
 1000 RETURN                                                            478.
      END                                                               479.
```

$DATA 480.